Thesis: Development of Phase-Field Model for studying Rapid Solidification by incorporating Continuous Growth Model Kinetics

Bashir Mitchell

February 2023

UNIVERSITY OF
BIRMINGHAM

University of Birmingham Research Archive

e-theses repository

This unpublished thesis/dissertation is copyright of the author and/or third parties. The intellectual property rights of the author or third parties in respect of this work are as defined by The Copyright Designs and Patents Act 1988 or as modified by any successor legislation.

Any use made of information contained in this thesis/dissertation must be in accordance with that legislation and must be properly acknowledged. Further distribution or reproduction in any format is prohibited without the permission of the copyright holder.

Contents

1 Introduction **6**

1.1 Motivation 6

1.2 Model Context 7

1.3 Model Development Aims 9

2 Literature Review **10**

2.1 Microstructure Formation during Additive Manufacture 11

2.2 Predicting Solidification and Microstructure Formation 14

2.3 Multi-Scale Modelling of Additive manufacturing 18

2.4 Rapid Solidification Modelling Review 21

2.5 Phase Field Modelling Review 24

2.6 Extended Irreversible Thermodynamics 36

3 Theory **38**

3.1 Reaction Rate Theory 38

3.2 Redistribution Potential 42

3.3 Fluxes for Characterising Solidification 44

3.3.1 Redistributive Flux 45

3.3.2 Cooperative Growth Flux 53

3.3.3 Diffusive Growth Flux 58

3.4 Bulk Diffusion as a Redistributive Flux 61

4 Models **66**

4.1 Diffuse Interface Model Utilising Cooperative Growth and Redistributive Flux 66

4.1.1 Cooperative Growth Flux in Diffuse Interface Model 69

4.1.2 Redistributive Flux in Diffuse Interface Model 74

4.1.3 Diffusion in Liquid and Interfacial Region with diffusivity acceleration 79

4.2 Modelling the Thermodynamics 81

4.2.1 Alloy System Parameters 85

4.3 Non Phase Field Diffuse Interface 89

5 Numerical Experiments and Implementation 93

5.1 Implementation of Diffuse Interface Model with Redistributive and Cooperative Growth Fluxes 93

5.2 Evolution of a Simple System 99

5.3 Partitioning vs Interface Velocity Numerical Experiments 100

5.3.1 Simulation Setup 104

5.3.2 Quantifying Partition Coefficient for Diffuse Interfaces 108

6 Results 110

6.1 Binary Alloys 110

6.2 Extension to Ternary Case Al-Sn-Cu 112

6.3 Discussion of Partitioning Results 116

6.4 Inconel System Demonstration 121

7 Conclusions 123

7.1 Overview 123

7.1.1 Motivation 123
7.1.2 Model Development 124
7.1.3 Notable Results 125
7.2 Other Findings 126
7.2.1 Redistributive Flux as a description of Diffusion 126
7.2.2 Curvature Potential in Diffuse Interfaces 127
7.2.3 Non-Phase Field Diffuse Interface 128
7.3 Potential Future Work 128
7.3.1 Solute Partitioning Predictions 128
7.3.2 Prediction of Microstructure Morphology 129

8 APPENDIX **131**

8.1 Low Driving force limit of Pair Wise Swapping Scheme 131
8.2 Derivation of Curvature Potential 132
8.3 anti derivative of $\phi(1-\phi)$ for standard travelling wave solution 134

Glossary

$\boldsymbol{D_i^\alpha}$ Diffusivity of element i in the α phase.

$\boldsymbol{H}$ PF energy penalty for coexisting phases.

$\boldsymbol{J_i}$ Lattice fixed frame flux of element i.

$\boldsymbol{R}$ molar gas constant.

$\boldsymbol{T}$ temperature in kelvin K.

$\boldsymbol{V_c}$ Maximum crystallisation velocity.

$\boldsymbol{X_i^S}$ $\boldsymbol{X_i^L}$ Concentration in the solid and liquid phases.

$\boldsymbol{\epsilon}$ PF gradient energy term.

$\boldsymbol{\eta_i^\alpha}$ Redistribution potential of element i in the α phase.

$\boldsymbol{\gamma_{ij}}$ Redistribution rate coefficient between elements i and j.

$\boldsymbol{\mu_i^\alpha}$ Chemical potential of element i in the α phase.

$\boldsymbol{\nabla}$ Gradient Operator in 1,2 or 3 dimensions..

$\boldsymbol{\phi^S}$ $\boldsymbol{\phi^L}$ Order Parameter or phase fraction.

$\boldsymbol{\psi_i^S}$ $\boldsymbol{\psi_i^L}$ product of phase fraction and composition of a given phase.

$\boldsymbol{j_i}$ Number fixed frame flux of element i.

$\boldsymbol{k}$ Partition Coeffcient, ratio of compositions on the solid and liquid sides of an interface.

$\boldsymbol{v_D}$ Redistributive Velocity from the CGM.

CGM Continuous Growth Model.

FID Finite Interface Dissipation Models.

KKS Kim Kim Suzuki phase field model.

LPBF Laser powder bed fusion.

PF Phase Field Model.

1 Introduction

1.1 Motivation

In recent years there has been interest in the development of a range of new near net shape manufacturing techniques, broadly classified as Additive Manufacturing (AM), whereby components are built up layer by layer into a 3D geometry. The advantages of these techniques are that they permit the creation of complex and detailed shapes that would other wise be difficult or produce via casting, or would result in a lot of waste material if produced by a subtractive machining process[1]. Additive manufacturing techniques have been applied to a variety of materials from plastics to ceramics [2] however this thesis will focus on the modelling challenges associated with the AM of metals. It is of interest for industries as varied as aerospace and biomedicine. In the aerospace industry AM permits the fabrication of components from Nickel Super Alloys (Inconel718/625) that are otherwise incredibly difficult to machine [3][4] whereas in bio-medicine AM is useful for efficiently producing patient specific custom implants out of durable, and non-bio reactive stainless steels (316L)[5].

The additive manufacturing of alloys such as these is typically performed by either a Directed Energy Deposition (DED) or Laser Powder Bed Fusion (LPBF) approach [6], both of which involve the rapid melting and consolidation of a metal powders to form the cross sectional layers for the desired geometry. These manufacturing techniques come with a need to be able to predict material properties as a function of material composition and processing parameters (such as laser power and laser scanning speed). These factors may influence the frequency and mode of defects that form [7], which may potentially have seriously adverse effects on a materials important performance metrics such as toughness and fatigue resistance.

The appearance of defects in materials during manufacture can be explained and predicted by considering the micro-structural evolution during the manufacturing process. In this case it is necessary to predict the microstructure formation during the re-solidification of the melted metal powder.

The modelling of the LPBF and DED processes overall requires a holistic multi-scale and multi-physics approach, wherein it is necessary to consider the macroscopic thermal fields around the molten and solid material, as well as microscopically the structures that form as the liquid solidifies [8]. This thesis will be primarily concerned with the microscopic modelling of solute distribution and its effect upon micro structure formation. The formation of microstructures such as dendrites have been well studied for conventional casting methods, however the re-solidification conditions for LPBF and DED processes are distinct, with much faster solidification rates and steeper thermal gradients the process more so resembles the conditions under a repetitive welding processes[9]. Thus it has been necessary to reconsider some of the assumptions made in models of microstructure formation (such as phase field models and cellular automota) when utilizing them under the more extreme thermodynamic conditions of additive manufacture.

1.2 Model Context

Much of the work on the multi-scale modelling of LPBF resembles closely the the modelling of weld pools and their heat affected zones [10]. The smallest length scale for relevant physics is the micrometer scale wherein microstructures can be resolved and distinguished, however simulating the entire domain (on the order of centimetres) at this resolution would be numerically intractable. Instead a simulation of the temperature field at the scale of the

weld pool is weakly coupled to a micro structure model - often times a phase field model (PFM)[11]. The models are coupled "weakly" in the sense that the results of temperature field model are used to inform the microstructure model, but not vice versa - ultimately however it is argued that the effect solidification has on the temperature field (for example by releasing latent heat) is quite negligible compared to the heat deposited by the laser. Solidification rates R and temperature gradients G from various parts of the weld pool are thus taken from the temperature field model and applied to the microstructure model, with the resultant microstructures being mapped to different R and G values. These results can then be used to generate and predict microstructure maps in terms of process parameters such as laser scan speed and power.

Due to the speed of solidification, the models used for predicting microstructure have been re-examined in recent years. In particular the effect of solute trapping on the resultant microstructures. To better predict the onset and magnitude of solute trapping phenomena, some of the original assumptions made in phase field modelling, such as the assumption of immediate relaxation to local equilibrium [12] [13], have been re-examined. This has resulted in the development of new diffuse interface models, many of which are PFM [14] [15], which attempt to reproduce the solute trapping dynamics predicted by older sharp interface models of rapid solidification developed in late 80s and early 90s such as the Continuous Growth Model [16] and the Local Non-Equilibrium Model [17] as such models have been shown to characterise the solute trapping phenomena remarkably well [18]. The work of this thesis is intended to be a contribution to, and extension of, these efforts.

1.3 Model Development Aims

To summarise the aims of this thesis are to make a model capable of being extended to 2D or 3D that reproduces the behaviour of Rapid Solidification Theory models such as the Local Non-Equilibrium Model (LNM) or the Continuous Growth Model (CGM). This will achieved by mapping the 1D sharp interface model (either CGM or LNM) behaviour to a diffuse interface models behaviour. Phase-Field models appear to be a promising framework to utilize in pursuit of this goal due to their phenomenological utility and the ease with which they can be generalised to higher dimensions. The development of this model will be based on a firm and robust understanding of the atomistic processes and fluxes with govern the successful sharp interface models of RS, and then attempting to replicate those processes in the in a Phase Field Model. The scope of work in this thesis will be limited to 1 dimensional phase field simulations to focus on accurately reproducing the kinetics of an interface and the distribution of solute under rapid solidification conditions. It is essential to accurately model these effects as the emergence of interface morphologies such as dendrites are directly dependent upon the composition profile and resultant solutal under cooling around the interface.

2 Literature Review

The thermal condition and histories during additive manufacturing are quite complex and varied. The Laser Powder Bed Fusion process (LPBF) is an additive manufacturing process that produces near net shape components however the properties, consistency and quality of the components are often varied and difficult to predict with current modelling techniques [1]. The LPBF process involves a high powered laser which is used to selectively melt and re-solidify a small region of metal powder into a continuous solid piece. This is performed over a 2D cross section of the desired 3D component in a powder bed. In order to build the next layer of the component a layer of powder is distributed over the build bed and the process is repeated for the next cross section with the Final component consisting of these bonded 2D layers [19]. The process parameters of the LPBF process such as Laser Power Output and Laser Scan speed must be correctly chosen in order to allow complete consolidation of powder particles and bonding between layers whilst not depositing so much energy in a region that it causes fusion of powder beyond the intended region [20].

Defects which are found during additive manufacturing may occur across multiple scales. In Taheri et al. 'Review of Defects in the LPBF processes'[21] a defect was defined as any property of the microstructure which is differed from a desired isotropic and fully dense solid of the target alloy. Such defects were porosity, lack of fusion, micro cracks, hot tears, variations in texture and grain size as well as unwanted variations in composition. Porosity may occur when a mesh of solidifying material prevents in filling of liquid melt as the material shrinks during solidification and cooling. It may also occur due to the formation and entrapment of gas bubbles [22]. Lack of fusion is usually a result of the laser not depositing

enough energy to fully melt and resolidify the particle powder into a continuous solid. This is also another source of porosity. Micro cracks and hot tears occur due the high frequency of thermal stresses experienced by the material as the laser makes repeated passes over the material [23]. Steep thermal gradients in the melt pool almost inevitably result in anisotropic texture[21].

2.1 Microstructure Formation during Additive Manufacture

The scope of this project will primarily be concerned with the microstructure formation on the scale of dendrites during the rapid re-solidification. In a holistic approach to understanding the LPBF process the thermal gradients driving this re-solidification may be determined from FEA analysis of laser heat deposition in the powder and the subsequent convection of the liquid melt as there exist sophisticated simulations in this regime of the problem such as those by Saad A. Khairallah et al. [24].

During solidification there are four distinct regimes of solidification behaviour shown in fig 3. It can be seen that as the solidification rate increases there is a transition from planar to cellular then to dendritic growth.

During re-solidification in LBPF of 316L it has been experimentally observed that the resultant phases are fully austenetic. These phases have a microstructure contains elongated grains of elongated columnar cells. These indicate the solidification progressed by way of competing colonies of cellular dendritic growth. XRD (X-Ray Diffraction), EBSD (Electron Back Scatter Diffraction), and TEM (Transmission Electron Microscopy) were utilized in a recent study by Krakhmalev et al [25] to confirm these results for 316L stainless steel during LPBF process. There have been contradictory studies that observed delta ferrite and

martensite[26][27], however there is also a body of evidence corroborating the former[28][7].

Cellular dendrites in the same colony appear to inherit the crystal structure of the substrate the nucleate from as can be seen in the EBSD map in fig 1. The single color regions of correspond to single crystallographic orientation and these color regions match up with the dendrite colonies. There is additional confirmation that cells in the same colony have the same crystallographic orientation as it was found that during the cooling of LPBF processed martensitic stainless steel the martensitic needles that formed during cooling would grow through cell boundaries however would stop at colony boundaries (the dashed lines in fig.1). [29]

In regards to this project this is relevant because it confirms the regime of solidification in LPBF is relevant for models of dendrite growth. In this case a phase field model. Competitive growth of cellular dendrites will not have to account for different crystal orientations within colonies because it has been experimentally found that there is little to no misorientation between cells within a colony. Therefore simulation of the growth of a single dendrite colony will also only need to account for growth anisotropy due to a single imposed arbitrary crystallographic orientation. Also, due to austenite being the only final phase observed, there should not be a need to consider a multi phase model at this stage. This sets a manageable initial goal for the project whilst still investigating a physically relevant system of 316L stainless steel. It is acknowledged that although only a single final phase was experimentally observed this does not rule out that there might be transient meta stable phases forming during the solidification process. An ultimately accurate description of the microstructure evolution may need to consider these phases, however it is difficult to find experimental in situ measurements of microstructure and phase formation during the LPBF process.

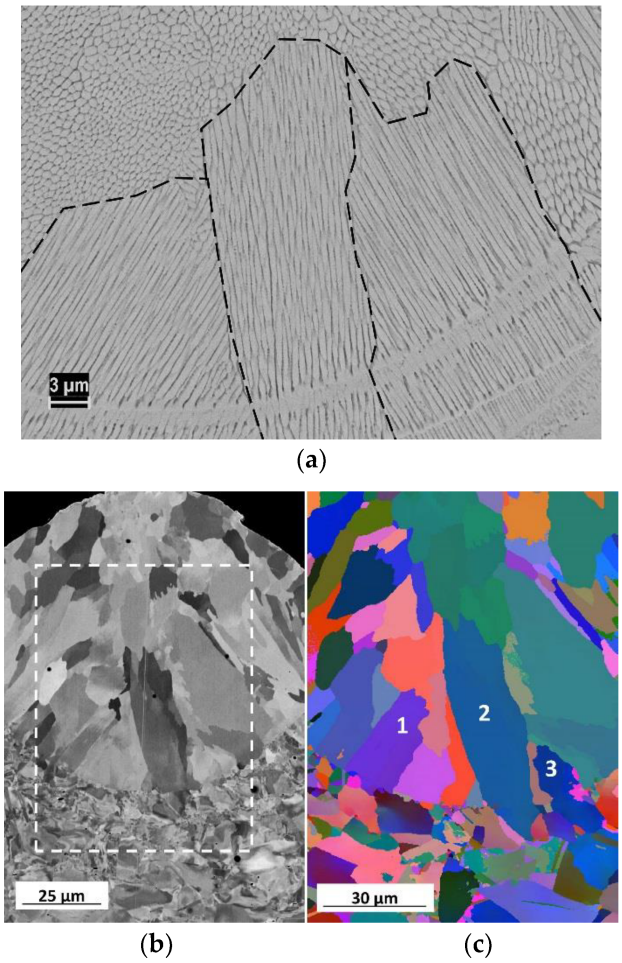


Fig. 1. *Scanning electron microscopy micrograph of the etched cross section of the LPBF 316 L. Seperate colonies are marked by the dashed lines. (b) channeling contrast SEM image of a cross section of the LPBF 316 L (c) an electron back-scattering diffraction orientation map of the marked region in (b). Grains 1, 2, and 3 show the epitaxial (layer upon layer) nucleation of colonies from some nucleation site. Figure taken from [30]*

In fig 1 the grains outside of the dashed region are seen to consist of much smaller and distinctly non columnar cells. Initially these were thought to cross sections of colonies of columnar cellular growth which were not growing in the plane of the slice, however after further reading it is believed that these represent a transition from columnar to equiaxed grain growth. This effect has been simulated for chill cast of Al-Cu Alloys by H. B. Dong and P. D. Lee using cellular automaton- finite difference scheme.[31] The results of their simulation can be seen in fig 2. The thermal under cooling would extend past the region of columnar dendrite growth due to solute pile up reducing the stabilising the liquid phase just ahead of the growing cells. This would permit randomly modelled new growth of equiaxed cells from nuclei in the liquid melt to occur resulting in the equiaxed region. Equiaxed regions of dendrite colonies are observed in the final microstructures of solidified 316L hence it is believed a similar mechanism may be taking place.

2.2 Predicting Solidification and Microstructure Formation

The formation of defects such as porosity and hot tears as well as other properties such as grain size can be predicted by which microstructures form during solidification [21]. It has been know for some time that the formation of microstructure and solidification modes are sensitive to the processing and manufacturing conditions that a material undergoes, as shown in Elmer et al [32] wherein different processing parameters for casting, welding and rapid solidification yielded up to 5 different microstructure morphologies. The key to making predictions for which of these morphologies will appear is to understand the relevant physics that initiates and drives a materials micro-structural evolution during the solidification process [33].

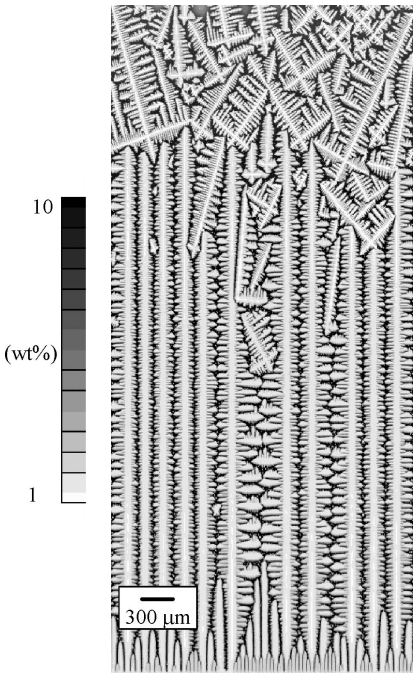


Fig. 2. *Result of Cellular Automaton - Finite Difference scheme simulation of cellular dendritic growth transitioning to an equiaxed growth regime [31]. A heterogeneous nucleation event was a modelled as a stochastic process with a higher likelihood of occurring during a greater degree of solute adjusted under cooling. Solute build up ahead of the advancing solid phase region (due to the lower solubility of Cu in the solid phase) results in a dendritic break down; however the appearance of heterogeneous nucleation (and thus equiaxed grains) is caused by applying a monotonically increasing liquidus isotherm velocity.*

The formation of dendritic microstructures can be predicted by the presence of constitutional super cooling in the liquid region just ahead of a solid - liquid interface. Constitutional super-cooling occurs under the following condition:

$$G < mc_{\infty}\left[\frac{1}{k} - 1\right] v/D \tag{1}$$

Where G is the thermal gradient, m is a parameter derived from the systems phase diagram (slope of the solidus line), c_{∞} is the far field solute composition and k is the interface partitioning coefficient (c_s/c_l). This expression was originally derived by Mullins and Sekerka [34] utilising a linear stability analysis to find conditions under which small perturbations of the interface would grow. Intuitively this condition results in unstable perturbations as when a small bump of material projects out into the liquid it will encounter material that is more under cooled than the material adjacent to the non perturbed surface, thus the perturbed region will grow faster thus destabilising the planar interface. It should be noted that the instability condition will always hold if v is sufficiently large, implying that above a certain interface velocity all planar interfaces ought to break down into a dendritic growths. This however is not physically the case and it is shown by Kurz and Trivedi in [35] that some of the assumptions made in Mullins and Sekerkas constitutional super cooling criterion must be re-examined in the high interface velocity regime. Their adjustments yield a return to planar stability above a certain interface velocity with the generally observed pattern of planar growth $\rightarrow$ cellular growth $\rightarrow$ dendritic growth $\rightarrow$ cellular growth $\rightarrow$ planar growth seen with increasing interface velocities. This is shown schematically in figure 3.

In addition to predicting whether or not the dendritic microstructures form, it is also

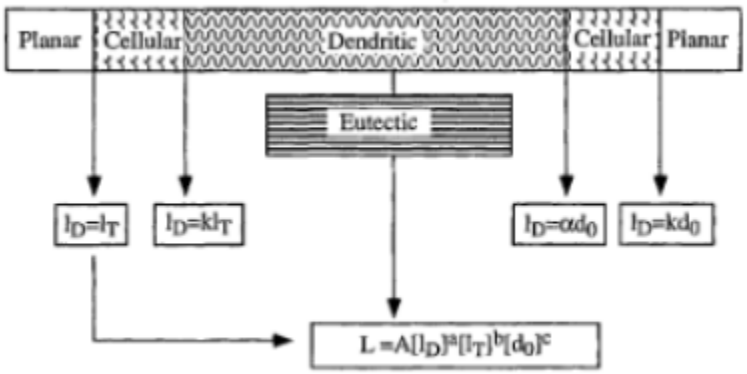


Fig. 3. *Solidification Regimes from a Dendritic growth overview by R. Trivedi and W. Kurz [36], with increasing interface velocity (left to right)*

useful to be able to predict the shape of those dendrites as has been done by McFadden and Browne [37] using Ivantsov dendrite growth model. The approach outlined however is not entirely predictive as it is necessary to know properties such as dendrite tip velocity in order to predict a dendrite tips radius or the resultant composition profile around the dendrite. This is a shortcoming that is also shared by the stability analysis provided by Mullins, Sekerka, Kurz and Trivedi. When predicting microstructure formation it is not always possible to know ab priorii what the the solidification velocity is limiting the utility of stability analysis and Invantsov Solutions to dendrite growth. Nevertheless these models do point towards the relevant physics and processes that need to be considered in the development of models that do predict microstructure given the thermal and material conditions alone, namely the necessity of coupling thermal, solutal and phase fields together.

2.3 Multi-Scale Modelling of Additive manufacturing

The modelling of additive manufacturing is typically approached as a multi-scale physics problem with dedicated models for the micrometer and millimeter length scales. On the micro-meter length scales there are several features of interest that models are used to predict, such as the nucleation and competitive growth of different grains [38], solute segregation behaviour in order to predict the formation of inter-metallic phases [39] and general micro structure morphologies. The modelling of microstructure morphology evolution is is effectively a moving boundary problem wherein equations governing the movement of material need to solved for each domain (a solid domain and liquid domain in the case of solidification) and the boundary defining the extent of these domains itself evolves according the movement of material across the boundary. Phase field simulations are a useful numerical tool for tackling such problems and have been used in the modelling of additive manufacturing by groups such as Karayagiz [11] and Radhakrishnan [40] to predict the size, shape and primary arm spacing of dendrites for the Ni-Nb and Ni-Fe-Nb systems under different processing conditions. These alloys systems were taken as simplified analogues for the high performance Nickel Super Alloy Inconel718 of interest for additive manufacture.

The Micro-structure models are typically used in conjunction with a model of the thermal field from either an analytical solution such as the Rosenthal Equation [41], or a numerical model of weld pool temperature across the domain of interest. This approach used in much of the contemporary work on phase field modelling of rapid solidification processes mirrors the set up of numerical experiments used to make predictions of microstructure formation of welding processes such as those [10] Farzardi et al, who pioneered this approach to predict the

microstructure in Al-Cu welds. The Thermal Field model of the weld pool is used to inform the temperature conditions for a separate micro-structural phase field simulation at a smaller length scale at various points across the melt pool geometry. It is from these microstructure models that a prediction of the distribution of microstructure across the weld pool can be made. The microstructure models use a linear approximation of the thermal field at a given location as input:

$$T(x, y, z, t) = T_0 + G(z - Rt) \tag{2}$$

Where T is the temperature field at points in space defined by x, y, z - and G is the Thermal Gradient at the given location in the melt pool and R is the growth rate, specifically the component of velocity perpendicular to the temperature Isotherm. This approach is known at as applying a frozen temperature field and it is important to note that is only a weak one directional coupling of the mesoscopic phase field model and the macroscopic thermal field simulation. In reality the solidification response from the meso-scale simulation would affect the release and the diffusion of latent heat from the interface region, which would in turn affect evolution of the temperature field which would in turn effect the microstructure formation etc... Ultimately the frozen temperature field assumption ignores this potential interplay, however for many alloy systems involving the potential transitions between planar and dendritic growth the breakdown of planar stability is primarily driven by solutal under-cooling ahead of the interface instead of the actual temperature profile alone. In these cases a frozen temperature field assumption is assumed to be fairly accurate as in spite of any rejected latent heat the thermal profile is presumed to have relaxed to a linear profile due to

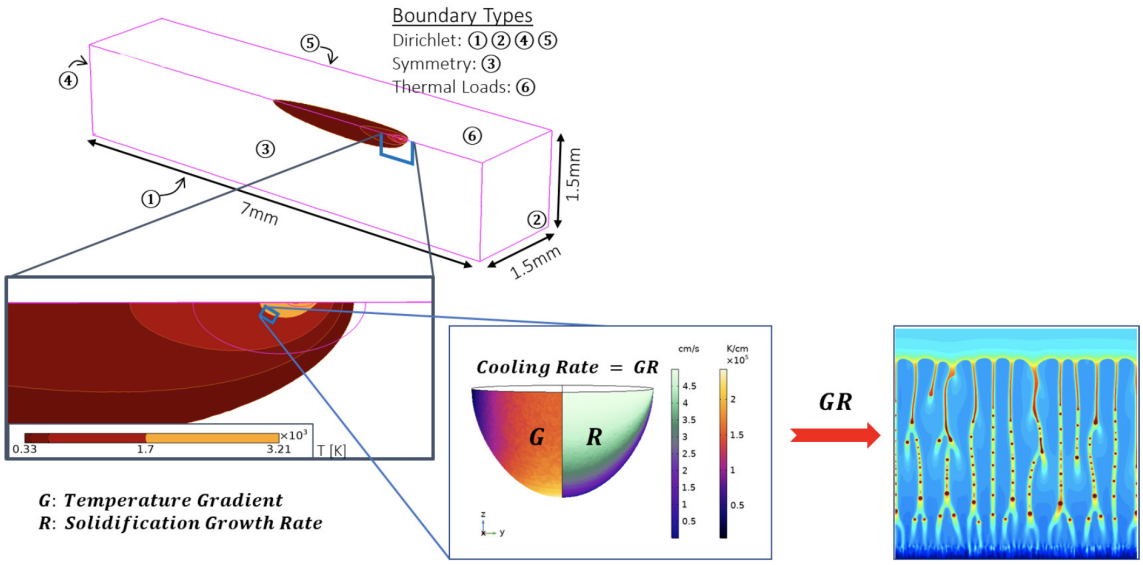


Fig. 4. *A schematic representation of the multiscale approach to modelling a the LPBF process. This figure is taken from Karayagiz et Al [11] paper on the modelling of Ni-Nb as a binary analogue for Inconel718 during additive manufacture. This figure demonstrates how a temperature field model is used to determine G and R parameters (growth rates and temperature gradients) at locations around the weld pool geometry. These thermal conditions are then applied to a phase field simulation at a smaller length scale to predict microstructure morphologies*

the Thermal Diffusivity typically being much higher than the solutal diffusivity.

More recently Karayagiz et al [11] applied this approach when investigating the Ni-Nb system as a simplified proxy of more complex Nickel Super alloys, with the set up for the different domains in the numerical experiment shown in figure 4. As with previous work they apply the frozen temperature field approach to inform the thermal conditions for their microstructure simulations at various points throughout the weld pool, however they are noteworthy and relevant to this thesis for being amongst the first to begin applying a class

of phase field models with a property known as finite interface dissipation (FID). Karaygiz characterises finite interface dissipation as being able to control the rate of transport of components across the phase interface, allowing systems to be accurately modelled both near equilibrium and in strong disequilibrium. The Phase Field model used was itself quite novel based directly on the work of Steinbach, Zhang and Plapp [15].

2.4 Rapid Solidification Modelling Review

Elements are typically more stable in one phase than another, this is no different for solid and liquid phases during solidification. During growth there will be a difference between the rates at which different atomic species are incorporated into the growing phase and an exchange of solute between phases, as can be seen quite directly in certain molecular dynamics simulations [42]. The result of this is a partitioning of the solute either side of the interface towards an equilibrium state, with the degree of partitioning over some region limited by how long the interface it self is in that region. If the interface spends very little time in a given location, such as by moving very fast, then there is not much time for partitioning to occur and there is a smaller difference between the compositions on either side of the interface. This phenomena is known as solute trapping.

During rapid solidification, it is impossible to ignore the effect solute trapping will ultimately have on the resultant microstructure. As Interfaces begin to move faster, there is less time for solute to partition along either side of the interface, thus the amount of solute rejected ahead of the interface can end up being drastically diminished. Given that the mechanism of dendrite formation is sensitive to the size and shape of the solute pile ahead of the interface - it is important for an accurate model of rapid solidification to account for solute trapping.

During very slow solidification it is often sufficient to assume that solid and liquid sides of the interface are in local equilibrium with each other, however if this same assumption were to be made under conditions of extremely fast solidification then there would be a double contradiction wherein if the interface were in a state anywhere near local equilibrium then the chemical driving force for rapid growth would not exist, and simultaneously there would simply not be enough time for the processes of redistribution at the interface to segregate solute into their preferred phases. Consequently the conditions around a rapidly advancing interface are necessarily far from equilibrium.

Amongst the most influential research quantifying the the effects of interface motion on the degree of solute trapping is in the experimental and theoretical work of Smith and Aziz. In their seminal work [16] they introduced a procedure for measuring the degree of solute trapping in thin samples of various aluminium alloys and presented the highly influential continuous growth model that could fit their observed trapping quite well. In their experiments thin 4000 Angstroms aluminium films were ion implanted with either copper, tin, germanium and indium atoms to a depth distributed about approximately 500 Angstroms, upon pulse laser melting it was assumed that due to short width of the film and the liquid hold time of a few millisecond that the solute profiles would likely have relaxed to fairly uniform state. Because the initial solute profile was uniform, it was possible to infer that any solute profile in the resultant solidified aluminium film would be the result of solute being rejected from the advancing solid phase. Due to the fact that solid and liquid aluminium have different electrical resistances, it was possible to model the films as resistors in parallel and then infer the solid fraction at given time by measuring the resistance across the film. Thus it was possible to get a measurement of the interfaces position and velocity at points

along the short width of the film. The amount of rejected solute combined with the measured interface velocity could then be used to infer what the rate of partitioning must have been.

Kittl Sanders and Aziz would go on to gather Experimental data for several other binary alloy systems and demonstrate the efficacy of the continuous growth model in phenomologically modelling rapid solidification processes [43][44]. Even though the Continuous growth model has enjoyed widespread application by virtue of its conciseness and simplicity it is not without its short comings. For example some critics observe that it is impossible for the model to ever predict the onset of complete solute trapping. Due to the fluxes in the model arising instantaneously it will always predict at least a small degree of partitioning as the interface travels irregardless of the speed.

In attempt to remedy this several groups have turned to extended irreversible thermodynamics (EIT) to produce model that do predict complete solute trapping at a finite velocity, with one such approach being the Local Non-Equilibrium Model (LNM) proposed by Sobolev [17]. In the LNM fluxes between disequilibriated systems don't arise instantly - that there is some relaxation time over which they appear. Thus if the time scale allowed for some process is too short, for example if the interface is to passes too quickly over a small region of space wherein we would expect partitioning to occur, then the effect of the driving force is entirely suppressed. This permits solute trapping to be complete, ie no solute pile up ahead of the interface what so ever, at a finite interface velocity. This phenomena is proposed to occur when the interface moves an order of magnitude faster than the velocity at which atoms rearrange themselves at the interface [45] - a fast but still finite interface velocity.

2.5 Phase Field Modelling Review

Phase field models are a class of models that have been successfully applied in modelling the growth of dendrite structures. They are characterised by modelling the interface between phases as a diffuse region which simplifies the numerical issues found in sharp interface models. The classic problem of a pure material solidifying is encapsulated by the three equations:

$$\partial_t u = D\nabla^2 u \tag{3}$$

$$v_n = D(\partial_n u]^- - \partial_n u]^+) \tag{4}$$

$$u_i = -d_0(\theta)\kappa - \beta(\theta)v_n \tag{5}$$

where u is some normalised temperature field, v_n is the velocity of the interface in the direction of its normal vector, $\partial_n u]^-$ is the normal derivative of u on the solid side of the interface, $\partial_n u]^+$ is the normal derivative of u on the liquid side of the interface, u_i is the temperature of the interface, κ is the curvature ,d_0 is anisotropic capillary length and β the anisotropic interface coefficient. There have been several attempts to directly solve the full time dependent free boundary problem stated above with explicit tracking of the sharp interface such as by using variational algorithms [46] and front tracking on multiple rotated lattices [47] however these methods are not easily extended into 3 dimensions.

Phase field models on the other hand couple the equations of motion of u and an order parameter ϕ which is a single number that takes a constant value in the bulk phases and has

a smoothly varying intermediate value in the diffuse interface. The equations of motion are often justified by demonstrating that they reduce to the classical description of the problem above in the sharp interface condition (the analytical solution when the numerically necessary width of the interface approaches 0)[48]. Due to the fact that it is not necessary to explicitly track the interface phase field models are straight forward to implement computationally and extend into 3 dimensions. The method is not however without its drawbacks. The parameters that inform the interface thickness will influence the interfaces behaviour. The origin of the term order parameter can in the context of solidification be seen to reference whether or not a given phase displays long range order. For example 1 for a solid ordered crystal and 0 for a disordered liquid. Encapsulating all the information about the phases into a single number results in the information about the crystal structure and resulting preferred growth directions being lost [49]. Fortunately this is reasonably straightforward to account for such as by adding a direction dependence on the interfacial energy density as is done in the Kim Kim Suzuki model [12] or by adding an increased driving force for certain growth direction as was done by Kobayashis group [50].

The following is a brief overview of origin of the phase field equations main moving parts. In order to stabalise phase field about two arbitrary values a starting point is the Ginzberg-Landau Free Energy functional used in the continuum theory of phase transitions [51] which is of the form:

$$G = \int_{\Omega} \mathscr{L}(\phi, \nabla\phi) d\Omega = \int_{\Omega} \epsilon^2 |\nabla\phi|^2 + H\phi^2(1-\phi)^2 d\Omega \tag{6}$$

Where ϵ is a parameter with units of interfacial energy density and H is a factor that

determines the height of the energy barrier to coexisting phases. These factors have opposite effects on the stable interface width Kinetics. It has been suggested in some reviews [52] that atomistic simulations can be used to inform these parameters[53]. Ω is simply the domain over which system is being considered, this domain could be 1, 2 or 3 dimensional and defined in whatever coordinate system is most convenient. Suppose that the spatial distribution of ϕ(x) were to evolve such that the above functional were locally minimized. It can be seen that there are two energy penalties imposed on ϕ(x). There is the double well potential $H\phi^2(1-\phi)^2$ which will discourage a value of ϕ that is not equal to 1 or 0, and then there is the $\epsilon^2(\frac{d\phi}{dx})^2$ which adds a significant penalty for too sharp and sudden a change in ϕ. Consequently this energy functional would be generally minimized by regions with a uniform ϕ value of either 1 or 0, with those regions being separated by thin but finite transitions, features that would correspond to single phase regions, and the interfaces between those regions respectively. The above form of the free energy potential is known commonly as the double well potential however it is not the only potential that has been used. The double obstacle potential proposed by Steinbach is an alternative with desirable properties for numerical simulation such as being guaranteed to converge to 0 or 1 within a finite width[54].

In order to find how to change a local region of $\phi(x)$ in order to reduce the contribution to total free energy G a simple relaxation Ansatz guarenteed to evolve the system towards a state that minimizes the functional 6 is often proposed:

$$\frac{\partial \phi}{\partial t}(x) = -M\frac{\delta \mathscr{L}}{\delta \phi}(x) \tag{7}$$

$$\frac{\delta \mathscr{L}}{\delta \phi} = \frac{\partial \mathscr{L}}{\partial \phi} - \nabla \cdot \frac{\partial \mathscr{L}}{\partial \nabla \phi}$$

$$\frac{\partial \phi}{\partial t} = -\epsilon^2 \nabla^2 \phi + H\phi(\phi - 1)(\phi - 1/2) \tag{8}$$

This equation of motion is sufficient to describe the behaviour of an interface in a pure material in absence of any temperature or solute fields. This yields the flattening of curved interfaces and the shrinking of particles as the only way to reduce the energy of the system is to reduce the amount of interfacial area. In order to model more complex pattern formation the relative stability of the phases needs to adjusted by coupling them to other fields such as temperature or solute. This is generally done by adding terms to the free energy functional G then $\frac{\partial \phi}{\partial t}$ is re derived. In the case of of a solutally controlled system the new function of G would look like:

$$G = \int_{\Omega} \epsilon^2 |\nabla \phi|^2 + H\phi^2(1 - \phi)^2 + g(\phi) f_{chem}(\phi, c) d\Omega \tag{9}$$

Where g(ϕ) is necessary in order for the driving force to vanish in the bulk of the material. This form of the free energy functional was used in the KKS model and by Plapp in [12] and [55] to get equivalent equations of motion. In Plapps Model the chemical potential field was coupled to the phase field equation instead of the solute field.

Multiphase field models have also been implemented. There are two main approaches, either to implement separate order parameters for each phase as was done by Steinbach et al.[56] where the double obstacle potential is also utilized in order to keep the energy of a triple point higher than the energy of a regular interface as can be seen in figure 5. The other

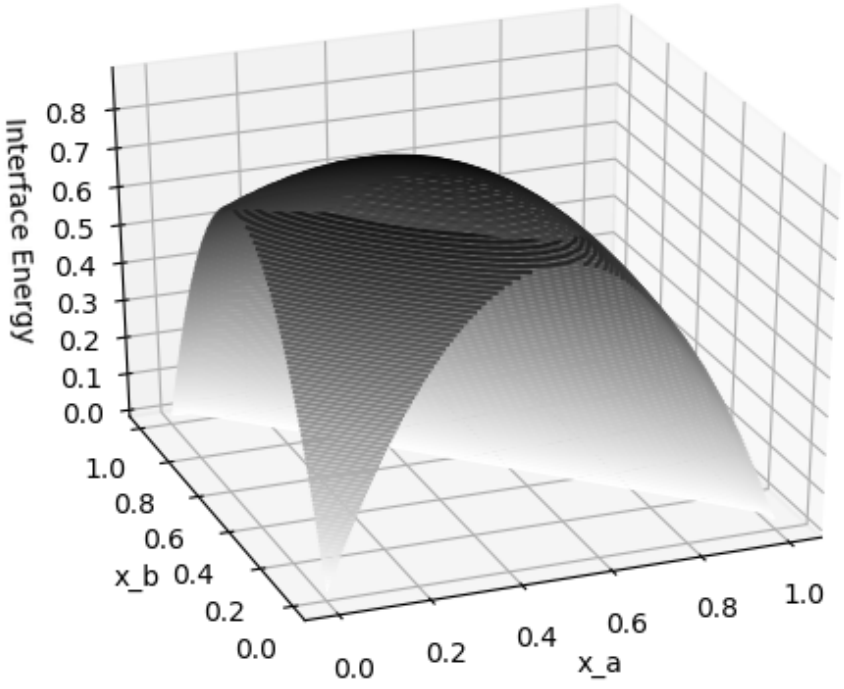


Fig. 5. *plot of the double obstacle potential for a 3 phase system where* $\phi_A + \phi_B + \phi_C = 1$

method involves adding another field which tracks the crystal orientation of each point in space and uses this information to determine how regions of phase should evolve[57].

In order to better understand the development of phase field models it is useful to review a few specific influential phase field models from the past 30 years. The earliest work considered here is the Kobayashi Model [50], which demonstrated phase fields modellings capacity to capture the relevant physics for predicting dendrite formation. Following on the from Kobayashis work the Wheeler Boettinger McFadden (WBM)[58] and Kim Kim Suzuki (KKS) models [12] developed shortly thereafter explored how solute and thus solutal under cooling could instigate dendrite formation. More contempory work by groups such as Steinbach [15] and Galenko [14] have in turn built off the frame work offered by the KKS model and attempted to develop phase field models for the highly non-equilibrium regimes of interest in this project. The kobayashi model in its most basic form consists of the following kinetic equations[50]:

$$\frac{\partial \phi}{\partial t} = M(-\epsilon^2 \nabla^2 \phi + H\phi(\phi - 1)(\phi - 1/2 + m(u, \theta))) \tag{10}$$

$$\frac{\partial u}{\partial t} = \nabla \cdot (D(\phi)\nabla u) \tag{11}$$

in this model the factor m is a function which takes values in the range $-1/2 < m < 1/2$. This effectively results in the double well potential being 'tilted' to make one phase more stable than the other as can be seen if the expression is integrated with respect to ϕ as shown in fig 6. The θ dependence of m allows this driving force to be increased in preferred growth directions in a straight forward way. This is achieved in many models of 2 dimensional

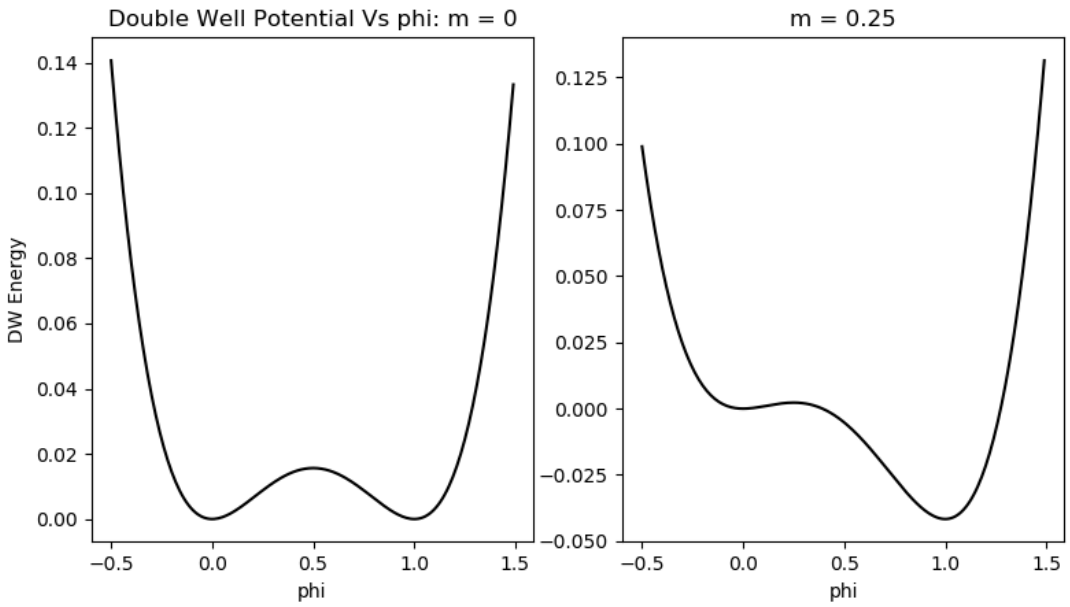


Fig. 6. *How the parameter m affects the relative stability of either phase. In the case on the right the solid phase at 1 will be more stable and if this is the case through the domain then solidification will occur.*

growth with 4 perpendicular preferred growth directions by multiplying m or ϵ by a factor of $1 + \eta cos(4\theta)$.

u is the aforementioned normalised temperature field whose time evolution is given by equation 11. In this model it is assumed that the temperature of different phases coexisting at a point in the diffuse interface region is the same. The phases do not however have the same enthalpy. Were the problem to be formulated using enthalpy rather than temperature the same resulting behaviour would occur when the total enthalpy at a point distributes itself between phases to minimize the Gibbs Free Energy for an imposed Total enthalpy and phase fraction. This principle is utilised in the KKS model as well when considering how solute would distribute itself between solid and liquid phases at a point. This is contrary to WBM early treatments of the problem where it was assumed that solute was distributed evenly across the solid- liquid mixture which required the addition of extra potential terms[12]. This is effectively a restatement of a result found by Mathis Plapp where a whole class of phase field models were shown to be congruent when considering a derivation from a grand canonical potential [55]. Kobayashis results in a 1994 paper of dendrite growth in 3 dimensions gave qualitatively accurate models of temperature controlled solidification an example of which can be seen in fig 7.

The KKS model has the following equations of motions which are derived from the Free energy functional in equation 9:

$$\frac{1}{M}\phi_t = \nabla \cdot \epsilon^2 \nabla\phi + h'(\phi)G(c_S, c_L) - wg'(\phi) \tag{12}$$

$$c_t = \nabla \left[D(\phi)H(\phi, c_S, c_L)\nabla ln\frac{c_L}{1-c_L} \right] \tag{13}$$

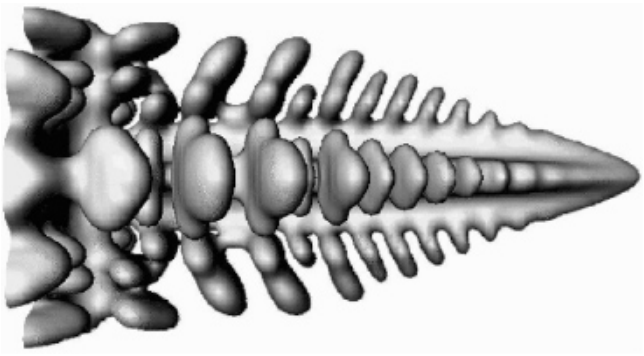


Fig. 7. *Result of Kobayashis Simulation in 3d with anisotropy included*

$$\frac{\partial G_s}{\partial c_s} = \frac{\partial G_l}{\partial c_l} \tag{14}$$

The second equation is given by the continuity equation of a solute flux driven by chemical potential gradient. The diffusion coefficient is the weighted average of the present phases. The final equation is justified by assuming that the free energy of each point in the system relaxes to the minimum free energy attainable at that point for an imposed ϕ and c. This condition is used to fix the final degree of freedom in the model to determine the values of c_s and c_l, the concentration of the solid and liquid phases respectively. This is necessary as it is the concentrations in the respective phases that informs the driving force for phase growth, and drive diffusion across the interfacial region. This condition can be derived by considering the conventional free energy G at point x to be function of ϕ, c, c_s and c_l. Suppose G(ϕ,c , c_s, c_l) is defined as the weighted average of the phase free energies:

$$G = \phi G_s(c_s) + (1-\phi) G_l(c_l) \tag{15}$$

The total derivative of this expression is:

$$dG = \frac{\partial G}{\partial \phi} d\phi + \frac{\partial G}{\partial c} dc + \frac{\partial G}{\partial c_s} dc_s + \frac{\partial G}{\partial c_l} dc_l = \phi \frac{\partial G_s}{\partial c_s} dc_s + (1-\phi) \frac{\partial G_l}{\partial c_l} dc_l \tag{16}$$

as by definition dϕ and dc are 0 because they're imposed as constants. Noting the constraint:

$$c = \phi c_s + (1 - \phi)c_l$$

$$dc = 0 = \phi dc_s + (1 - \phi)dc_l$$

If these are substituted back into equation 16 for dG = 0 which should be a minimum one gets the intended result:

$$\frac{\partial G_s}{\partial c_s} = \frac{\partial G_l}{\partial c_l} \tag{17}$$

The above condition is often referred as the 'local equilibrium' condition. According to the authors of the paper this local equilibrium condition at points in the interface does not guarantee that there will be equilibrium solute partitioning by the interface. It was shown in the original paper that solute partitioning is in agreement with the solute partitioning and entrapment expected from Aziz[59] analysis of rapidly advancing interfaces [12], at least for relatively modest interfacial velocities. A partition coefficient of the following form was expected and derived:

$$k(v) = \frac{k_e + (v/v_d)}{1 + (v/v_d)}$$

where k is the partition coefficient, v is the interface velocity, k_e is the equilibrium partition coefficient (slow interface velocity) and v_d is the diffusive speed. The KKS model has been used by various authors to model binary alloy solidification [13][60]. It has also been extended to incorporate a temperature field as well in some cases. The multiple fields (phase, solute, temperature) and requirements for very small time steps in a simple explicit euler method

have pushed some to optimize the numerical computation by solving the phase field equation on an adaptive mesh[61].

The manner in which Steinbachs model differs from many contemporary phase field models such as the KKS model [12] and WBM model [58] is that permits it additional control over the rate of transport of components across the phase interface - in the other models, in order to evaluate the solute diffusion gradients and driving forces for growth in the interfacial region, it is typical to assume an effective composition for each of the coexisting phases. In models that assume local equilibrium, the set of compositions is in turn assumed to be that which minimizes the Gibbs Free Energy subject to the constraints of the given phase fractions and overall composition of the phase mixture. Crucially in Steinbachs model it is this assumption of local equilibrium that is dropped and instead a set of kinetic equations in introduced to describe how the compositions of the phases at a point redistribute solute at a finite rate. The key adjustment in Steinbachs model can be seen below in the equation below:

$$\phi_\alpha \dot{c_\alpha} = \nabla(\phi_\alpha D_\alpha \nabla c_\alpha) + P\phi_\alpha\phi_\beta(\mu_\beta - \mu_\alpha) + \phi_\alpha\dot{\phi}_\alpha(c_\beta - c_\alpha) \tag{18}$$

This equation describes the evolution of the composition field c_α in the α phase, its most crucial feature being the second term on the RHS on the equation which determines the rate at which solute is effectively redistributed bewteen the phases and in the absence of a pre-existing concentration difference between the phases is the only term which would permit solute to build up in one phase relative to the other. The first term is simply a diffusion equation but limited to single phase, and the third term acts a source term that

must necessarily occur if there is a change in ϕ and $c_\beta \neq c_\alpha$.

Ultimately because concentration gradients do not appear instaneously across the diffuse interface, due to finite rate at which compositions at points along the phase field model attempt to relax towards the local equilibrium set of compositions, the transport of solute across the interface region can be inhibited if the time scale of this relaxation is not much shorter than the time the time it takes for an interface to pass over some point in space. Conversely in the case where the interfaces motion is slower, the time scale of relaxation may be short enough to replicate the behaviour of local equilibrium condition. Whether or not the time scale is short enough depends entirely on the parameter controlling relaxation speed - which in the case of Steinbachs work is the parameter P in equation 18, which they refer to as the interface permeability.

Steinbach's finite interface dissipation model has been applied by several groups and has been extended to the multi-component and multi-phase case [62]. It generally appears to be quite popular with many groups, however it is not the only approach to reproducing highly non-equilibrium solidification behaviours. In Galenkos work a phase field model is proposed based on Extended Irreversible Thermodynamics, wherein a second order time dependence of the the phase and composition fields is introduced by deriving the Governing Equations from an Entropy Production Rate Maximisation principle [14]. Galenkos model behaviour is functionally similar to the Finite Interface Dissipation model, however this behaviour originates from a "reversed" kinetic assumption. In the FID, the appearance of driving force to transport solute to opposite ends of the diffuse interface (i.e. solute partitioning) is delayed due to the finite rate at which composition fields of the phases relax towards a locally equilibrium configuration. Instead in Galenkos work the driving force is present instantly,

however the systems reaction to that driving force ramps up over a finite relaxation time, an effect which appears as a second order time dependence in the equations of motion. This is in contrast to Steinbachs approach and all other discussed phase field models which have equations of motion that have a strictly first order time dependence. Ultimately however, the end result is qualitatively similar. There is an enhanced suppression of partitioning at higher interface velocities. Galenkos approach does have a certain theoretical robustness, given that it does not abandon the local equilibrium assumption as Steinbach does, nonetheless it is the latters work that is paralleled most closely in the development of the models in this thesis.

2.6 Extended Irreversible Thermodynamics

The models discussed so far have all had the feature that so long as two simulations have the exact same value for every parameter (ϕ and c) through out the domain at time t, then any subsequent evolution of the two systems will be identical. The history of the system will not effect its evolution, it is entirely determined by its current state. Under rapid solidification conditions this may not be the case. Models which extend the space of thermodynamic variables to include $\partial\phi/\partial t$ allow the interfacial velocity to directly influence partitioning. Phase field models incorporating this have been developed[14].This approach is based in extended irreversible thermodynamics which is a relatively recent extension of Non-equilibrium thermodynamics.

An interfaces velocity has been shown to directly affect the partitioning of solute however the relation stated above, which comes from the Aziz continuous growth model, requires an infinite growth velocity for partitionless growth. In reality a finite growth speed should be able to account for this which has been shown the models developed by P Galenko and D

Jou [63]. In their work partitionless growth occurred once the interface velocity V became greater than D/δ where δ is the interface width and D is the diffusivity of the solute.

The above works have personally spurred interest in how diffusion occurs in the hyperbolic regime rather than the parametric one (diffusion equations of the form similar to Ficks Second Law or the Heat Equation). In parametric diffusion the driving force for diffusion is assumed to instantaneously cause a finite flux however in hyperbolic diffusion the this flux arises smoothly over some relaxation time. An analogy can be drawn to that of a sky diver. The sky diver experiences a dissapative force proportional to their velocity much like a flux of atoms would as they bump past other atoms. Once this force equals the force of gravity (analogous to some constant chemical potential potential difference) they are in a steady state travelling at the terminal velocity (which is analogous to the induced flux in parabolic diffusion). This is similar to the Maxwell Cataneo equation which describes how a temperature field changes when accounting for the relaxation rates of the heat fluxes[64]:

$$t_{relax}\frac{\partial^2\theta}{\partial t^2} + \frac{\partial\theta}{\partial t} = \frac{k}{\rho c}\frac{\partial^2\theta}{\partial x^2} \tag{19}$$

Clearly this reduces to the heat equation when the relaxation time t_{relax} is very short. θ is the normalised temperature in the above equation.

3 Theory

3.1 Reaction Rate Theory

To make any kind of prediction of the rate of some reaction, be that an explicit chemical reaction, a change of state reaction or even the movement of atoms between lattice sites, it is necessary to propose some kind of kinetic model. Transition State Theory (TST) provides a widely utilised and straight forward frame work to characterise the rates of reactions in terms of a few physically meaningful constants and thermodynamic driving forces [65]. Although the models are not wholly predictive and need to be calibrated to observed experimental results, the models capture phenomologically accurate behaviour of many systems with just a few constant parameters. Typically these parameters characterise some base line attempt frequency and base line activation probability of a given reaction.

At its most general, transition state theory posits that the reactants A and products B represent a pair of meta-stable local equilibria in the overall configuration space of A and B's common constituents. These local equilibria are energy minima, wherein order for a molecule to reach nearby points in the configuration space would require some extra energy. It is assumed that molecules fluctuate randomly about the local minimas of A and B in the configuration space due to random thermal interaction with each other, however if a molecule is sufficiently perturbed in configuration space, it may end up being pushed out of its current local minima and settling in a different one. This would be observed as the transition of that molecule from one state to another. In this picture, the rate at which molecules transition from state A to state B is simply the rate at which molecules in state A accrue enough energy and are perturbed in the appropriate direction in configuration space to overcome

the energetic barriers between A and B. This overall rate can be thought of as the product of two things: the rate of oscillation about of molecules about the local minima A (known as an attempt frequency f), and the fraction of those oscillations that have enough energy to overcome the energy barrier along their trajectory through configuration space between A and B (This is effectively a probability thus we denote it $P^{A\to B}$). Both these factors are highly temperature dependent. Firstly rate of oscillation is, at least in simple solids, almost a direct proxy for temperature. Secondly from the maxwell-boltzmann distribution of energy levels, it can be seen that at higher temperatures the molecules are more evenly spread out across their accessible energy levels, up to the limiting case of an infinite temperature wherein molecules are equally like to be found across every possible energy level.

$$p_i = \frac{1}{Z} e^{-\epsilon_i / kT} \tag{20}$$

As a consequence of this more molecules are likely to be found in a higher energy configuration necessary for overcoming the energy barrier between the states.

It is often sufficient to bundle the complexity of the potential energy surface across configuration space along a single dimension known as the reaction coordinate [65], with the likelihood of traversing the potential energy surface between states A and B being dependent on the difference in energy between the states A and B and some base-line energy barrier Q_0 always present between the states. The rate of atoms moving from A to B, denoted by $k^{A\to B}$, in this simplified model can be tractably expressed as:

$$k^{A\to B} = f X^A P^{A\to B} = f X^A \exp\left(\frac{-Q_0}{kT}\right) \exp\left(\frac{-(E_B - E_A)}{kT}\right) \tag{21}$$

Where f is the attempt frequency of transtions from A to B, Q_0 is a baseline energy barrier, T is the temperature and $E_B - EA$ is the energy difference between states B and A. It must be noted that transitions between states are generally not one directional, typically there is a conjugate reverse process occurring simultaneously which eventually yields a dynamic equilibrium once the forwards and backwards rates cancel out. This is the case for any system where the equilibrium state can be considered as microscopically time reversible which holds by definition for any thermodynamic system[66]. Thus in order to get the rate at which molecules move between states one takes the difference between these forwards and backwards rates:

$$k^{A\leftrightarrow B} = k^{A\rightarrow B} - k^{B\rightarrow A} = f(X^A P^{A\rightarrow B} - X^B P^{B\rightarrow A}) \tag{22}$$

The factor f can be safely assumed to be shared by the states if they are at least in thermal equilibrium, the factors X^A and X^B represent the overall number of molecules in the system that are in state A and B respectively. These prefactors to in the forwards and backwards rates are necessary because it would not make sense for molecules to transition from a state, that no atoms are currently in.

Kinetic Equations of this form were originally proposed by Eyring and Polanyi as a means of characterising the rates of chemical reactions [67], however it was soon after used in the context of diffusion as well by Rosav and Powe [68]. Their work assumes a vacancy exchange mechanism to describe how molecules can diffuse throughout a liquid phase, thus it was not too much of an extension when work by Hilert [69] [70] used a similar treatment for solid lattices where vacancy exchange is considered the predominant mode by which solute diffuses

throughout a material. The fundamental conception of diffusion as a thermally activated process is used in many modern frameworks for diffusion modelling such as the CALPHAD approach and justified with appeals to transition state theory. Although Transition state theory approaches to diffusive processes will be considered in this thesis, more important is the application of TST to processes such solute redistribution across and interface, and the process of phase change. Solute redistribution is not too far a conceptual stretch from diffusion, however the states that atoms are transitioning between are between different phases, rather than within the same phase. Smith and Azizs seminal work on the Continuous Growth Model (CGM) already utilizes a TST model to inform the rate at which solute redistributes across the interface between phases [16], and has been a significant and direct influence on the models developed in this thesis. The growth of phase however is generally not presented as an atomistic process in the same way that diffusion or solute redistribution is, instead it is conceptualised as the reorganising of a large number of atoms. Still it does not seem incongruous to treat the configurational rearrangement of atoms that occurs during a phase change as any different to the configuration rearrangement of atoms that occurs during a chemical reaction, or during diffusion. In Molecular dynamics simulations of the rapid solidification of Silicon, it has been observed that TST yields good fit to experimentally observed solidification rates [71].

With the aforementioned caveats in mind,the subsequent sections of this chapter, transition state theory will be utilised to construct thermodynamically driven fluxes describing the process of:

- a diffusive flux, which causes the phase and composition of adjacent phases to change.

- a redistributive flux, which reorders the atoms across in the interface in a manner that does not cause any phase growth. This is enforced by considering a pair wise swapping mechanism.

- a cooperative growth flux, meant to model the spontaneous ordering or disordering of atoms either to or from either a solid or liquid state.

These fluxes will subsequently be incorporated into diffuse interface models to widen their applicability, with TST offering a consistent foundation from which to derive the relative rates of the processes we wish to incorporate into the model. It is important to be able to control the relative rates of these processes, as it is their relative rate that determines how much solute segregation occurs and thus whether or not conditions for dendritic or planar growth are present.

3.2 Redistribution Potential

In the subsequent sections we make use of a potential introduced by Aziz and Smith [16] called the redistribution potential. The redistribution potential denoted in this thesis as η is useful in a kinetic model of fluxes when the configurational component of the driving force for a reaction is already accounted by some feature of the kinetic model. For example, consider some general flux of element i acting between the phases α and β:

$$k_i \propto X_i^{\alpha} \exp\left(\frac{-\Delta G}{RT}\right) - X_i^{\beta} \tag{23}$$

This model of k_i assumes a principal of mass action, meaning the rate at which i moves from one phase to the other is proportional to the concentration X_i^{α} and X_i^{β} in each phase,

with their relative rates being modified by an additional barrier ΔG, seen by the α to β reaction. For this model, the configurational component of the driving force for a reaction is accounted for by the compositional factors X_i^α and X_i^β in the forwards and backwards rates. When this system is in chemical equilibrium, ie when $\mu_i^\alpha(\vec{X}^\alpha) = \mu_i^\beta(\vec{X}^\beta)$ for every element in the system, then k_i should be 0 for each i.

$$X_i^\alpha \exp\left(\frac{-\Delta G}{RT}\right) = X_i^\beta \tag{24}$$

naively we might propose that the barrier ΔE is equal to the chemical potential difference between the states α and β ($\Delta G = \mu_i^\alpha - \mu_i^\beta$), however clearly the this would not satisfy the above equation 24. If however, we substitute in the difference in redistribution potential, defined as:

$$\begin{aligned} \eta_i &= \mu_i - RT \ln X_i \\ \Delta E &= \eta_i^\alpha - \eta_i^\beta \end{aligned} \tag{25}$$

We instead now find that equation 24 is satisfied under the condition of thermodynamic equilibrium. The exact form of a redistribution potential could in principal vary depending on the kinetic model used, however for models in this thesis the definition above is wholly applicable and sufficient. Ultimately this is the motivation to introduce the redistribution potential η_i as a concise manner of expressing thermodynamically informed barriers in reaction rate style models without evaluating redundant logarithmic terms inside the exponential. In this case it permits k_i to be written as:

$$k_i \propto X_i^\alpha \exp\left(\frac{-(\eta_i^\alpha - \eta_i^\beta)}{RT}\right) - X_i^\beta \tag{26}$$

3.3 Fluxes for Characterising Solidification

There are three fluxes which can be used to describe all the processes that occur between the solid phase and liquid phase during solidification, these being the aforementioned diffusive, redistributive and cooperative growth fluxes. In this section these fluxes are modelled using thermodynamically informed reaction rate theory to give us models of the relative rates of these processes. These fluxes are then used to in the development of the diffuse interface models in section 4. Ultimately due to the nature of these fluxes this yielded two kinds of model, one where the redistribution of solute and growth of phase were separated and could be independently controlled, and another where the of growth phase and redistribution of solute was mediated by a single process.

The Redistributive Flux and the Cooperative Growth Flux are derived in sections 3.3.1 and 3.3.2. They are effectively multi-element generalisations of the fluxes that Aziz and Smith utilized when deriving their seminal work on the continuous growth model[16]. The redistributive flux can be thought of as a direct exchange mechanism between different elements across the interface, whereas the cooperative growth is imagined as an in-place process where the atoms in a region adjacent to the growing phase spontaneously re-order themselves to match the structure of that phase. These fluxes affect the evolution of the system in independent ways, which makes it easier to control the relative rates of phase growth and solute redistribution. The Cooperative growth flux alone will not result in any partitioning behaviour of solute across the interface, whereas the redistribution fluxes will not contribute to the interfaces actual motion.

The diffusive growth flux, discussed in subsection 3.3.3, is flux that assumes a vacancy

exchange mechanism and which can cause both solute redistribution and phase growth. The advantages of a model based purely on the diffusive mechanism is that it has fewer variables resulting in it being more predictive and, by being both conceptually and numerically simpler, is more straight forward to implement. However due to the growth of phase during rapid solidification not being a purely diffusive process (i.e. not mediated primarily by a net flux of vacancies across the interface) a model utilising purely this approach is not appropriate in the context of rapid solidification, though it may find use in modelling situations with slower phase growth such as during oxidation. For these reasons, although the redistributive flux is presented and discussed, it is not utilised in the solidification models developed for this work. Its incorporation though could be the subject of future work to model the growth of phase with both diffusive and cooperative components.

The fluxes derived in the following sections are meant to be as general as possible, thus it was interesting to see if they could be applied to situations other than solidification. Conceptually, if the redistributive flux were to be acting across an imaginary boundary within a single phase instead of across a boundary between distinct phases, then it ought to produce an effect identical to that of number fixed frame diffusion. In section 3.4 we compare how the redistributive flux can be used to model diffusion, and the circumstances under which it behaves similarly to conventional approaches to number-fixed frame diffusion.

3.3.1 Redistributive Flux

In this section we introduce, generalise and adapt the redistributive flux of the Continuous Growth Model for use in a diffuse interface model. When deriving the Continuous Growth Model, Aziz and Smith proposed a model of redistributive flux between the solid liquid phase

acting at the interface[16]. This flux would dissipate free energy by rearranging atoms either side of interface whilst keeping the total number of atoms either side of the interface fixed. For a simple binary system of A and B between a solid S and liquid L phase, the rate at which A atoms increase on the solid side of the interface and decrease on the liquid side of the interface is denoted as k_A^S. This rate is given by :

$$k_A^S = k_{B,A}^{S\longleftrightarrow L} - k_{A,B}^{S\longleftrightarrow L} \tag{27}$$

Where k_A^S is the total rate at which the number of A atoms in S increases (or conversely the rate at which the number of A atoms in L increases), and $k_{B,A}^{S\longleftrightarrow L}$ and $k_{B,A}^{S\longleftrightarrow L}$ are the rates for the forwards and backwards reaction in this binary system. In order to find k_A^S one needs to consider two possible scenarios across the interface between the solid and liquid phases. Either an A atom in the solid is attempting to exchange places with a neighboring B atom in the liquid, or conversely a B atom in the solid is attempting to exchange with an A atom in the liquid. The overall rates at which these exchanges successfully occur are denoted by $k_{A,B}^{S\longleftrightarrow L}$ and $k_{B,A}^{S\longleftrightarrow L}$ respectively and can be expressed as follows:

$$k_{B,A}^{S\longleftrightarrow L} = f_{BA} X_B^S X_A^L P_{B,A}^{S\longleftrightarrow L} \tag{28}$$

In this expression f_{BA} is the attempt frequency of exchanges across per unit area of the interface, the quantity $X_B^S X_A^L$ is the probability that a randomly selected exchange event is between a B atom in the solid and an A atom in the liquid, and finally the factor $P_{B\longleftrightarrow A}^{S\longleftrightarrow L}$ is a thermodynamically informed probability that a given attempt will succeed in overcoming the thermodynamic barrier to reaction and succeed in causing the atoms A and B to swap

places.

In order to generalise the rate equation 28 to the multi-component case, it is helpful to reframe $k_{B,A}^{S\longleftrightarrow L}$ as the rate at which A atoms in general join S from L $k_A^{L\longrightarrow S}$, this quantity is identical to $k_{B,A}^{S\longleftrightarrow L}$ for the A B binary. For multi-component systems however there will be a seperate term for each extra element in the system that A could swap with, instead of just B. For the sake of generality we will relabel our elements to the arbitrarily definable i and j, and a pair of general phases α and β. The rate at which i leaves α and joins β, $k_i^{\alpha\longrightarrow\beta}$, is given by:

$$k_i^{\alpha\longrightarrow\beta} = X_i^{\alpha}\sum_j f_{ij}X_j^{\beta}P_{i,j}^{\alpha\longleftrightarrow\beta} \tag{29}$$

This expression is found by summing all the possible pairwise swaps that would result in an i atom moving from α to β in a manner that is identical to considering the swapping of separate independent binary cases. It is optional to either include or exclude the contribution of an i atom swapping with another i atom from $k_i^{\alpha\longrightarrow\beta}$ as the contribution of this particular swap will cancel out when taking the difference of the forwards and backwards rates. For further details see figure 8. Conversely the rate at which i atoms leave β and join α can be derived following the exact same logic:

$$k_i^{\beta\longrightarrow\alpha} = X_i^{\beta}\sum_j f_{ji}X_j^{\alpha}P_{j,i}^{\alpha\longleftrightarrow\beta} \tag{30}$$

Analagously to Aziz and Smiths work, the factor f_{ji} is again representative of some attempt frequency, and the term $P_{j,i}^{\alpha\longleftrightarrow\beta}$ is the probability that any given exchange attempt between i and j succeeds. The net rate of change of i between α and β is simply the difference

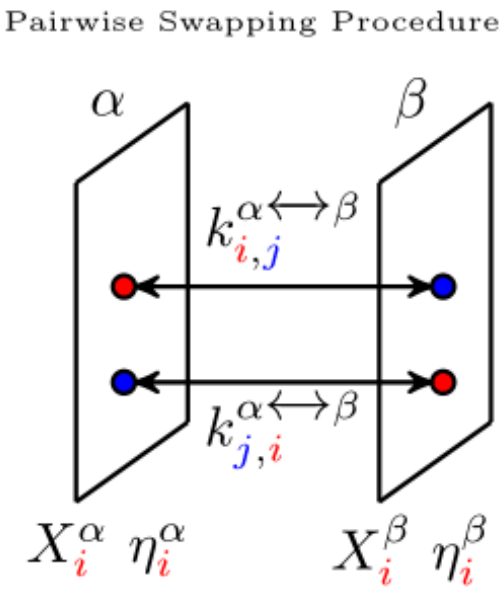


Fig. 8. *This figure shows a schematic of the pairwise swapping procedure for a pair of elements i and j. In order to find the overall rate at which i atoms moving from α to β, $k_i^{\alpha \rightarrow \beta}$, one needs to take the sum of all $k_{i,j}^{\alpha \longleftrightarrow \beta}$ over the elements j in phase β. Thus $k_i^{\alpha \rightarrow \beta} = \sum_j k_{i,j}^{\alpha \longleftrightarrow \beta} = \sum_j X_i^{\alpha} X_j^{\beta} f_{ij} P_{i,j}^{\alpha \longleftrightarrow \beta}$*

of these two rates, for the following order of subtraction this yields the increase in i on β and the decrease in i on α:

$$k_i^{\alpha\longleftrightarrow\beta} = k_i^{\alpha\rightarrow\beta} - k_i^{\beta\rightarrow\alpha} = \left[X_i^{\alpha}\sum_j f_{ij}X_j^{\beta}P_{i,j}^{\alpha\longleftrightarrow\beta}\right] - \left[X_i^{\beta}\sum_j f_{ji}X_j^{\alpha}P_{j,i}^{\alpha\longleftrightarrow\beta}\right] \tag{31}$$

With the factors factors f_{ij} and f_{ji} being equal under the assumption of microscopic reversibility [66]. Due to the number fixed nature of this flux (i.e. the overall numbers of atoms in α and β do not change) it is convenient to only evaluate the flux for N-1 elements in an N element system, with the change in the unevaluated element being inferred from the number fixed property. Another important property of the number fixed frame, in addition to preserving the number of atoms in each phase, is that the choice of unevaluated element should not affect the evaluated fluxes. Both these properties of number fixedness can be readily verified by taking the sum of all $k_i^{\alpha\longleftrightarrow\beta}$ and observing that they sum to 0. Consequently the redistributive flux derived here will not contribute to the net growth of phase.

The final component to be determined before this rate equation can be used are the values of the probabilistic factors $P_{j,i}^{\alpha\longleftrightarrow\beta}$ and $P_{i,j}^{\alpha\longleftrightarrow\beta}$. In reaction rate theory, these probabilities are dependent on the height of the Energy barriers between the states in the model. The choice of barriers is an important one in reaction rate theory and, in the absence of some firm and rigourous theory of the energy potentials in configuration space, it is common to utilize the thermodynamic quantity of chemical potential to construct these barriers in order to ensure that they evolve the system retains some phenomologically correct behaviours [16]. These include and conformance with experimentally observed low driving force behaviours and equilibrium conditions, as well as some desirable high driving force behaviours - such

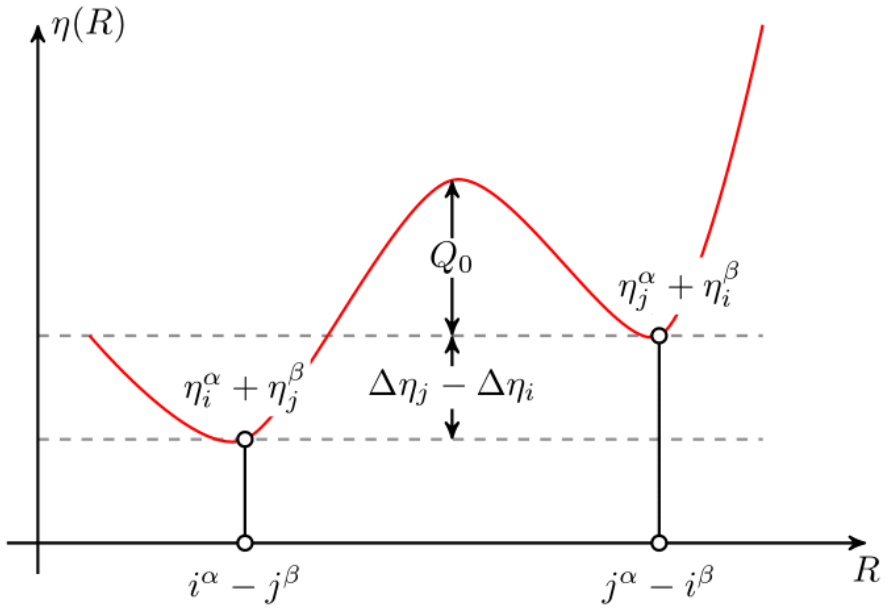


Fig. 9. *This construction is identical to the one proposed by Aziz and Smith in their seminal work [16]. It is only valid if $\eta_i^\alpha + \eta_j^\beta < \eta_j^\alpha + \eta_i^\beta$, otherwise the barrier between the two states might disappear - thus implying they would not exist as distinct local equilibria.*

as the total rate of a reaction not exceeding the physical parameters f_{ij}. After all it would not make physical sense for the successful exchange attempt frequency to exceed the overall attempt frequency.

In the CGM paper the probabilistic factors for the forwards and backwards reactions were derived by considering a barrier construction much like that in figure 9. In this construction, the thermodynamically less stable state (the configuration at a high redistribution potential η) sees a base-line energy barrier of Q_0, whereas the more stable state sees a larger barrier of $Q_0 + |\Delta\eta|$. The larger energy barrier suppresses the rate of reaction in one direction, moreso than the other, resulting in a net rate of change between the states. The resultant probabilistic factors $P_{B,A}^{S\leftrightarrow L}$ and $P_{A,B}^{S\leftrightarrow L}$ are:

$$P_{B,A}^{S\leftrightarrow L} = \exp\left(\frac{-(Q_0 + (\eta_A^S + \eta_B^L) - (\eta_B^S + \eta_A^L))}{RT}\right)$$
$$P_{A,B}^{S\leftrightarrow L} = \exp\left(\frac{-Q_0}{RT}\right) \tag{32}$$

These probabilities are appropriate for the binary alloys where the B,A state is more thermodynamically stable (in terms of redistribution potential) than the A,B state, if the reverse were true however, then one of these probabilities would be greater than one and therefore completely unphysical. Additionally it cannot be guaranteed (for non-ideal solutions) that one configuration will be more stable across the whole composition space, thus the above equation cannot be said to be generally valid across a wide range of compositions and temperatures. It is straightforward however to apply a few numerical tricks to create an expression that represents the intended construction of both states seeing a positive barrier. To this end it is helpful to split the probability into two parts, one for each element:

$$P_{i,j}^{\alpha\leftrightarrow\beta} = P_i^{\alpha\rightarrow\beta} P_j^{\beta\rightarrow\alpha} \tag{33}$$

with each part defined as follows:

$$\begin{aligned} P_i^{\alpha\rightarrow\beta} &= \exp\left(\frac{-Q_i + ((\eta_i^\alpha - \eta_i^\beta) - |(\eta_i^\alpha - \eta_i^\beta)|)}{2RT}\right) \\ &= \exp\left(\frac{-Q_i + (\Delta\eta_i - |\Delta\eta_i|)}{2RT}\right) \end{aligned} \tag{34}$$

$$\begin{aligned} P_i^{\beta\rightarrow\alpha} &= \exp\left(\frac{-Q_i - ((\eta_i^\alpha - \eta_i^\beta) + |(\eta_i^\alpha - \eta_i^\beta)|)}{2RT}\right) \\ &= \exp\left(\frac{-Q_i - (\Delta\eta_i + |\Delta\eta_i|)}{2RT}\right) \end{aligned} \tag{35}$$

This construction will result in perfectly valid probabilities for any combinations of η_i^α and η_i^β, and reproduces probabilities in equation 32 - when it would be physically appropriate

to do so. This can be seen as the η terms completely cancel out whenever the element i is in the state that it is less stable in, and the barriers value is increased by $|\Delta|\eta$ if i is in a state that it is more stable in. The expression also reproduces the linear phenomenological law in the low driving force limit and converges to the highest physically possible flux in the limit that $|\Delta\eta| \to \infty$.

Given that the redistributive flux in this work is composed solely of binary pairwise contributions, the probabilities evaluated in this way for each pair of elements in the system are sufficient to complete our model. Thus the resultant equations of the redistribution rate are:

$$\gamma_{ij} = f \exp\left(\frac{-Q_{ij}}{RT}\right) \tag{36}$$

$$\begin{aligned} k_i^{\alpha \leftrightarrow \beta} = X_i^{\alpha} \exp\left(\frac{\Delta\eta_i - |\Delta\eta_i|}{2RT}\right) \cdot \sum_j \gamma_{ij} X_j^{\beta} \exp\left(\frac{-\Delta\eta_j - |\Delta\eta_j|}{2RT}\right) \\ - X_i^{\beta} \exp\left(\frac{-\Delta\eta_i - |\Delta\eta_i|}{2RT}\right) \cdot \sum_j \gamma_{ij} X_j^{\alpha} \exp\left(\frac{\Delta\eta_j - |\eta_j|}{2RT}\right) \end{aligned} \tag{37}$$

As a review of the definitions, this expression yields the signed net movement of atoms from α to β. The factor γ_{ij} is a kinetic factor for each pair of elements in the system - it defines the maximum frequency at which a given pair of elements can exchange places. X_i^{α} and X_i^{β} are the molar fraction of element i in the α and β phases, $\Delta\eta_i$ is the redistribution potential difference between the phases for element i ($\Delta\eta = \eta^{\alpha} - \eta^{\beta}$), and R and T are the molar gas constant and system temperature respectively.

To apply this redistributive flux in a 2D or 3D context it is necessary to consider how the shape of the interface might affect the flux. A strongly curved interface, such as might be

found at the growing tip of a dendrite, can have the effect of shifting the relative position of the free energy curves of a pair of phases. This would in turn affect driving forces for growth and redistribution between those two phases, as the redistribution and chemical potentials are derived from the relative difference between those curves. In order to apply this redistributive flux to 2D or 3D simulations, the effect of this curvature should be accounted for. This can be done quite straight forwardly by simply adding $\Delta\mu^C$ to the redistribution potential difference, $\Delta\eta_i$. Simply making the substitution $\Delta\eta_i \rightarrow \Delta\eta_i + \Delta\mu^C$. In this case the curvature potential difference for a uniformly curved (or 2d) surface is defined as:

$$\Delta\mu^C = \frac{2\sigma}{R} \tag{38}$$

or in the case of a 3 dimension surface:

$$\Delta\mu^C = \frac{2\sigma}{R_1 + R_2} \tag{39}$$

3.3.2 Cooperative Growth Flux

Phase growth occurs when more atoms adsorb onto a growing phase than disassociate from it. At an atomistic scale the growth of a phase α would be observed as the successful adsorption and incorporation of atoms or groups of atoms from the adjacent β phases structure (or lack there of) onto the α phase, with the composition of the newly extending α phase being dependent on the relative rates at which different atomic species associate and disassociate with the growing α phase. This process does not occur independently for atoms either side of the interface for example certain complexes of atoms may more readily adsorb onto a growing phase, or if an atoms immediate neighbors are adsorbed onto the interface, then it will be

more likely to be adsorbed as well.

In this work it is assumed this process can be approximated by combining a pair of mechanisms - the redistributive flux and the cooperative growth flux. The cooperative growth flux imagines that the atoms adjacent to the growing interface are leashed to some imaginary potential lattice site for the growing phase, thus there is no competition between rates of association and disassociation of different elements. This is elaborated in figure 10 in which new layers of the growing α would form at the previously existing β phases composition. The effect of competing association and disassociation is intended to be accounted for by the redistributive flux described in section 3.3.1.

A cooperative growth flux of this form is proposed as it does not result in any solute being pushed ahead of the interface thus does not contribute to the redistribution of solute between the phases. This is useful in our model as it isolates the redistributive flux as being the only process which can initiate a composition change between phases. It should be noted that this mechanism may appear to contradict the claim that cooperative growth does not contribute to redistribution given that the composition of the growing phase will change as a layer of material at a different composition is incorporated, this effect however is restricted purely to the growing phase. For completeness the magnitude of this effect for a 2 phase system with phase fractions ϕ^α and ϕ^β, if the α phase cooperatively grows into the β phase by an amount $\delta\phi^\alpha$, then the new composition in the α phase, $(X^\alpha)'$, will be:

$$(X^\alpha)' = \frac{\phi^\alpha X^\alpha + \delta\phi X^\beta}{\phi^\alpha + \delta\phi} \tag{40}$$

Given a clear definition of how this flux should affect the system, it is then necessary to

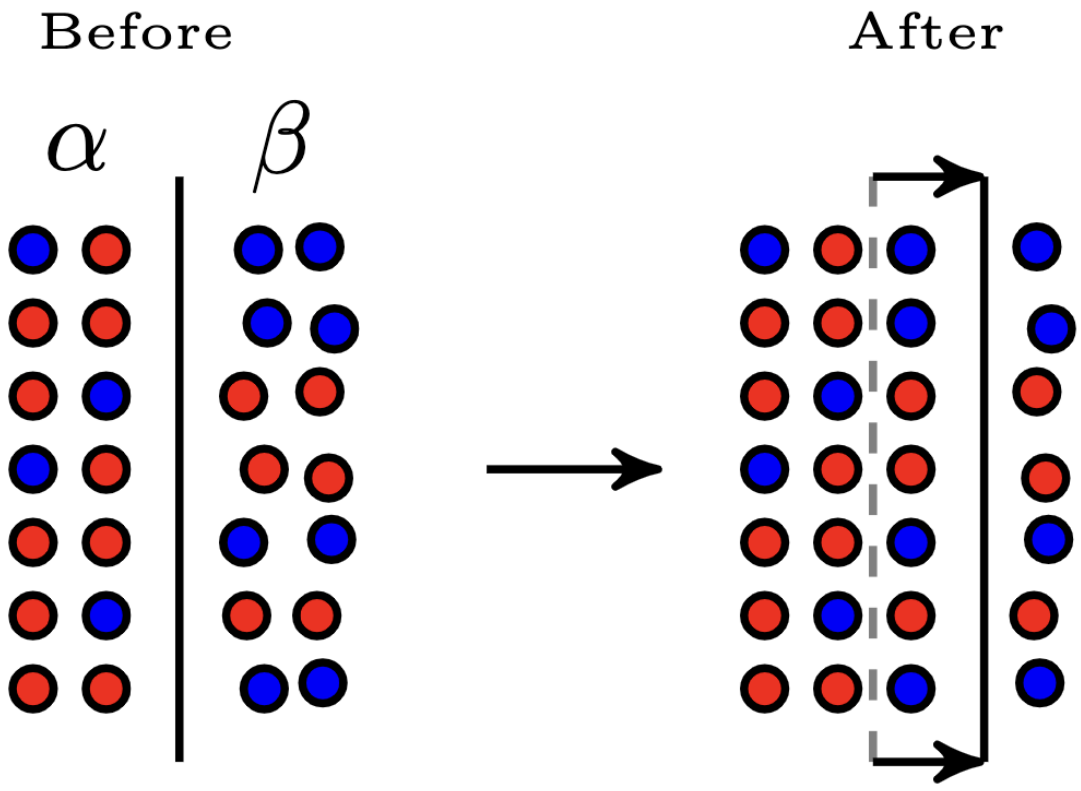


Fig. 10. *Illustration of Cooperative Growth Mechanism, a layer of β phase adsorbs onto the existing α phase. As a result the overall composition of the β phase remains unchanged, however the α phase composition is adjusted slightly due to the newly incorporated β phase.*

find an expression for the rate at which this flux should occur given some driving force. It may be tempting to reapply the concepts used when deriving the redistributive flux, imagining a forwards rate for parts of a layer freezing - and a backwards rate for parts of a layer melting, with the net motion of interface being a difference between the two. There is a problem however introducing a concurrent freezing and melting process, as according to equation 40 this would result in the redistribution of solute between the solid and liquid phases, which is an effect that is intended to be controlled solely by the redistributive flux. Instead it is assumed that either the freezing mode, or the melting mode of cooperative growth acts exclusively over some local area of the interface, at rate determined by a common phenomenological model for the growth rate of crystalline solids. To this end the following equation is utilised [72], where K is the attachment rate of atoms to a solidifying crystal phase:

$$K = \alpha \left[1 - \exp\left(\frac{\Delta G}{RT} \right) \right] \tag{41}$$

Where ΔG is thermodynamic the driving force for this process, R and T are molar gas constant respectively, and α is defined as the maximum attachment rate at a negative infinite driving force. To ensure that our system evolves in the correct direction and with the appropriate magnitude, ΔG is the free energy released by the change in phase. For the cooperative growth flux, given the before and after scenarios in 10, this value for ΔG should be $\sum_i^N X_i^L(\mu_i^S - \mu_i^L)$, which is the free energy released X_i^L i atoms rearrange into a solid state, at the solid - liquid interface. This expression is only physically meaningful so long as $\Delta G < 0$, as it is only phenomologically valid for solidification - ie positive values of K. For this reason, a more complete expression for K which would be physically meaningful both

when there is a driving force for melting or a driving force for freezing would be:

$$K = \begin{cases} \alpha \left[1 - \exp\left(\Delta G^F / RT\right)\right] \text{ if } \Delta G^F < \Delta G^M \\ \\ \alpha \left[\exp\left(\Delta G^M / RT\right) - 1\right] \text{ if } \Delta G^M < \Delta G^F \end{cases} \tag{42}$$

The driving forces for melting ΔG^M, and driving forces for freezing ΔG^F apply to a pair of mutually exclusive and asymmetric processes. The freezing process occurs when liquid layers are adsorbed onto the solid phase (at the liquid phases composition) thus its driving force according to a consideration of the overall free energy before and after the reaction is:

$$\Delta G^F = \sum_i^N X_i^L (\mu_i^L - \mu_i^S) \tag{43}$$

whereas in the case of melting, a layer of solid material is assumed to disassociate and join the liquid phase (at the previously solid phases composition). Consequently the free energy released by this process is:

$$\Delta G^M = \sum_i^N X_i^S (\mu_i^S - \mu_i^L) \tag{44}$$

The effect of curvature on growth can be included as well by adding either a curvature potential term $\Delta\mu^C$ to G^F and (with an opposite sign) to G^M however when incorporated into a phase field style model as done in section 4.1.1, it is unnecessary as the phase field terms them selves naturally yield an apparent driving force to reduce interfacial area. Applying a curvature potential adjustment to the interface driving force would in that case result in the effect of curvature being double counted when simulating the evolution of curved interfaces.

3.3.3 Diffusive Growth Flux

Although the diffusive flux was not ultimately utilised in the rapid solidification models in this work, it is still important to acknowledge it here as a sensible and physical pathway by which phase growth and redistribution can occur. The diffusive growth fluxes are meant to model a process whereby an atom in one phase exchanges places with a vacancy in a neighboring phase. The net result of this exchange would naturally be the growth of one phase at the expense of the other, and a change in composition of two phases if there are multiple different elements involved. The diffusive flux can be represented as a special case of the Redistributive flux 37, however with an extra "element" labelled v being introduced to represent the vacancies, and all the cross term kinetic factors γ_{ij} being 0 for non-vacancy interactions. This effectively results in the redistributive flux only allowing pairwise swaps between an atom and a vacancy across the adjacent phases. With these changes the resultant equation of for the net flux of i atoms between a pair phases α and β is:

$$\begin{aligned} k_i^{\alpha\leftrightarrow\beta} = X_i^{\alpha} \exp\left(\frac{\Delta\eta_i - |\Delta\eta_i|}{2RT}\right) \cdot \gamma_{iv} X_v^{\beta} \exp\left(\frac{-\Delta\eta_v - |\Delta\eta_v|}{2RT}\right) \\ -X_i^{\beta} \exp\left(\frac{-\Delta\eta_i - |\Delta\eta_i|}{2RT}\right) \cdot \gamma_{iv} X_v^{\alpha} \exp\left(\frac{\Delta\eta_v - |\eta_v|}{2RT}\right) \end{aligned} \tag{45}$$

If it is assumed that the vacancy species reaches equilibrium much faster than the material elements in the systems, then it can be assumed that $\Delta\mu_v = 0$. This allows the above equation to be somewhat simplified:

$$k_i^{\alpha\leftrightarrow\beta} = \gamma_{iv} X_v \left[X_i^{\alpha} \exp\left(\frac{\Delta\eta_i - |\Delta\eta_i|}{2RT}\right) - X_i^{\beta} \exp\left(\frac{-\Delta\eta_i - |\Delta\eta_i|}{2RT}\right)\right] \tag{46}$$

$$X_v = \begin{cases} X_v^{\alpha} \textbf{ if } \Delta\eta_v > 0 \\ X_v^{\beta} \textbf{ if } \Delta\eta_v < 0 \end{cases} \tag{47}$$

Where in these expressions, the $\gamma_{iv}X_v$ may simply be absorbed into some general Mobility Constant M_i. It may seem that this "Constant" could change due the condition in equation 47, this would only be the case for systems that very strongly non-ideal with respect to their vacancy thermodynamics. So long as $|G_{v,0}^{\alpha} - G_{v,0}^{\beta}|$ is generally much greater than any RK Polynomial/ enthalpy of mixing terms in the free energy function difference, then M_i is guaranteed to be constant. This rate was derived through a procedure that is conceptually identical to that proposed by Larsson et al in [73], however due to a difference in the choice of barrier construction, they arrive at a slightly different flux equation:

$$J_i = \frac{M_i RT}{V_m \Delta z}\sqrt{X_i^{\alpha}X_i^{\beta}X_v^{\alpha}X_v^{\beta}}\,2\sinh\frac{\Delta\mu_i}{2RT} \tag{48}$$

In their barrier construction, instead of only the more η Stable state seeing a larger energy barrier (as seen in figure 9), both the $i^{\alpha} \leftrightarrow va^{\beta}$ exchange process and the reverse $i^{\beta} \leftrightarrow va^{\alpha}$ exchange process see a modified barrier of a half the magnitude for each reaction (as shown in figure 11). This construction of barriers however can potentially introduce an unphysical scenario if $|(n^{\beta} - n^{\alpha})/2| > Q_0$, as in this situation one of the states would be seeing negative energy barrier, resulting in a likelihood of overcoming the barrier in excess of 1. It is this incongruity that permits equation 48 to produce fluxes in excesses of what the maximum attempt frequency f could physically permit- albeit perhaps only at extremely large driving forces. The barrier construction in 9 avoids this pitfall hence the equation 46 has the advantage of remaining physically coherent at arbitrarily large driving forces.

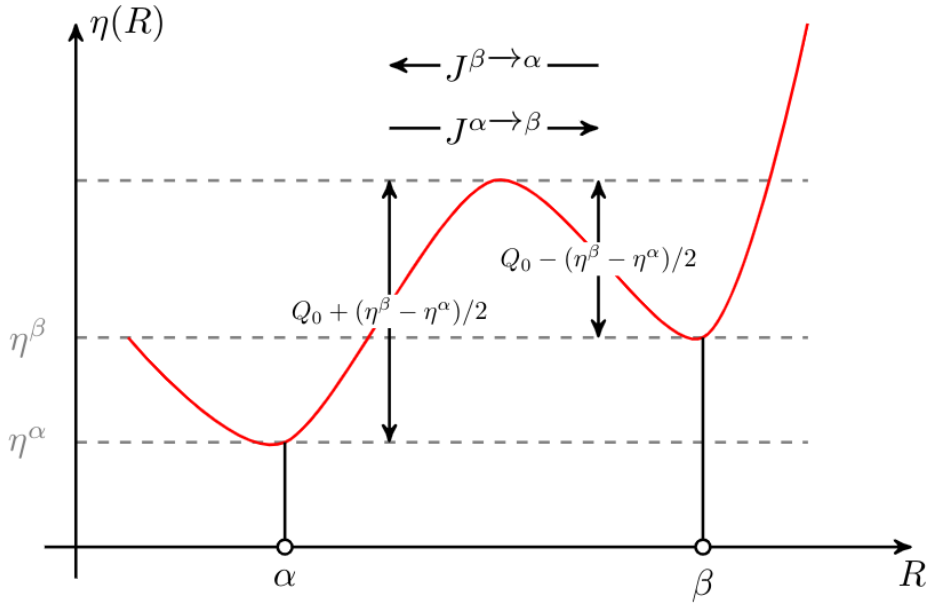


Fig. 11. *A thermodynamic barrier construction based off the assumptions used by Larsson and Hillert [70] [73] in reaction rate treatments of diffusion by a vacancy exchange mechanism. In this construction the barrier height decreases from the perspective of the higher energy state and increases from the perspective of the lower energy state.*

Given that this thesis is attempting to model highly non-equilibrium solidification processes, the property of remaining physically coherent at large driving forces is what motivated the decision to primarily utilize Aziz and Smiths construction over other thermodynamic barrier constructions common in the literature [70].

During solidification the growth of phase is not a purely atomistic process that can be modelled at the scale of individual exchanges of particles across the interface instead, as can be seen in recent molecular dynamics simulations [74], it is an in place re ordering of many particles into a new stable configuration. This is especially the case for rapidly solidifying melts. To address this shortcoming Larsson and Borgenstam extended their model to combine

the diffusive flux with a cooperative growth flux [75], however the approach makes it difficult to disentangle the contribution to the growth rate of the competing processes. There ought to be some theoretical maximum rate at which the interface grows, and an approach which combines two processes that lead to phase growth would need to contrive some limit to prevent that maximum being exceeded. For these reasons in this work it was decided to further develop models using fluxes that affected the system in relatively independent ways (ie. the cooperative growth flux and the redistributive flux).

3.4 Bulk Diffusion as a Redistributive Flux

The most widely adopted approaches for modelling number or volume fixed diffusion fluxes are based on Anderson and Agrens proposed methods for Numerical simulation of diffusion fluxes [76] which forms the basis for the CALPHAD approach to modelling diffusion in alloys [77]. The number fixed fluxes (denoted as NFF) are useful because it is convenient in most numerical models for each discrete point in the model to represent a fixed number or volume of material. Not doing so would necessitate the expansion or distortion of the discrete control volumes used to approximate the system as each control volume could represent a differing volume or number of atoms. An approach that could prove cumbersome in a single dimension and would be very difficult to account for in 2 or 3 dimensions. Formally the NFF is defined as a set of fluxes j_i that satisfies:

$$\sum_i j_i = 0 \tag{49}$$

NFF are typically derived by transforming the Lattice Fixed Fluxes, which are propor-

tional the chemical potential gradient and generally neither volume or number fixed, using a moving frame of reference where the movement is relative to the Lattice Fixed Frame. The moving reference frame introduces a flux proportional to the velocity of the reference frame that can be straight forwardly selected to cancel out the non-zero net flux that is apparent in the Lattice Fixed Frame.

The Redistribution Flux that describes the rearrangement of solute at an interface between phases is also necessarily number fixed. Although these two approaches to a NFF have been derived in separate contexts and for distinct purposes (as illustrated in figure 12), it appears that the redistributive process ought to be applicable to both diffusion within and between phases. This is because even though the redistributive flux was originally proposed as acting across a real interface between thermodynamically distinct phases, there is no reason it could not be imagined to occur across a "psuedo interface" within a single phase, thus behaving like a diffusion flux. Consequently the redistributive flux could offer a unified approach to treat NFF diffusion across a domain with phase boundaries present. However, in order to use widely available kinetic coefficients, such as CALPHAD Mobilities, in the redistributive flux - some regime of equivalence between pairwise swapping procedure and conventional approach would have to be demonstrated for diffusion throughout a single phases.

This regime of equivalence can be found by applying the redistributive flux to operate between two nearby spatial regions at z and $z + \delta z$ within the same phase, and taking low driving force limits to examine how the resultant equation relates to the the conventional approach based on a moving frame of reference. The redistributive flux derived in section 3.3.1 is:

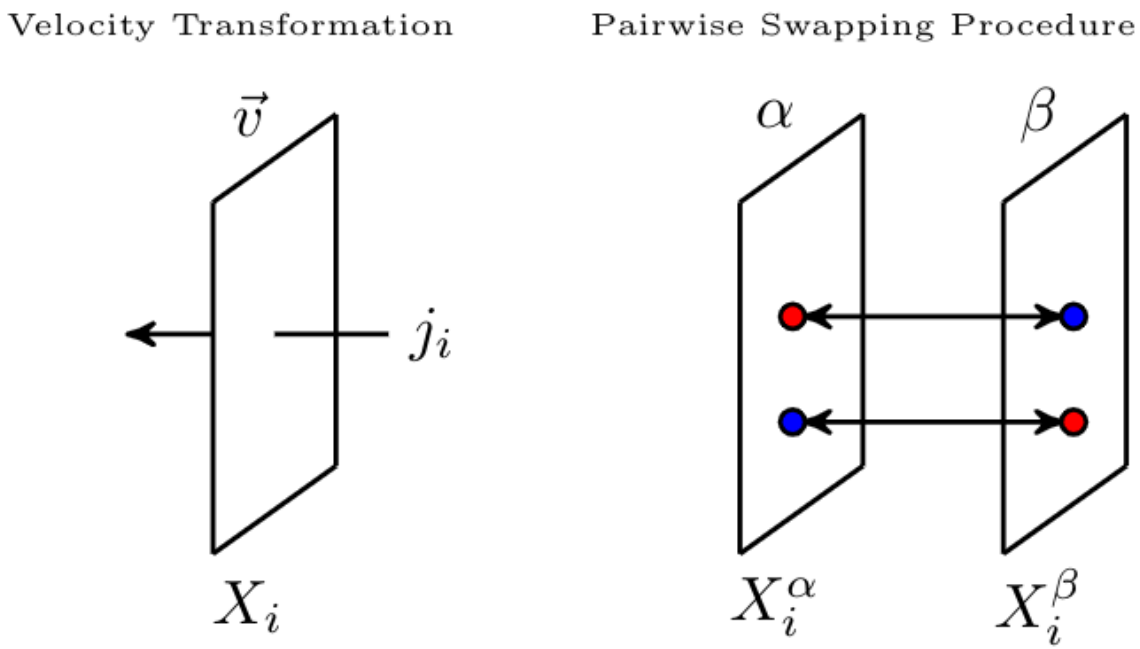


Fig. 12. *Pair of distinct contexts in which a number fixed flux can be derived.*

$$k_i^{\alpha\leftrightarrow\beta} = X_i^\alpha \exp\left(\frac{\Delta\eta_i - |\Delta\eta_i|}{2RT}\right) \cdot \sum_j \gamma_{ij} X_j^\beta \exp\left(\frac{-\Delta\eta_j - |\Delta\eta_j|}{2RT}\right) \\ -X_i^\beta \exp\left(\frac{-\Delta\eta_i - |\Delta\eta_i|}{2RT}\right) \cdot \sum_j \gamma_{ij} X_j^\alpha \exp\left(\frac{\Delta\eta_j - |\eta_j|}{2RT}\right) \tag{50}$$

This net rate of i atoms moving between α and β, $k_i^{\alpha\leftrightarrow\beta}$ can be converted to flux through a single phase quite straight forwardly. To apply this through a single phase, we imagine that α is some region of phase at location z, and β is some nearby location $z + \delta z$. As a further simplification for sake of this derivation, it will also be assumed that $\Delta\eta_i$ is always negative. This results in the flux between z and $z + \delta z$ being:

$$j_i/\delta = X_i(z)\exp\left(\frac{-\delta\nabla\eta_i}{RT}\right)\cdot\sum_j \gamma_{ij}X_j(z+\delta z) \\ -X_i(z+\delta z)\cdot\sum_j \gamma_{ij}X_j(z)\exp\left(\frac{-\delta\nabla\eta_j}{RT}\right) \tag{51}$$

And then taking the low driving force limit where $\delta\Delta\eta_i$ is quite small and substituting in Chemical potential μ_i instead of η_i the following expression is found (Full derivation in appendix B):

$$j_i/\delta = X_i\left[-\frac{\delta\nabla\mu_i}{RT}\right]\cdot\sum_j \gamma_{ij}X_j - X_i\cdot\sum_j \gamma_{ij}X_j\left[-\frac{\delta\nabla\mu_j}{RT}\right] \tag{52}$$

For comparison the number fixed flux derived by considering a moving reference is:

$$j_i = J_i - X_i\sum_j J_j \\ = -M_iX_i\frac{\nabla\mu_i}{RT} + X_i\sum_j\left[-M_jX_j\frac{\nabla\mu_j}{RT}\right] \tag{53}$$

From these expressions it can be seen that the two fluxes are certainly not generally equivalent. As much was to be expected given that the description of diffusion given by equation 53 has N independently variable kinetic coefficients (one for each M_i) in an N element system, whereas the flux derived from the swapping procedure in equation 52 has N(N-1)/2 independent kinetic coefficients (one for each symetric pair of γ_{ij} and γ_{ji}). Nonetheless there is at least one scenario under which variables can be selected to make the equations equivalent, that is when $M_i = M_j$ for all elements in the system. It can be readily verified that both equation 53 and 52 are equivalent when the following substitution is made:

$$\gamma_{ij}\delta^2 = M = M_i = M_j \tag{54}$$

It is interesting to note that it is only under these conditions that the conventional NFF behaves as a valid redistribution flux. By valid we mean that if the flux were permitted to operate between two distinct phases held at fixed phase fractions, then the system would eventually relax to a pair of compositions with parallel (though not necessarily common) free energy curve tangents. Such a property of a redistributive flux is generally considered physically desirable as the parallel tangent composition minimizes a systems Gibbs Free Energy when phase fraction and overall composition are fixed. This introduces the possibility to derive a redistributive flux between phases by considering a lattice fixed fluxes boosted to a moving frame of reference fixed on the interface. Such an approach would not be entirely unprecedented as Larsson et al [73] [70] applied fluxes very similar to lattice fixed frame fluxes to describe the growth of phases, however a transformation of those fluxes to a number fixed frame via a velocity boost would not generally yield redistributive fluxes that relax a system to a composition satisfying the parallel tangents condition.

In conclusion it does not to seem to be generally possible to relate kinetic coefficients between the conventional models of number fixed frame diffusion and the suggested model based on a swapping procedure as they are describing fundamentally different behaviours in their common domain of diffusion through a bulk phase. Therefore although the swapping scheme presented here may be a conceptually and thermodynamically consistent scheme for describing the redistribution of components over an interface between phases, it is difficult to apply to the context of diffusion through a bulk phase as it has only been found to be reconcilable with the CALPHAD approach to diffusion [77] under the specific condition of equal mobility across all elements shown in equation 54.

4 Models

4.1 Diffuse Interface Model Utilising Cooperative Growth and Redistributive Flux

In this chapter we incorporate the redistributive flux and cooperative growth flux into a diffuse interface model in order to produce a model that can behave like (and thus be informed by) a continuous growth model (CGM), whilst sidestepping the awkward numerical challenge of a moving boundary problem. The present model is based on work done by N Warnken on a phase field model for non-local equilibrium phase transformations. The model separates contributions from curvature and thermodynamic driving forces. Phase changes are calculated from reaction rate consideration as outlined by Larsson, Strandlund and Hillert [73], in the low driving force regime [78] [79]. Phase field models were chosen as the diffuse interface model of choice onto which to map the sharp interface behaviour as their behaviour and kinetics is well studied, additionally their numerical implementation can be straight forwardly extended to 2 and 3 dimensional cases. The redistributive and cooperative fluxes (from sections 3.3.2 and 3.3.1) are incorporated into the phase field model by considering how the flux would affect a sharp interface model, and then replicating that effect in the diffuse interface model. Ultimately there are several Key features of the model that should be inherited from the redistributive and cooperative growth fluxes:

- Fluxes that contribute to redistribution should not contribute to growth of phase - i.e. they should not increase or decrease the phase fraction ϕ.
- The amount of solute partitioning should monotonically decrease with increasing inter-

face velocity (ideally following the same relationship as the CGM).

- Phase Field models behaviour interface velocity should correlate with some measure of the average driving force for cooperative growth across the interface.

The phase field model used is conceptually similar to the KKS and FID (finite interface dissipation) phase field models in regards to the domain of the simulation. This domain consists of a pair of phases, representing a solid phase S and liquid phase L with the presence of either phase being tied to a phase field variable ϕ, and a separate composition field for each element, in each phase in the system. Regions where ϕ is close to either 1 or 0 are thermodynamically and kinetically treated as unambiguously single phase - whereas a value of ϕ between 0 and 1 is thermodynamically modelled as a mixture of phases, with the rate of interaction between phases (i.e. growth and redistribution of solute between phases) being scaled by a factor $\phi(1-\phi)$. Overall this results in one field ϕ for the phase field and two composition fields for each element in the system. A novel feature of this work however is that instead of representing the system in terms of phase fractions ϕ^S, ϕ^L, and phase compositions X^S and X^L, the domain is instead expressed in terms of molar fraction of each element in a given phase, which is denoted by the quantity ψ. The conversion between these two representations of the domain is quite straight forward:

$$\begin{aligned} \psi_i^S &= \phi^S X_i^S \\ \psi_i^L &= \phi^L X_i^L \end{aligned} \tag{55}$$

The decision to represent the domain with these quantities was made to aid in the conciseness of the resultant equations describing the evolution of the domain. This evolution is

described in terms of 2N first order differential equations w.r.t time for an N element system, with it being possible to split the rates of change for ψ_i^S and ψ_i^L in two parts:

$$\begin{aligned} \dot{\psi}_i^S &= \dot{\psi}_i^{S,diff} + \dot{\psi}_i^{S\longleftrightarrow L} \\ \dot{\psi}_i^L &= \dot{\psi}_i^{L,diff} - \dot{\psi}_i^{S\longleftrightarrow L} \end{aligned} \tag{56}$$

with $\dot{\psi}_i^{S,diff}$ and $\dot{\psi}_i^{L,diff}$ representing the independent process of diffusion throughout each phase, and $\dot{\psi}_i^{S\longleftrightarrow L}$ describing the exchange processes (redistribution and growth) occurring between phases in the mixture that's modelled to exist at points in the diffuse interface. Diffusion throughout a phase should not contribute directly to the phase growth or shrinkage. This yields the conditions:

$$\begin{aligned} \sum_i \dot{\psi}_i^{S,diff} &= 0 \\ \sum_i \dot{\psi}_i^{L,diff} &= 0 \end{aligned} \tag{57}$$

Which essentially just dictates that diffusion ought to be number fixed mechanism operating between control volumes / simulation points. As a slight simplification, it is assumed that $\dot{\psi}_i^{S,diff} = 0$ given that the diffusivity of elements in the solid phase is often orders of magnitude smaller than the diffusivity in the liquid phases. Together these equations describe the transition of material between solid and liquid states in the interfacial region, and the transport of material spatially by diffusion of solute across the interfacial and bulk regions (for the liquid phase) - however material transport due to convective effects is not included at it was deemed beyond the scope of this work.

4.1.1 Cooperative Growth Flux in Diffuse Interface Model

When mapping the cooperative growth flux onto the phase field model, there are several properties that must to preserved in both representations of the physical system. Firstly the interfaces motion in response to some driving force should be the same in both cases. This introduces the complication of how to correspond the range of compositions that exist across a phase field models interfacial region, with the pair of distinct compositions either side of sharp interface - and the associated driving force in each model. This complication diminishes however if the composition in each phase is roughly uniform across the the interface, as this would result in a constant thermodynamic driving force across the phase field model - making it easier to predict the resultant phase field models interface velocity and draw correspondence with a sharp interface model. Stated formally, a point on the solid side of the interface at $z^{\phi\rightarrow 1}$ should have approximately the same solid and liquid composition as another point on the liquid side at $z^{\phi\rightarrow 0}$. In terms of ψ this condition is:

$$\begin{aligned} \frac{\psi_i^S(z^{\phi\rightarrow 0})}{\sum_j \psi_j^S(z^{\phi\rightarrow 0})} &\approx \frac{\psi_i^S(z^{\phi\rightarrow 1})}{\sum_j \psi_j^S(z^{\phi\rightarrow 1})} \\ \frac{\psi_i^L(z^{\phi\rightarrow 0})}{\sum_j \psi_j^L(z^{\phi\rightarrow 0})} &\approx \frac{\psi_i^L(z^{\phi\rightarrow 1})}{\sum_j \psi_j^L(z^{\phi\rightarrow 1})} \end{aligned} \tag{58}$$

The addition of an accelerated interfacial diffusion (discussed further in section 4.1.3), meant to smooth out the composition profile through the interfacial region, makes this assumption valid over a wider range of interface velocities. However as the interface transitions from a diffusion controlled growth mode to a temperature controlled growth mode the assumption of a uniform concentration profile will become invalid, consequently the assumed driving force would instead have to be inferred from the interfaces actual resultant motion

under those circumstances.

In addition to reproducing the predicted interface velocity, the phase field implementation of the cooperative growth mechanism should not, by it self, result in a composition change in either the solid, or the liquid phase field (assuming both phases start at the same composition). Any redistribution of solute between the phases is instead intended to be wholly controlled and initiated by the redistributive fluxes proposed in section 3.3.1. The separation of the phase field domain itself into distinct phases and the growth of the more thermodynamically stable phase is guaranteed by monotonically decreasing the following energy functional:

$$F = \int_{\Omega} d\Omega \left[\frac{\varepsilon^2}{2} |\nabla \phi|^2 + H\phi^2(1-\phi)^2 + \frac{\sqrt{H}}{\epsilon\sqrt{2}} \frac{P}{S}(X^S, X^L)\phi^2(1-\frac{2}{3}\phi) \right] \tag{59}$$

The rate of change of ϕ for the phase field model is derived by a fairly typical procedure, taking the variational derivative of the energy functional in equation 59 with respect to ϕ and proposing a relaxation Ansatz that would be guaranteed to reduce the energy functional on each time-step. A driving force is added to this model by the addition of the ϕ^3 terms in the functional which act to tilt the double well potential effectively rendering one of the phases energetically more favourable than the other. The composition dependent factor P may vary from 1 to -1 corresponding to maximally tilted configuration of the double well potential. This tilt however was suppressed by a factor S as otherwise a large enough variation of P across the interface could result in the formation of a spurious stable phases. Values of kinetic coefficients in the phase field model are then selected such that these extremum of tilted double well configurations correspond the maximum allowed freezing and melting

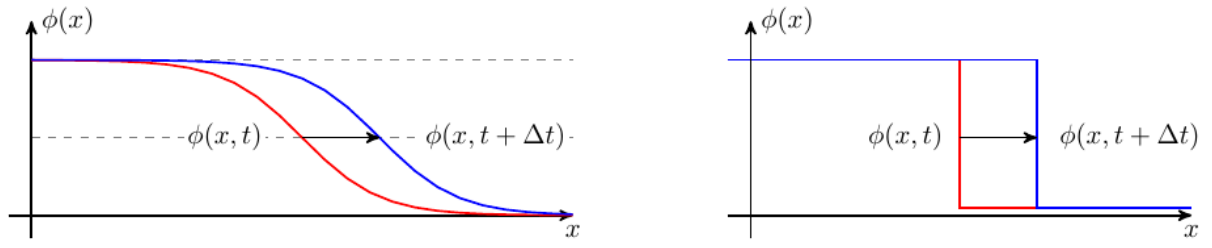


Fig. 13. *One condition for a proper mapping of a phase field model (left) to a sharp interface model (right), would be for the total area difference under the blue and red curves to be equivalent when the driving forces are same. An equivalent area difference would represent an equivalent amount of material Incorporated into the growing phase.*

velocity. The resulting phase field equation characterising the overall rate of change of ϕ is found to be:

$$\begin{aligned}\frac{\partial \phi}{\partial t} &= V_c S\left(-\frac{\delta F_{int}}{\delta \phi}\right) \\ &= V_c S((-\epsilon^2 \nabla^2 \phi + 2H\phi(1-\phi)(1-2\phi)) + 2\frac{\sqrt{H}}{\epsilon\sqrt{2}}\frac{P}{S}\phi(1-\phi))\end{aligned} \tag{60}$$

This particular phase field energy functional and driving force term was chosen as the widely known 1-D travelling wave solutions to phase-field equations of this form make it relatively straight forward to verify that its behaviour can be made analogous to the cooperative growth fluxes proposed in section 3.3.2. This is done by taking direct inspiration from those fluxes, and setting the factor P to be equal to:

$$P = \begin{cases} \left[1 - \exp\left(\Delta G^F / RT\right)\right] \ \textbf{if} \ \Delta G^F < \Delta G^M \\ \\ \left[\exp\left(\Delta G^M / RT\right) - 1\right] \ \textbf{if} \ \Delta G^M < \Delta G^F \end{cases} \tag{61}$$

Where ΔG^F and ΔG^M are the driving forces for freezing and melting respectively as defined in section 3.3.2. For a given driving force across the interface ΔG we should expect the same interface velocity in both a sharp interface and diffuse interface representations of a given interface. As illustrated in figure 13 the rate at which material is incorporated into a given phase in a diffuse interface model should be equal to the rate at which atoms are incorporated into that same phase in the sharp interface model. Thus we demand the following equality should hold:

$$\Delta x = J_{coop} \cdot \delta \cdot \Delta t = \int_{-\infty}^{\infty} \frac{\partial \phi}{\partial t} \cdot \Delta t \cdot dx \tag{62}$$

In this expression Δx is the distance that the 1-D interface should progress over a short time interval Δt. This is equivalent to:

$$\frac{V_c P}{\delta} = \int_{-\infty}^{\infty} \frac{\partial \phi}{\partial t} dx \tag{63}$$

Where V_C is the maximum crystallisation velocity, δ is the inter atomic spacing, and P is the driving force factor from equation 61. It is straight forward to show that by comparison of the 1-D travelling wave solution to equation to the 1-D sharp interface that this condition holds if and only if both interfaces move at the same velocity v for a given driving force ΔG. The interface velocity given by the cooperative growth mechanism acting on a sharp interface is simply:

$$v = V_c P \tag{64}$$

whereas the interface velocity of the phase field model can be found by utilising the

travelling wave solution, as is done in the KKS model [12]).

$$\phi(x,t) = \frac{1}{2}\left(1 - \tanh\left(\frac{\sqrt{H}}{\epsilon\sqrt{2}}(x - v\cdot t)\right)\right) \tag{65}$$

By substituting equation 65 into equation 60, this yields:

$$\begin{aligned} 2v\frac{\sqrt{H}}{\epsilon\sqrt{2}}\phi(1-\phi) &= V_c 2\frac{\sqrt{H}}{\epsilon\sqrt{2}}P\phi(1-\phi) \\ v &= V_c P \end{aligned} \tag{66}$$

Therefore demonstrating that for some driving force, this phase field model will respond identically to a sharp interface model governed by the cooperative growth mechanism.

Typically in phase field models the state of the system is defined in terms of an order parameter ϕ and the composition fields X^S and X^L. In this work however the evolution of the phase and composition fields in this model are found by instead evolving the ψ_i^S and ψ_i^L fields. These fields are equivalent to as ϕX_i^S and $(1-\phi)X_i^L$ respectively and can be thought of as the molar fraction of atoms in some control volume that are element i and in a given phase. It is therefore necessary to convert $\frac{\partial\phi}{\partial t}$ to a set of $\frac{\partial\psi_i}{\partial t}$ for each element.

The properties of the cooperative growth flux can be preserved across points in the interfacial region by considering how much ψ_i^L should become ψ_i^S, or vice versa. In the case of freezing the change in ϕ, $\Delta\phi$, at some point in the interface will be positive and should correspond to $\Delta\phi$ amount of liquid being incorporated into the solid phase. The fraction of this incorporated liquid that is of element i is of course simply X_i^L. Therefore $\Delta\psi_i^S = \Delta\phi X_i^L$. As a result the composition of the solid phase fraction X_i^S may change, however because every element is incorporated proportionally to their concentration in the liquid phase fraction, the overall composition of the liquid phase X_i^L will remain unchanged for all i. This preserves the

desired properties of cooperative growth flux outlined in section 3.3.2. A near identical line of reasoning can be applied when considering the process of melting (ie. when ϕ is negative). In each case the rate of change of ψ_i from liquid to solid is simply therefore:

$$\frac{\partial \psi_i^C}{\partial t} = \begin{cases} \frac{\partial \phi}{\partial t} X_i^L \textbf{ if } \frac{\partial \phi}{\partial t} > 0 \\ \\ \frac{\partial \phi}{\partial t} X_i^S \textbf{ if } \frac{\partial \phi}{\partial t} < 0 \end{cases} \tag{67}$$

4.1.2 Redistributive Flux in Diffuse Interface Model

In order to apply a redistributive flux to the diffuse interface phase field model produced in section 4.1.1 it is important to acknowledge some important conceptual differences between the diffuse and sharp interface models. In a sharp interface model there is clear delineation between the phases and which fields are relevant to solving the systems evolution for a given point in space, however for the diffuse interface model there is a region of space between $\phi = 1$ and $\phi = 0$ where this delineation becomes quite ambiguous. Instead of a sharp delineation between the phases it is instead common to allow the fields associated with each phase to overlap in this region of space. Points in this region are then thermodynamically and kinetically treated as a mixture of the two phases which are capable of exchanging solute between each other.

For a sharp interface model the redistributive fluxes directly act to partition solute by transferring solute spatially between the adjacent phases. In this diffuse interface phase field model however, the overall redistributive process is effectively occurring via two tightly coupled processes as shown in figure 14. The diffusion of solute from one "side" of the diffuse

interface to the other (from where $\phi = 0$ to where $\phi = 1$) denoted as j_i^D, and the exchange of solute between the "mixture" of phases coexisting at each point labelled j_i^R. As solute is re-partitioned between the mixtures of phases at each point in the interface region by j_i^R, a concentration gradient will emerge within each phase which gives rise to j_i^D that describes the diffusion of solute across the interfacial region. Clearly both of these processes are necessary in order to observe any kind of partitioning behaviour and the overall solute redistribution will be limited by each process.

An absolutely rigorous mapping of the diffuse interface solute redistribution to sharp interface solute redistribution would need to consider both of these effects however in this work we simplify our attempt to recover sharp interface behaviour by making j_i^R the rate controlling step for overall redistribution, rather than the diffusion of solute through the interface region j_i^D. This is achieved by utilizing diffusivity acceleration (elaborated in section 4.1.3) in the interfacial region. The accelerated diffusion has the additional property of flattening the composition fields in the interfacial region by allowing diffusion to act through them faster, which makes the assumptions used to predict the overall rate of redistribution in the diffuse interface model (shown in equation 68 - an assumption of uniform composition) more accurate.

In order to make a direct comparison of diffuse interface redistribution to sharp interface redistribution we consider the scenario where the composition fields, $X^S(x)$ and $X^L(x)$, across the diffuse interface are constant. Under these conditions the overall rate at which solute is redistributed across the entire diffuse interface should be equivalent to the rate at which solute is redistributed across the sharp interface $k_i^{\alpha \longleftrightarrow \beta}$, this can be expressed across a one dimension domain as:

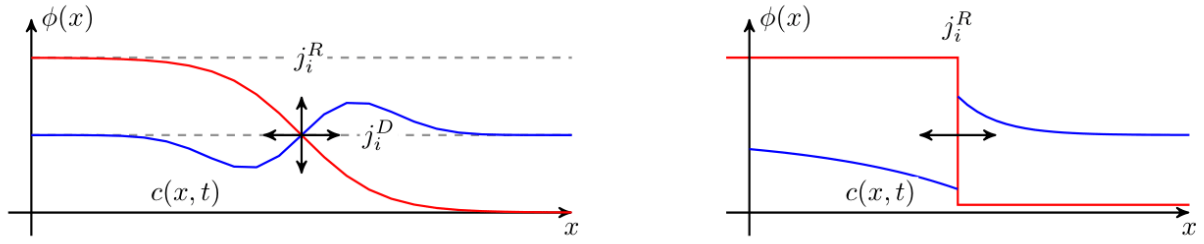


Fig. 14. *A schematic representation of the difference between redistribution across a sharp, discontinuous interface (right), and a diffuse interface (left). Redistribution across a sharp interface can be expressed by the single flux j_i^R, whereas in order for solute to move across the diffuse interface it must first be exchanged from α to β by j_i^R (represented by the vertical arrow at a point in the interface), then be transported across the interfacial region by j_i^D. If either of j_i^R or j_i^D is completely suppressed, then growth will be completely partitionless*

$$k_i^{\alpha\longleftrightarrow\beta}(X^S, X^L) = \int_{-\infty}^{\infty} \frac{\partial \psi_i^{\alpha\longleftrightarrow\beta}}{\partial t} dx \tag{68}$$

By kinetically and thermodynamically treating interfacial regions of the phase field model as mixture of the α and β phases, it is assumed that the redistributive process from section 3.3.1 $k_i^{\alpha\longleftrightarrow\beta}$ is acting between the coexisting phases at that point. The rate however is modified by a factor of $A\phi(1-\phi)$ which is imagined to represent how much "area" there is between the coexisting phases for $k_i^{\alpha\longleftrightarrow\beta}$ to act over. In this expression A is a normalisation factor dependent upon the phase field model parameters. A modification of this sort is also simply practically necessary to localise the redistribution process to only the interfacial region and prevent the redistribution of solute between phases in areas where there is only one phase present. These assumptions yield the expression:

$$\frac{\partial \psi_i^{\alpha \longleftrightarrow \beta}}{\partial t} = A\phi(1-\phi)k_i^{\alpha \longleftrightarrow \beta} \tag{69}$$

which can be directly substituted into equation 68 to get:

$$k_i^{\alpha \longleftrightarrow \beta}(X^S, X^L) = \int_{-\infty}^{\infty} A\phi(1-\phi)k_i^{\alpha \longleftrightarrow \beta}(X^S, X^L)dx \tag{70}$$

Given that the factor $k_i^{\alpha \longleftrightarrow \beta}(X^S, X^L)$ is considered to be uniform across space (due to the assumption of an approximately uniform composition through the interfacial region), it can be extracted from the integral and canceled out, meaning this equation has only a single unknown A that can be straight forwardly solved for by substituting in the steady state 1-D travelling wave solution. This substitution is worked through in appendix section 8.3 yielding:

$$A = 2\frac{\sqrt{H}}{\epsilon\sqrt{2}} \tag{71}$$

which can be substitued back into the original expression for $\frac{\partial \psi_i^{\alpha \longleftrightarrow \beta}}{\partial t}$.

$$\frac{\partial \psi_i^{\alpha \longleftrightarrow \beta}}{\partial t} = 2\frac{\sqrt{H}}{\epsilon\sqrt{2}}\phi(1-\phi)k_i^{\alpha \longleftrightarrow \beta} \tag{72}$$

The ϕ terms can be multiplited by the X_i^S and X_i^L terms in $k_i^{\alpha \longleftrightarrow \beta}$ (according to $\psi_i^S = \phi^S X_i^S$ and $\psi_i^L = \phi^L X_i^L$) to yield the diffuse interface redistribution equation that is used in this model:

$$\frac{\partial \psi_i^{\alpha \longleftrightarrow \beta}}{\partial t} = 2\frac{\sqrt{H}}{\epsilon\sqrt{2}}\left[\psi_i^{\alpha} \cdot \sum_j \gamma_{ij}\psi_j^{\beta} p_{i,j}^{\alpha \longleftrightarrow \beta} - \psi_i^{\beta} \cdot \sum_j \gamma_{ij}\psi_j^{\alpha} p_{j,i}^{\alpha \longleftrightarrow \beta}\right] \tag{73}$$

In this equation the all terms retain their previous meaning, where the $p_{i,j}^{\alpha\longleftrightarrow\beta}$ is a factor between 0 and 1 proportional to the likelihood that an i atom in the α phase would successfully swap places with an adjacent j atom in the β phase, and $p_{j,i}^{\alpha\longleftrightarrow\beta}$ is proportional to the likelihood of the inverse process succeeding. The γ^{ij} here again represents a factor combining the baseline probability of the i and j atoms swapping with an attempt frequency of the exchange process for those elements. If we assume that this redistribution process would be microscopically reversible under equilibrium conditions then, according to Onsager[66], we can then also insist that $\gamma_{ij} = \gamma_{ji}$. The product of γ_{ij} and $p_{i,j}^{\alpha\longleftrightarrow\beta}$ is essentially the same as $P_{i,j}^{\alpha\longleftrightarrow\beta}$ from section 3.3.1.

For ideal solutions it is straightforward to demonstrate that these factors are constant as a consequence of the redistribution potential itself also being a constant, however for many thermodynamic systems such as the Al-Sn system investigated in this thesis this is a poor assumption to make. Generally, for non-ideal solutions, the $p_{j,i}^{\alpha\longleftrightarrow\beta}$ and $p_{i,j}^{\alpha\longleftrightarrow\beta}$ terms will have a composition dependence.

In pursuit of generalizing to 2 or 3 dimensional simulations, the effect of interface curvature would need to be incorporated into the redistributive process as this would modify the equilibrium state of the interface for a given curvature. The macroscopic curvature of the interface can be incorporated in the model by addition of the curvature potential mentioned in section 3.3.1. As is shown in Appendix section 8.2 the effective curvature potential for phase field model 60 derived from the free energy functional given by 59 is:

$$\Delta\mu^C = \frac{\epsilon}{\sqrt{2H}} \frac{RT}{\phi(1-\phi)} \frac{\delta F_{int}}{\delta\phi} \tag{74}$$

Where $\frac{\delta F_{int}}{\delta \phi}$ denotes a partial derivative with respect to only the interfacial terms of the Free energy functional (the first two terms in equation 59). This concept of a curvature potential is borrowed from the work of N Warnkenn [79] where curvature and thermodynamic driving forces are separated. It is possible to incorporate this contribution into the calculation of $p_{i,j}^{\alpha\longleftrightarrow\beta}$ and $p_{j,i}^{\alpha\longleftrightarrow\beta}$, however it is numerically more convenient to take the low curvature limit to extract this term from the exponential part of the equation. Not doing so would require the curvature potential $\Delta\mu^C$ to be evaluated in regions where it approaches becoming undefined as $\phi \to 1$ or 0. Ultimately we arrive at the following equation of motion:

$$\begin{aligned}\frac{\partial \psi_i^{\alpha\longleftrightarrow\beta}}{\partial t} = 2\frac{\sqrt{H}}{\epsilon\sqrt{2}}\left[\psi_i^{\alpha}\cdot\sum_j \gamma_{ij}\psi_j^{\beta}p_{i,j}^{\alpha\longleftrightarrow\beta} - \psi_i^{\beta}\cdot\sum_j \gamma_{ij}\psi_j^{\alpha}p_{j,i}^{\alpha\longleftrightarrow\beta}\right] \\ + 2\frac{\sqrt{H}}{\epsilon\sqrt{2}}\left[X_i^L p_{i,j}^{\alpha\longleftrightarrow\beta} + X_i^S p_{j,i}^{\alpha\longleftrightarrow\beta}\right]\phi(1-\phi)\frac{\Delta\mu^C}{RT}\end{aligned} \tag{75}$$

Which is made numerically tractable everywhere when we substitute equation 74 to get:

$$\begin{aligned}\frac{\partial \psi_i^{\alpha\longleftrightarrow\beta}}{\partial t} = 2\frac{\sqrt{H}}{\epsilon\sqrt{2}}\left[\psi_i^{\alpha}\cdot\sum_j \gamma_{ij}\psi_j^{\beta}p_{i,j}^{\alpha\longleftrightarrow\beta} - \psi_i^{\beta}\cdot\sum_j \gamma_{ij}\psi_j^{\alpha}p_{j,i}^{\alpha\longleftrightarrow\beta}\right] \\ - \left[X_i^L p_{i,j}^{\alpha\longleftrightarrow\beta} + X_i^S p_{j,i}^{\alpha\longleftrightarrow\beta}\right]\frac{\delta F_{int}}{\delta\phi}\end{aligned} \tag{76}$$

4.1.3 Diffusion in Liquid and Interfacial Region with diffusivity acceleration

Due to the findings in section 3.4, it was deemed impractical to try and treat diffusion as a redistributive process. Instead diffusion is modelled in the conventional way for phase field models with separate composition fields for each phase [12] [15]:

$$\frac{\partial \psi_i^{diff}}{\partial t} = -\nabla\cdot\phi^L j_i^D \tag{77}$$

In this expression, the rate of change of ψ_i in the liquid phase is derived from the continuity

equation (appropriately in the absence of any source terms) on the diffusion fluxes j_i^D. The fluxes j_i^D are Fickian and driven purely by the concentration gradient in X_i^L however they are suppressed by the amount of ϕ^L actually present as caused by the factor ϕ^L. It would have been more physically accurate to use the chemical potential gradients as the driving force for diffusion, however for numeric simplicity and performance reasons the fickian approximation was used instead. This suppression both localises the liquid diffusion to the liquid phase, and for our choice of variables in terms of ψ it also appropriately scales down the flux. D_i^L is simply the diffusivity of element i in the liquid. Given the higher diffusivity of solute in the liquid, diffusion in the solid is completely ignored in this model.

In addition to simulating diffusion in the liquid however, an enhanced mode of diffusion is permitted in the interface region in order to permit the redistributive flux to be rate controlling for the partitioning of solute across the interface. This has the effect of levelling off the composition fields in the interfacial region making the assumption of a uniform concentration field more valid. This acceleration is achieved by the addition of an acceleration factor α which is incorporated into like so:

$$\begin{aligned} \frac{\partial \psi_i^{diff}}{\partial t} &= -\nabla \cdot (\alpha \phi^L j_i^D) \\ \alpha &= (1 + \alpha_0 \phi (1 - \phi)) \\ j_i^D &= J_i^D - X_i^L \sum_j^N J_j^D \\ J_i^D &= -D_i \nabla X_i^L \end{aligned} \tag{78}$$

Under this expression, the $\phi(1-\phi)$ is largest in the centre of diffuse interface allowing material to diffuse across this region faster and bring the compositions either side of the

interface closer together than they would have otherwise been. In our experiments the factor of A was typically given a value of 10 as a trade off between achieving the desired composition field flattening, but also not having to reduce the time step of the simulation due to the diffusion fluxes being an order of magnitude larger than the would otherwise have been.

4.2 Modelling the Thermodynamics

Throughout several chapters in this thesis chemical and redistribution potentials are used in order to inform the direction and magnitude of redistribution and growth fluxes. To evaluate the chemical and redistribution potentials at a reasonable speed requires either an efficient means of looking up chemical potential with some third party piece of software, storing and interpolating a domain of relevant chemical potential values, or simply evaluating an explicit analytical expression of the chemical potentials. It was this latter approach that was chosen in this work. Approximate Free Energy curves were found for the relevant phases and elements in a given alloy by fitting over a small region of compositions space relevant to the simulation against the output of the more sophisticated models used by Thermo-Calc [80]. The limited scope of the fit was necessary as the simplified free energy models used were simply not detailed enough to fully reproduce the output of the more sophisticated free energy models over the whole composition space.

The free energy models of phases in this project were based off the highly general CALPHAD approach to thermodynamic modelling [81]. The Free Energy function used for both liquid and solid phase consisted of an Ideal Gibbs Free Energy term in addition to an Excess Free Energy Terms up to order 3 in X_i RK polynomial terms which were deemed a necessary level of accuracy because this allows the Free Energy Function to produce a mis-

cibility gap, and control its location in composition space. Although the most state of the art thermodynamic models may have excess free energy terms up to a much higher power, or may utilize a more physically representative thermodynamic model (such as the compound energy formalism utilizing sub-lattice models for ordered solid phases [82]), for this work a relatively simple thermodynamic model was sufficient to accurately capture the shape of the free energy landscape around the relatively small composition space of interest. Additionally it was much simpler and more efficient to implement and run the simplified thermodynamic models. The Free energy functions took the form:

$$\begin{aligned} G(\vec{X},T) &= \sum_{i}^{N} \left[G_i^0(T) X_i + RT X_i \log\left(X_i\right) \right] \\ +1/2 \sum_i \sum_j & L_{ij}^0(T) X_i X_j + L_{ij}^1(T) X_i X_j (X_i - X_j) \end{aligned} \tag{79}$$

Where $G(\vec{X},T)$ is the Free energy density of the system at a given set of compositions $\vec{X}$ and temperature T, $G_i^0(T)$ is the Gibbs Free Energy of pure element i in the given phase, X_i is the molar fraction of element i, R is the universal gas constant, and L_{ij}^0 and L^1ij are the second and third order interaction terms between pairs of elements in the system. When implementing these models it is important to note at L_{ij}^0 terms are symmetric whilst the L_{ij}^1 terms are anti symmetric, thus $L_{ij}^0 = L_{ji}^0$ whereas $L_{ij}^1 = -L_{ji}^1$ and L_{ii} terms will always self cancel to can be considered to 0 or be ignored. Ultimately the models in this project utilize the chemical potential as a driving force, this can be derived in a relatively straight forward manner from the above model of Free Energy and is found to be:

$$\mu_i = G_i^0(T) + RT\log(X_i) \tag{80}$$

$$- \frac{1}{2}\sum_j^N \sum_k^N L_{jk}^0 X_j X_k - \frac{3}{2}\sum_i^N L_{jk}^1 X_j X_k (X_j - X_k) \tag{81}$$

$$+ \sum_j^N L_{ij}^0 X_i \tag{82}$$

$$+ \sum_j^N (L_{ij}^1 X_i^2) + 2\sum_j^N \sum_k^N L_{jk}^1 X_j X_k \tag{83}$$

This expression was derived from equation 79 by considering the pure element points on the tangent plane to the free energy surface as illustrated from the construction in figure 15.

In order to get chemical potential functions that could be used at a range of temperatures it was necessary to define temperature dependent functions for $G_i^0(T)$, L_{ij}^0 and L_{ij}^1. It should be noted that any potential ternary interaction between elements i,j and k has been neglected in this model. These functions were the following:

$$G_i^0 = a_i + b_i T + c_i T log(T) \tag{84}$$

$$L_{ij}^0 = \alpha_{ij}^0 + \beta_{ij}^0 T \tag{85}$$

$$L_{ij}^1 = \alpha_{ij}^1 + \beta_{ij}^1 T \tag{86}$$

The fitting procedure was ultimately used to determine what the values of a_i, b_i, c_i should be for each element in the system, and what α_{ij}^0, β_{ij}^0, α_{ij}^1 and β_{ij}^1 should be for each unique pair of elements i and j in the phase. These values were found by fitting the above model

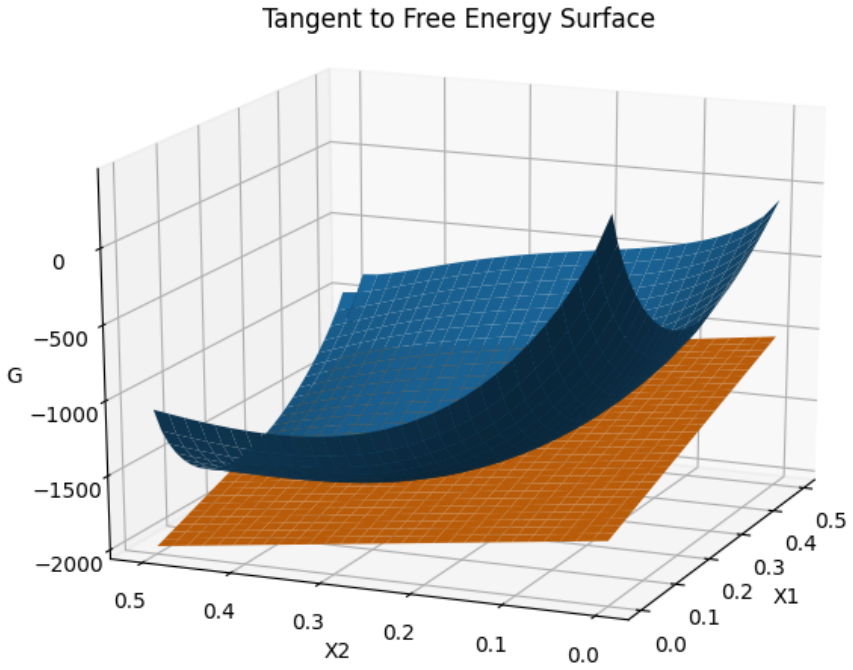


Fig. 15. *Given that chemical potential is defined by the* $G = \sum \mu_i X_i$*, defining* μ_i *as the end points for each element on the tangent plane (where it intersects the pure element points in composition space on the y-axis) will satisfy the definition. This is illustrated in the figure above, as the the tangent plane has the equation:* $G(X_1, X_2) = \mu_3 + (\mu_1 - \mu_3)X_1 + (\mu_2 - \mu_3)X_2$

, which can be rearranged to $G(X_1, X_2) = \mu_1 X_1 + \mu_2 X_2 + \mu_3(1 - X_1 - X_2)$, which is simply $G = \sum \mu_i X_i$ evaluated for 3 elements.

to Free Energies extracted from the open source SSOL2 database via Thermo-Calc across a representative trajectory of compositions between the solidus and liquidus compositions. The solidus and liquidus were chosen as end points for a composition trajectory as it would be unusual for the compositions inside the interface to exceed those bounds during any solutally controlled growth process. A simple python script was written utilizing the Scipy curvefit library to find best fit parameters for the above functions along that trajectory.

4.2.1 Alloy System Parameters

The methodology was applied to Al-Cu-Sn and its Al-Cu and Al-Sn subsystems to find the free energy descriptions of an amorphous Liquid and Al dominant FCC_A1 phase. For reference the values found for the G_0 and RK- polynomial mixing term parameters are outlined in the tables below for each system:

Table 1: **G_0 in the Al-Cu Binary System, values are given to 3 significant figures or the nearest whole number**

Phase	**Element**	a_i	b_i	c_i
FCC_A1	Al	-12387	201	-33.3
FCC_A1	Cu	-9349	158	-28.2
LIQUID	Al	-490	174	-31.4
LIQUID	Cu	-3506	149	-28.3

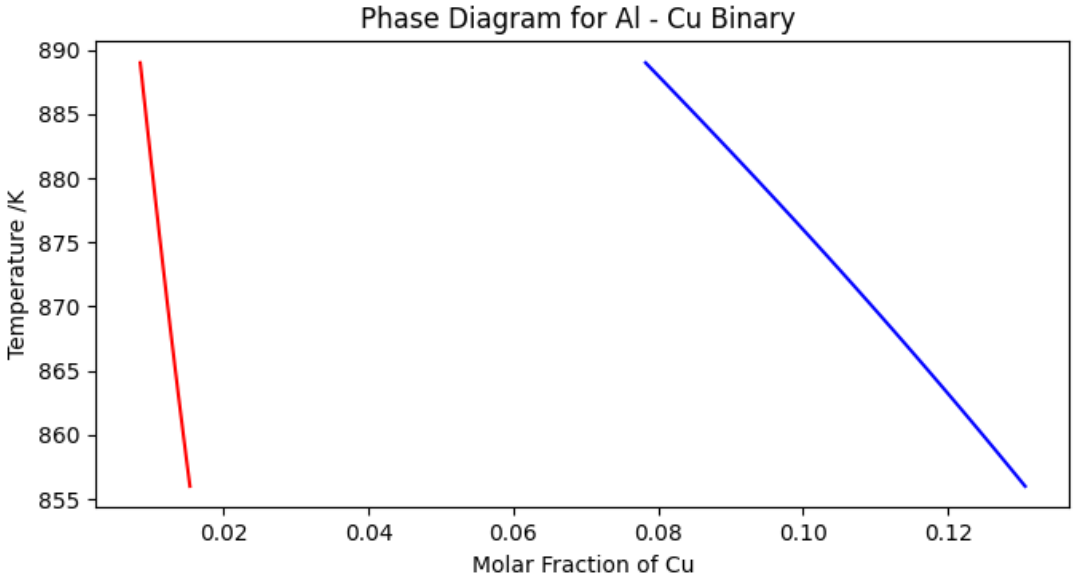


Fig. 16. *Plot of the Al Cu phase diagram over the temperature and composition range relevant to the numerical simulations in this paper*

Table 2: **Mixing Terms in the Al-Cu Binary System**

Phase	**Element Pair**	α_{ij}^0	α_{ij}^1	β_{ij}^0	β_{ij}^1
FCC_A1	Al-Cu	-52158	37505	2.00	-2.00
LIQUID	Al-Cu	-66556	30500	8.00	-7.40

Table 3: **G_0 in the Al-Sn Binary System, values are given to 3 significant figures or the nearest whole number**

Phase	**Element**	a_i	b_i	c_i
FCC_A1	Al	-12386	196	-32.7
FCC_A1	Sn	-4110	134	-28.5
LIQUID	Al	-175	172	-31.1
LIQUID	Sn	-1286	125	-28.5

Table 4: **Mixing Terms in the Al-Sn Binary System**

Phase	**Element Pair**	α_{ij}^0	α_{ij}^1	β_{ij}^0	β_{ij}^1
FCC_A1	Al-Sn	70280	-20781	-44.1	45.1
LIQUID	Al-Sn	23249	434	-52.3	47.2

Table 5: $\boldsymbol{G_0}$ **in the Al-Cu-Sn Ternary System**

Phase	**Element**	a_i	b_i	c_i
FCC_A1	Al	-12387	196	-32.7
FCC_A1	Cu	-9253	157	-28.1
FCC_A1	Sn	-4111	134	-28.5
LIQUID	Al	-175	172	-31.1
LIQUID	Cu	3624	148	-28.2
LIQUID	Sn	-1286	125	-28.5

Table 6: **Mixing Terms in the Al-Cu-Sn Ternary System**

Phase	**Element Pair**	α_{ij}^0	α_{ij}^1	β_{ij}^0	β_{ij}^1
FCC_A1	Al-Cu	-51368	36678	1.69	-1.69
FCC_A1	Cu-Sn	-240	-266	-0.01	0.008
FCC_A1	Sn-Al	50844	935	-0.797	-0.86
LIQUID	Al-Cu	-66120	29271	7.75	-7.14
LIQUID	Cu-Sn	-62.6	-69.1	0.024	0.045
LIQUID	Sn-Al	12998	-10899	-6.04	0.103

4.3 Non Phase Field Diffuse Interface

In this work the phase field model is used as numerically convenient stage on which the physical processes are playing out on. The redistribution and growth processes themselves are informed by the relative thermodynamics of the neighbouring phases and their interfacial properties, however the phase field terms in model simply react to what the other terms are doing to maintain a smooth monotonic interfacial region, a process which conveniently results in interface motion and growth under the desired circumstances.

An attempt was made to develop an explicitly discrete and physical model of the interfacial region compatible with the fundamentally discrete redistribution and cooperative growth mechanisms presented in sections 3.3.2 and 3.3.1. However this approach was not pursued further due to time constraints. Additionally the novelty of the approach would have made it difficult to validate the response of the diffuse interface to the composition field throughout it. It was simply much easier to utilise the phase field models whose behaviour was well known and could be corroborated across multiple sources.

Atomic planes are prescribed some measure of order ϕ, with $\phi = 1$ representing a completely coherent lattice plane and $\phi = 0$ representing a disordered plane of atoms. Values of ϕ between 0 and 1 represent planes which have ordered and disordered areas across them. For simplicity we will assume that ϕ is the area fraction of a lattice plane that is ordered.

If an ordered region of the lattice plane is stacked onto another ordered region, the ordered planes stabilize each other and the ϕ values of the planes do not change. If a disordered plane region is stacked upon another disordered plane region, then there is no atomic ordering present for atoms to adsorb onto thus once again the ϕ values of the planes do not change.

However, if a disordered plane region is stacked upon an ordered plane region, or vice versa, then it is possible that atoms from the disordered plane may arrange themselves onto the ordered substrate or alternatively atoms may disassociate from the ordered plane region as there is no additional plane of ordered atoms locking them in place. Additionally we consider what happens when disordered region is sandwiched between two ordered regions, and the opposite when an ordered region is sandwiched between two disordered planes. In total this gives us 6 possible scenarios that would appear locally, as shown in figure 17

Take two adjacent atomic planes labelled 1 and 2 of area A. From simple statistical considerations, the area A_2^1 of ordered plane on 1 stacked upon disordered plane on 2 is simply:

$$A_2^1 = A\phi_1 \left(1 - \phi_2\right) \tag{87}$$

conversely the area A_1^2 of disordered plane 1 stacked upon ordered area of plane 2 is:

$$A_1^2 = A\phi_2 \left(1 - \phi_1\right) \tag{88}$$

in this notation, the plane from which the ordered area is being considered is placed in super script whilst the plane from which the disordered area is being considered is placed in subscript. The rate at which atoms in an ordered region of plane 1 disassociate due to disordered regions of plane 2 can be expressed as:

$$\kappa_2^1 = f\rho A\phi_1 \left(1 - \phi_2\right) P_D(\phi_1) \tag{89}$$

Whilst the rate at which atoms in a disordered region of plane 1 adsorb onto ordered regions of plane 2 can be expressed as:

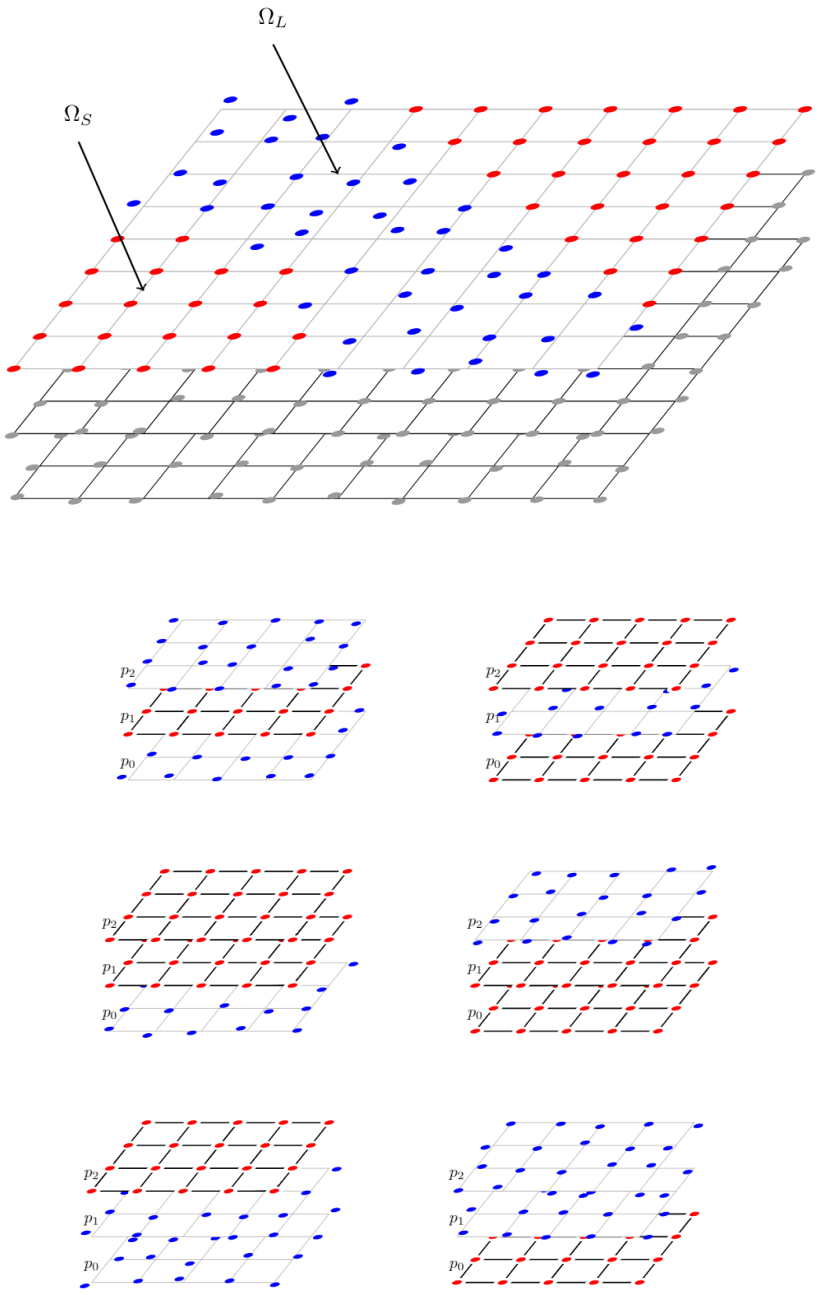


Fig. 17. *Diagram of 3 planes of atoms with disordered (blue) and ordered (red) regions denoted as* Ω_S *and* Ω_L *shown at the top. Locally small regions of these 3 stacked planes would appear as one of the six possible scenarios shown beneath, from which sensible assumptions can be made about what would happen to the plane* p_1 *sandwiched between* p_0 *and* p_2*.*

$$\kappa_1^2 = f\rho A\phi_2 \left(1-\phi_1\right) P_I(\phi_1) \tag{90}$$

where f is the attempt frequency per atom, ρ is the atomic density over area, $P_D(\phi_1)$ is the probability that an attempt at atomic disassociation succeeds and $P_I(\phi_1)$ is the probability that an attempt at incorporation into an ordered structure succeeds. The rate of change of ϕ_1 due to plane 2 is therefore:

$$\left[\frac{\partial\phi_1}{\partial t}\right]_{1,2} = \frac{\kappa_1^2 - \kappa_2^1}{A\rho} = f\left(\phi_2\left(1-\phi_1\right)P_I(\phi_1) - \phi_1\left(1-\phi_2\right)P_D(\phi_1)\right) \tag{91}$$

Any given plane is always sandwiched between two others, therefore in order to evaluate the entire rate of change of ϕ_1 it is necessary to consider the plane sandwiching plane 1 with plane 2. This plane will be labelled as plane 0. We find κ_0^1 and κ_1^0 through the exact same procedure as for κ_2^1 and κ_1^2. This yields:

$$\left[\frac{\partial\phi_1}{\partial t}\right]_{1,0} = \frac{\kappa_1^0 - \kappa_0^1}{A\rho} = f\left(\phi_0\left(1-\phi_1\right)P_I(\phi_1) - \phi_1\left(1-\phi_0\right)P_D(\phi_1)\right) \tag{92}$$

Thus the total rate of change of ϕ_1 can be evaluated:

$$\frac{\partial\phi_1}{\partial t} = \left[\frac{\partial\phi_1}{\partial t}\right]_{1,0} + \left[\frac{\partial\phi_1}{\partial t}\right]_{1,2} = f\left(\left(\phi_0+\phi_2\right)\left(1-\phi_1\right)P_I(\phi_1) - \phi_1\left(2-\phi_0-\phi_2\right)P_D(\phi_1)\right) \tag{93}$$

Rate of change of ϕ for atomic plane n as function of itself and the surrounding $n-1$ and $n+1$ planes.

$$\frac{\partial\phi_n}{\partial t} = f\left(\left(\phi_{n-1}+\phi_{n+1}\right)\left(1-\phi_n\right)\beta_I\left[\left(1-\alpha\right)+\alpha\phi_n\right] - \phi_n\left(2-\phi_{n-1}-\phi_{n+1}\right)\beta_D\left[1-\alpha\phi_n\right]\right) \tag{94}$$

5 Numerical Experiments and Implementation

This chapter covers details of how the phase field model outlined in chapter 4.1 was implemented and the numerical approximations used to do so. Additionally the set up and purpose of the numerical experiments that were performed with the resultant numerical model are also presented, with the results of those experiments discussed in chapter 6.

5.1 Implementation of Diffuse Interface Model with Redistributive and Cooperative Growth Fluxes

In this section we summarise and overview the governing equations used in this model, in addition to providing a few caveats that proved helpful during the numerical implementation. As has been noted already, this model differs from many other approaches to phase field modelling in its choice to model ψ_i^S and ψ_i^L fields as opposed to to the conventional ϕ, X_i^S and X_i^L fields. This choice of variables was used because any change in ψ_i^S results in an equal and opposite change in ψ_i^L, which makes implementing the redistributive flux and cooperative growth fluxes very straight forward. For these mechanisms, this choice of variables is seemingly the most natural way to characterise the system.

The differential equations governing the evolution of the system were approximated using a simple explicit forward euler time step on a uniform square grid. The new ψ_i^S and ψ_i^L for each discrete point in the domain is evaluated after each time step Δt by the expression:

$$\begin{aligned} \psi_i^S(t+\Delta t) &= \psi_i^S(t) + \Delta\psi_i^S(t) \\ \psi_i^L(t+\Delta t) &= \psi_i^L(t) + \Delta\psi_i^L(t) \end{aligned} \tag{95}$$

The overall $\Delta\psi_i^S$ for a given time step being given by:

$$\Delta\psi_i^S = \left[\frac{\partial\psi_i^C}{\partial t} + \frac{\partial\psi_i^{S\longleftrightarrow L}}{\partial t}\right]\Delta t \tag{96}$$

Whereas the overall change in ψ_i^L for the same time step can be partly determined from $\Delta\psi_i^S$ according to:

$$\Delta\psi_i^L = -\Delta\psi_i^S + \Delta\psi_i^{diff} \tag{97}$$

in these expressions $\frac{\partial\psi_i^C}{\partial t}$ is the rate of change of ψ_i^S due to the cooperative growth mechanism and $\frac{\partial\psi_i^{S\longleftrightarrow L}}{\partial t}$ is the rate of change of ψ_i^S due to the redistributive mechanism. The redistribution mechanism actually only needs to be solved for N-1 of the elements in the system, with the change in the final element being inferred from how the rest change. This is due to the number fixed nature of that mechanism, in fact it is often numerically more reliable to do so as this prevents the accumulation of numerical errors. The full expressions needed needed to evaluate $\frac{\partial\psi_i^C}{\partial t}$ are:

$$\frac{\partial\psi_i^C}{\partial t} = \begin{cases} \frac{\partial\phi}{\partial t}X_i^L \textbf{ if } \frac{\partial\phi}{\partial t} > 0 \\ \\ \frac{\partial\phi}{\partial t}X_i^S \textbf{ if } \frac{\partial\phi}{\partial t} < 0 \end{cases} \tag{98}$$

$$\frac{\partial\phi}{\partial t} = V_c(-\epsilon^2\nabla^2\phi + 2H\phi(1-\phi)(1-2\phi) + 2\frac{\sqrt{H}}{\epsilon\sqrt{2}}P\phi(1-\phi)) \tag{99}$$

$$P = \begin{cases} \left[1 - \exp\left(\sum_i^N X_i^L(\mu_i^L - \mu_i^S)/RT\right)\right] \textbf{ if } \sum_i^N X_i^L(\mu_i^L - \mu_i^S) < \sum_i^N X_i^S(\mu_i^S - \mu_i^L) \\ \\ \left[\exp\left(\sum_i^N X_i^S(\mu_i^S - \mu_i^L)/RT\right) - 1\right] \textbf{ if } \sum_i^N X_i^S(\mu_i^S - \mu_i^L) < \sum_i^N X_i^L(\mu_i^L - \mu_i^S) \end{cases} \tag{100}$$

whereas the expressions needed to evaluate $\frac{\partial \psi_i^{S\longleftrightarrow L}}{\partial t}$ are:

$$\begin{aligned}\frac{\partial \psi_i^{S\longleftrightarrow L}}{\partial t} = 2\frac{\sqrt{H}}{\epsilon\sqrt{2}}\left[\psi_i^{\alpha}\cdot\sum_j \gamma_{ij}\psi_j^{\beta}p_{i,j}^{\alpha\longleftrightarrow\beta} - \psi_i^{\beta}\cdot\sum_j \gamma_{ij}\psi_j^{\alpha}p_{j,i}^{\alpha\longleftrightarrow\beta}\right] \\ -\left[X_i^L p_{i,j}^{\alpha\longleftrightarrow\beta} + X_i^S p_{j,i}^{\alpha\longleftrightarrow\beta}\right]\frac{\delta F_{int}}{\delta\phi}\end{aligned} \tag{101}$$

$$p_{i,j}^{\alpha\longleftrightarrow\beta} = \exp\left(\frac{-(\Delta\eta_i + |\Delta\eta_i|)}{2RT}\right)\exp\left(\frac{(\Delta\eta_i - |\Delta\eta_i|)}{2RT}\right) \tag{102}$$

The numerically expensive parts of these expressions to evaluate are those terms with an explicit composition dependence, however it is only necessary to evaluate those terms within the interfacial region. It would not make sense to evaluate the redistributive mechanism, or the chemically driven parts of the cooperative growth mechanism in regions where ϕ approaches either 1 or 0 as these parts of the domain are physically meant to represent a single phase region that is not interacting with the other phase. What constitutes part of the interfacial region is ultimately an arbitrary distinction for a diffuse interface model, however in this work we found that the definition of an interfacial point as one where ϕ has a value between 0.05 and 0.95 was sufficient to not significantly alter the model behaviour whilst also providing a significant reduction in computation time. To be explicit in what this practically entailed, the quantities P and $\frac{\partial \psi_i^{S\longleftrightarrow L}}{\partial t}$ were not calculated and assumed to be 0 whenever $0.05 > \phi > 0.95$.

The only part of equations 98 and 101 that cannot be evaluated solely from the information at a single point in the model is the $\nabla^2\phi$ term, representing the second order spatial derivative of ϕ, which is used to evaluate $\frac{\partial\phi}{\partial t}$. This expression requires consideration of the ϕ value of the local neighborhood around a given point in the model and on discrete evenly spaced grids is commonly approximated as:

$$\nabla^2\phi(z) \approx \frac{\phi(z+\Delta z)+\phi(z-\Delta z)-2\phi(z)}{2\Delta z} \tag{103}$$

Where z denotes the spatial location of some point and Δz is the distance between grid points, in the case of a two dimensional grid with spatial dimensions y and z, the expression is instead:

$$\nabla^2\phi(y,z) \approx \frac{\phi(y,z+\Delta z)+\phi(y,z-\Delta z)+\phi(y+\Delta y,z)+\phi(y-\Delta y,z)-4\phi(y,z)}{4\Delta z} \tag{104}$$

Although much of the change in $\Delta\psi_i^L$ is accounted for by $-\Delta\psi_i^S$, it also has a diffusion component $\Delta\psi_i^{diff}$ that needs to be evaluated. This quantity represents the molar fraction change of element i in the liquid phase that occurs solely due to diffusion through the liquid phase over a time step Δt. In this model diffusion is simulated to occur between contiguous slabs of a single phase, with diffusion through the solid being entirely ignored as the diffusion coefficient in the liquid is orders of magnitude higher than that of the solid. As discussed in section 4.1.3, the rate of change of ψ_i^L due to interfacially accelerated diffusion is:

$$\begin{aligned}
\frac{\partial\psi_i^{diff}}{\partial t} &= -\nabla\cdot(\alpha j_i^D) \\
\alpha &= (1+A\phi(1-\phi)) \\
j_i^D &= J_i^D - X_i^L\sum_j^N J_j^D \\
J_i^D &= -D_i\phi^L\nabla X_i^L
\end{aligned} \tag{105}$$

Where D_i is the diffusivity of element i in the liquid phase. The fluxes J_i^D are lattice fixed frame fluxes based on Fickian diffusion and numerically evaluated at the mid point between two model points. The discrete approximation of J_i^D from z to $z+\Delta z$ is:

$$J_i^D(z+\Delta z/2) = -Dmin(\phi^L(z), \phi^L(z+\Delta z))\frac{X_i^L(z+\Delta z) - X_i^L(z)}{\Delta z} \tag{106}$$

This is an approximation of the lattice fixed frame flux outgoing from the model point at z and incoming to the model point at $z + \Delta z$. The decision to implement the ϕ^L factor as the minimum of $\phi^L(z)$ and $\phi^L(z + \Delta z)$ instead of an interpolated $\phi^L(z + \Delta z/2)$ was taken in order to suppress any spurious solute from regions where $\phi^L \to 0$. However when transforming to the number fixed frame to calculate j_i^D between two model points, the value of X_i^L is interpolated to a mid point value as any spurious solute diffusion would have already been suppressed by taking the minimum of the ϕ^L values of adjacent model points. The α term is likewise evaluated at an interpolated midpoint:

$$\alpha(z+\Delta z/2)j_i^D(z+\Delta z/2) = J_i^D(z+\Delta z/2) - \sum_i^N X_i^L(z+\Delta z/2)J_i^D(z+\Delta z/2) \tag{107}$$

Where the summation is over all N elements in the system. Given that each j_i^D is evaluated at a mid-point between points in the model, they are thought of as operating between adjacent model points. Thus each j_i^D value calculated in between a pair of points is an outgoing flux for one model point at z, and an oppositely signed incoming flux for its neighbor as $z + \Delta z$. By framing the discretely evaluated fluxes $j_i^D(z + \Delta z/2)$ as incoming and outgoing fluxes, the definition of the divergence (the net difference of fluxes across some boundary) can be leveraged to evaluate $-\nabla \cdot (\alpha j_i^D)$. This is done simply by adding the incoming j_i^D, and subtracting the outgoing j_i^D:

$$\frac{\partial \psi_i^{diff}}{\partial t}(z) = -\nabla \cdot (\alpha j_i^D(z))$$
$$\approx \alpha(z - \Delta z/2) j_i^D(z - \Delta z/2) - \alpha(z + \Delta z/2) j_i^D(z + \Delta z/2)$$

yielding the implemented numerical approximation of the set of equations in 105. To evolve the system in an accurate and numerically stable manner between time steps it is necessary for an appropriately sized time step Δt to be selected. Unlike implicit time step numerical schemes, the simple explicit forward time step scheme has no guarantee of numerical stability for arbitrarily an large time step [83], so instead an optimistic adaptive time stepping scheme was implemented to try to optimise for both stability and performance. The adaptive time step was implemented by simply scaling down a default time step of $\Delta t = 6 \times 10^{-11}$ seconds to a $\Delta t'$ such that it satisfies $\Delta t' |\dot{\psi}| < 0.01$ for all fields and points in the model. This constraint effectively limits the model to a $\Delta \psi_i$ of 0.01 or lower which is a convenient way to reduce the time step in the early stages of the simulation as the model relaxes to a diffuse interface and the initial highly non-equilibrium solute partitioning occurs.

Putting all of these steps together the fields in the model were updated each time step by the following procedure:

1. Use the current values of the fields ψ_i^S,ψ_i^L and temperature T of the system to calculate $\Delta \psi_i^S$ for N-1 elements in N element system.

2. Use current ψ_i^L to calculate $\Delta \psi_i^{diff}$.

3. If the largest $\Delta \psi_i^S$ is > 0.01, scale down Δt. Increment time by Δt.

4. Update $\psi_i^S \rightarrow \psi_i^S + \Delta \psi_i^S$.

5. Update $\psi_i^L \rightarrow \psi_i^L - \Delta\psi_i^S + \Delta\psi_i^{diff}$.

6. Update time dependent temperature field T to new values.

7. If time t > maximum time t or iterations > max iterations, finish.

8. Return to step 1.

5.2 Evolution of a Simple System

As a preliminary test to confirm that the redistributive and cooperative growth mechanisms are sufficient to evolve some system to equilibrium, the evolution of a simple two phase system with realistic thermodynamics was modelled. In this simplified model there is no spatial domain or diffusion, it consists of a single point with two phases ϕ^S and ϕ^L which can exchange solute by equation 75 and grow according to equation 60. The interfacial terms from equation 60 are 0 and can be ignored because the domain consists of a single point. This simplified model is effectively behaving like a point in the diffuse interface region, albeit with its phase fraction being allowed to change independent of its neighbors and the overall composition of the mixture being fixed.

The system being considered in this test was the Ternary Al-Cu-Sn at 878K, for which the parameters describing the thermodynamics can be found in tables 5 and 6. In each simulation, a system was initialised with a 50:50 mixture of the solid and liquid with the same composition. This was set up for a series of initial overall compositions and the compositions of each phase were tracked over time. The result of this simulation can be seen in figure 18. As expected and guaranteed by mass balance, the solidus, liquidus and initial composition all fall along a straight line- however interestingly the trajectory of the system towards this

equilibrium state does not stay along this line, but instead veer off into an S shaped trajectory. In principle there isn't anything prevent this from happening, nonetheless it is interesting to observe. The demonstration that the system ultimately relaxes to a valid pair of points along the solidus and liquidus demonstrates that the implementation of redistributive flux and cooperative growth fluxes in this work are at least thermodynamically consistent.

5.3 Partitioning vs Interface Velocity Numerical Experiments

In section 4 it was noted that a phase field model derived with reference to the fluxes in sections 3.3.2 and 3.3.1 ought to reproduce some of the expected behaviour of sharp interface models based on those fluxes. The most famous and widely applied of those sharp interface models being the Continuous Growth Model (CGM) developed by Aziz and Smith [16]. Their work yielded a ubiquitous and useful expression relating the amount of partitioning expected as a function of an interface velocity that has been widely utilized to phenomologically characterise partitioning during rapid solidification. The expression that was derived for a dilute alloy was:

$$k(v) = \frac{k_e(T) + v/v_D}{1 + v/v_D} \tag{108}$$

where k(v) is the velocity dependent solute partitioning, v is the interfaces velocity, v_D is the redistributive velocity of solute and $k_e(T)$ is the temperature dependent equilibrium partition coefficient.

The numerical experiments outlined here were meant to test whether or not the phase field model preserves this relation between interface velocity and partition coefficient - which

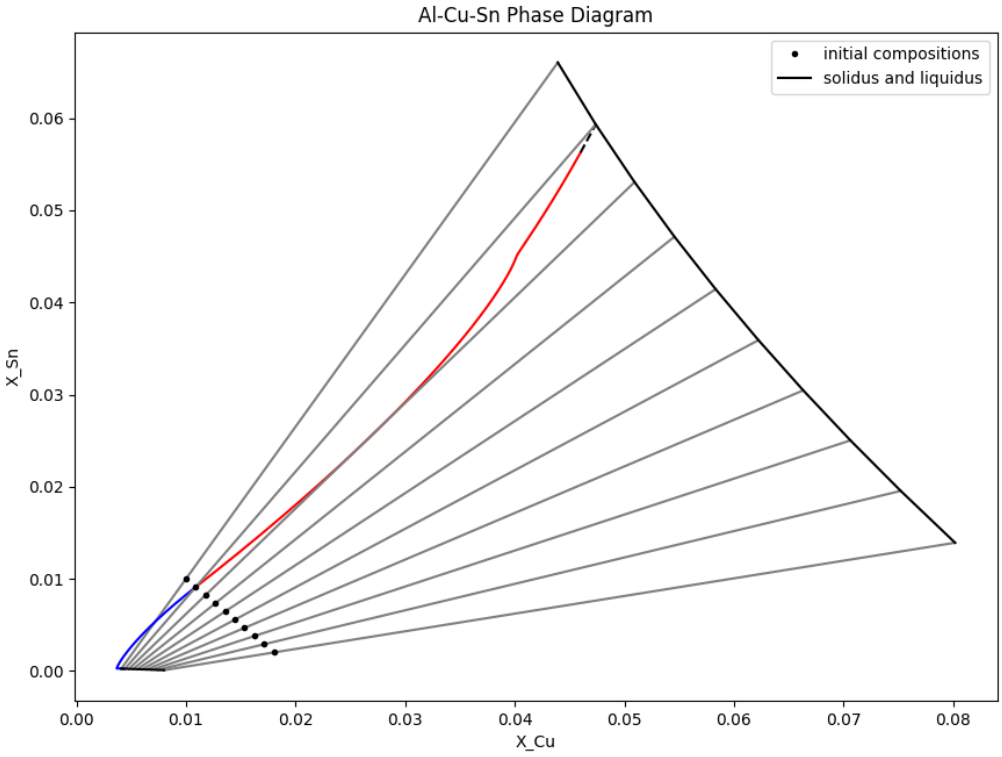


Fig. 18. *This phase diagram for the Al-Cu-Sn system was generated using the redistributive and cooperative growth fluxes. The black dots represent the initial condition of 50 : 50 phase mixture at varying compositions and the grey dashed lines map those initial conditions to a pair of liquidus and solidus compositions. The blue and red lines demonstrate a typical trajectory of the system as it evolves towards the solidus and liquidus compositions under the redistributive and cooperative growth mechanisms. The validity of the phase diagram was verified by checking that* $\Delta\mu = 0$ *for all elements.*

could potentially allow these types of phase field models to straight forwardly incorporate the kinetics derived from rapid solidification experiments that utilize the CGM. The kinetics of the CGM can be straight forwardly incorporated as γ_{ij} in equation 101 can be directly substituted for v_D from a CGM.

Additionally, due to the extension and generalisation of the redistributive fluxes provided in section 3.3.1 it is possible to make predictions of the partitioning behaviour systems with 3 or more elements by combining the partitioning behaviour of its constituent binary subsystems. If the γ_{ij}, γ_{jk} and γ_{ki} can be determined from some set of binary partitioning experiments, then predictions for a system containing those pairs of elements can be made by simply substituting in the γ_{ij} values found for the binary subsystems into overall multi-component system. An obvious limitation of this approach would be that the binary redistribution coefficients may be highly unrepresentative of the elements behaviour in a system with three or more elements. If an i-j binary alloy undergoes solidification at a markedly different temperature range than a i-k alloy system and given the temperature dependence of the γ_{ij} factors, it may be inappropriate to use the same γ factors at temperatures different from which they were derived at. As well as the differences in temperature, different pairs of elements may form into distinct thermodynamic phases during solidification. For example if an i-j system forms into an FCC phase at temperature T, however an i-k system forms a BCC phase at the same temperature T, then the phase that the i-j-k system forms at temperature T will render one of the γ factors for either the i-j or i-k system unrepresentative of the situation at the interface. This is assuming that redistribution between a BCC phase and a liquid phase is kinetically different to redistribution between an FCC phase and a liquid phase.

For a ternary system these concerns can be addressed by limiting the application of predictions to dilute alloys composed mainly of a single element, for which its subsystems form the same structured phases at a similar temperature range. Under these conditions it is safer to assume that processes mediating redistribution are well approximated by the redistribution that occurs for its binary system. In an (i,j,k) system which is predominantly i, it is only necessary that the i-j and i-k sub system form the same phase at a similar temperature range, simply because the number of j-k interactions will be much less than the number of i-j or i-k interactions. The j-k interaction can be neglected, without effecting too greatly the resultant partitioning behaviour of the system, provided the system is sufficiently dilute.

Ultimately the Al-Sn-Cu ternary system was selected as an appropriate candidate for prediction of partitioning behaviour as it satisfies the conditions outlined above. The Al-Sn and Al-Cu subsystems both form an FCC phase at around 900K, conditions under which there exist experiments characterising the rapid solidification of Al-Cu and Al-Sn with a CGM [59]. Thus it is possible to extract reasonable approximations of the $\gamma_{Al,Sn}$ and γ_{Al_Cu} parameters and utilize them in a prediction for the Al-Sn-Cu systems partitioning. This is assuming that the Al-Sn-Cu system is Aluminium rich and that the Sn-Cu interaction can be ignored by virtue of Sn and Cu both being very dilute.

As a further demonstration of the models generality and capability, a test run for a full Inconel718 simulation was run. This system contained 10 elements (Ni, Cr, Co, Mo, Nb, Ti, Al, C and Fe) and previous phase field modelling of it typically uses a representative binary system (such as Ni and Nb) instead of considering the whole alloy system [11]. Unfortunately there was a severe dearth of partitioning data for this system (or its binary sub-systems) thus

it was not possible to make an informed prediction of the partitioning behaviour, as could be done for the Al-Cu-Sn ternary.

5.3.1 Simulation Setup

The set up for these simulations consisted of an isothermal 1 dimensional domain with a seed region of solid on the left hand side of the simulation space and a liquid region extending indefinitely to the right. A snap shot of a typical simulation output after the system has been given some time to evolve can be seen in figure 19. For a given alloy and temperature, different solutal undercoolings are applied by having the domain start at different uniform compositions. The decision to apply a solutal under cooling in this way, rather than by lowering the isothermal temperature or applying a moving thermal gradient, was to make it easier to compare the partitioning behaviour of this model to the predicted solute trapping behaviour of the continuous growth model. By using an isothermal set up for the experiment we can compare our model behaviour to the simplest version equation 108 where k_e is a constant.

The simulations were typically run until the interface reached a steady state, however for certain initial conditions a true steady state could not be reached. By a true steady state we mean a condition where the interfaces solid phase is forming with the same composition C_0 as the far field liquid composition as explained by Tiller et al [84]. This inability to reach a steady state for for partition coefficients close to k_e is hypothesised to occur for two reasons, firstly it is assumed to be a result of the finite spatial domain and the choice of boundary conditions on that domain. For practical reasons, the simulation domain was only 200nm however to accommodate steady states that would take a longer time and distance

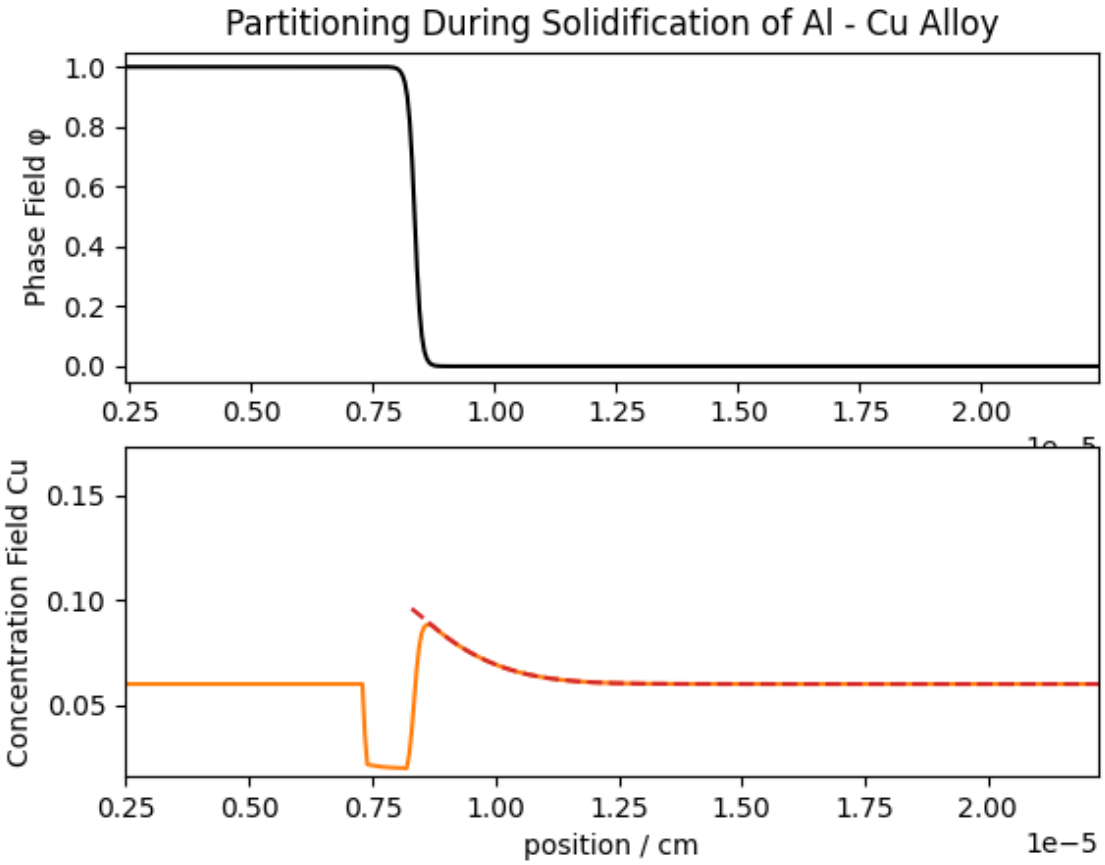


Fig. 19. *Snap shot of Phase Field simulation of an Al-Cu alloy (0.94 molar fraction Al) at 878K after 200000 iterations (3 microseconds simulated time). This particular under cooling results in slow solutally controlled growth, with a partition coefficient $k(v)$ quite close to k_e.*

to achieve the simulation domain was spatially shifted rightwards whenever the total phase fraction of solid across the domain exceeded an arbitrary threshold of 30% solid. This was done by removing the leftmost point from the simulation and adding a point with phase and composition matching the boundary conditions at the right hand side of the domain. This shifting domain and fixed composition of the far boundary effectively acts like a solute sink, which permits the formation of a nonphysical steady state. The 200nm length scale was chosen as it is of the same order of magnitude as the Al-Cu and Al-Sn rapid solidification experiments performed by Aziz and Smith [18] who studied the partitioning for a 300 nm Al film.

Secondly a steady state solution with a partition coefficient approaching k_e doesn't appear thermodynamically possible. Such an interface would need to have solid side composition of c_0 and a liquid side composition approaching c_0/k_e. If we take c_0 values between c_e^s and c_e^l (as compositions below c_e^s will solidify very rapidly and composition whereas compositions above c_e^l will certainly not solidify at all) and plot the driving forces for freezing and melting equations 43 and 44 as shown in figure 20, we see this always results in net driving force for melting so we won't observe even a slow rate of solidification with compositions of c_0 and c_0/k_e either side of the interface. Steady state behaviour with an equilibrium partition coefficient seems to necessitate an extra dimension into which inter dendritic solute rejection can occur, or some other kind of solute sink to allow the solid to grow at a composition different to the far field composition.

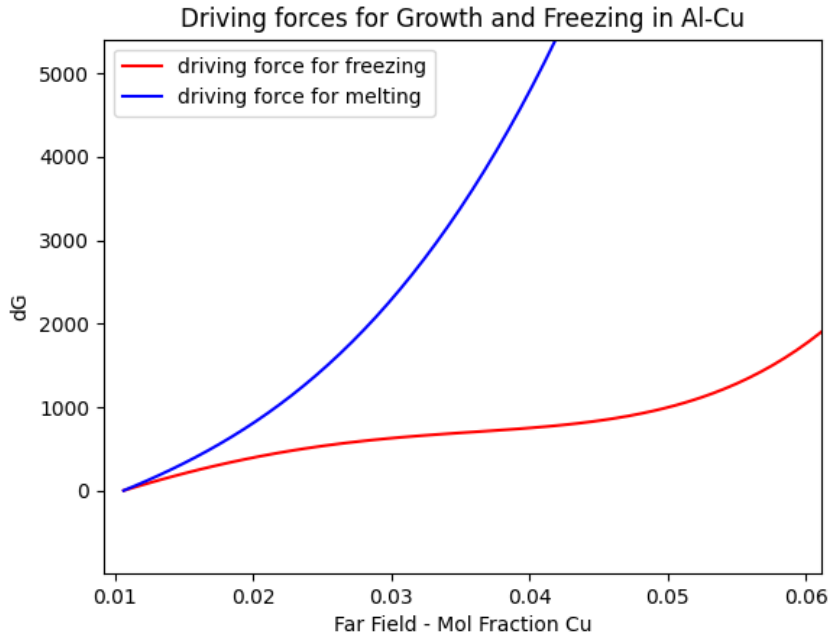


Fig. 20. *Plot of the driving forces for solidification and melting for the Al-Cu system at 878K for a solid side composition c^s a liquid side composition of c^s/k_e. From this plot we see that there is always a greater driving force for melting if we assume the partition coefficient at the interface is k_e. Thus this composition range (between c_e^s and c_e^l) will never be able to produce steady state 1-D solidification with a partition coefficient of k_e.*

5.3.2 Quantifying Partition Coefficient for Diffuse Interfaces

In a sharp interface model, the definition of the partition coefficient k is unambiguously simply the ratio of the composition on the solid side of the interface c^s divided by the composition of the liquid side of the interface c^l. In a diffuse interface model however, the partition coefficient is not so neatly defined due to a range of compositions existing across the interface. In this project the following definition of partition coefficient was proposed:

$$k_i = \frac{\int_{-\infty}^{\infty} \phi(1-\phi) X_i^S) dx}{\int_{-\infty}^{\infty} \phi(1-\phi) X_i^L dx} \tag{109}$$

Some have suggested to instead take the partition coefficient of the diffuse interface as the composition of the growing solid phase divided by the maximum of the solute concentration in the liquid phase [15] typically located somewhere within the interfacial region, or by simply taking the partition coefficient via extrapolated composition fields at $\phi = 0.5$ [12].

It was decided however that measuring the partition coefficient in a weighted manner across the interface would yield a more reliable number as this would not be affected by the numerical tricks necessary to keep the concentration fields well defined across the domain. For example the concentration of solute in the liquid becomes an increasingly ill defined concept as one approaches the solid side of the interface - ϕ approaches 1. A negligible amount of liquid phase at a fixed composition is modelled as existing throughout space to keep the liquid composition fields well defined (without meaningfully affecting the models behaviour), however the size of this numerically necessary addition may affect the size and position of the liquid concentration peak. Additionally, parts of the diffuse interface where more partitioning takes place (the middle regions of the interface) contribute more to the

overall measured partition coefficient by this measure.

6 Results

6.1 Binary Alloys

The results for the partitioning behaviour of Al-Sn and the Al-Cu binary alloy systems can be seen in figures 22 and 23 respectively. Typically simulations were run for 200000 iterations (corresponding to approximately 3 microsecond of simulated time) to yield an approximately steady state solution, however partitioning was also measured during shorter intervals as an imperfect method to sample the partitioning behaviour for velocities between this range. It was necessary to sample velocities during earlier iterations as otherwise there was consistent clustering of the resultant interface velocities between the diffusion controlled and non diffusion controlled solidification modes illustrated in figure 21.

After initial results were gathered, it was found that multiplying the Redistributive Velocity v_D by a factor of 0.5 in the phase field model yielded a much better fit with a CGM model using the same unaltered v_D. For all the results gathered in this section and the next this extra factor of 0.5 was used to effectively suppress the redistribution mechanism in the phase-field model. A theoretical justification for this extra suppression factor cannot be provided at the current time.

In figures 22, 23 and 25 the results of these simulations are denoted by either crosses or dots, whereas a dashed line represents the partitioning predicted by the continuous growth model whose behaviour the phase field models were expected to replicate. The constants in these continuous growth models were taken from Smith and Azizs early rapid solidification experiments with thin films of pulse laser melted dilute Aluminum alloys [18]. The constants used can be found in table 7, however it should be noted that the equilibrium factors k_e have

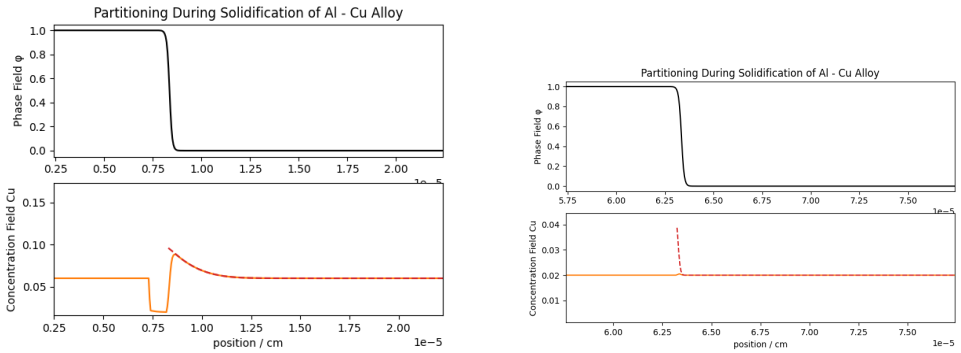


Fig. 21. *A snapshot comparing a high partitioning scenario (left) with a $k(v)$ close to k_e, to a low partitioning scenario where $k(v)$ is close to unity. It can be seen in the right hand image that the assumption of a uniform concentration across the interface, made during derivations in sections 4.1.1 and 4.1.2, does not hold so well. This uneven composition field may contribute to the over estimation of partitioning seen in figures 22 and 23*

been recalculated for the bespoke thermodynamic models discussed in section 4.2.

alloy system	D^L/cm^2s^{-1}	k_e	v_D/cm^2s^{-1}	composition range/ Mol Frac
Al-Cu	4.4×10^{-5}	0.11	6.7	0.0024 - 0.06 Cu
Al-Sn	4.9×10^{-5}	3.86×10^{-3}	36	0.0038 - 0.02 Sn

Table 7: This table contains the unique coefficients used for the Al-Cu and Al-Sn system simulations and continuous growth models. The equilibrium partition coefficient k_e is defined as the solid concentration divided by the liquid concentration of the non-Al element. Both simulations were performed at 878K.

For both the Al-Cu and Al-Sn systems the phase field model generally replicates the trend of the continuous growth model, however there is a notable under estimate of the partitioning at low interface velocities, and conversely an over estimate of the degree of partitioning at

higher interface velocities.

6.2 Extension to Ternary Case Al-Sn-Cu

Given that the phase field model was able to reproduce the CGM-like behaviour in the binary cases, this permitted the concept to be extended to the Ternary case. After all the Ternary case is simply composed of 3 pair wise interactions (Al-Sn, Al-Cu and Cu-Sn) for which the redistribution fluxes can be independently calculated. The contribution of the Cu-Sn interaction is however in this case effectively ignored by setting the redistribution flux interaction parameter between Cu and Sn - $\gamma_{Cu,Sn}$ - to zero. This was done because the strength of the Cu-Sn pairwise swapping interaction is essentially unknown at 878K between a Liquid and FCC_A1 phase. Given that these phases do not coexist at this temperature it is unsurprising that there haven't been any rapid solidification experiments that can be used to inform the value of $\gamma_{Cu,Sn}$ at 878K between FCC_A1 and Liquid phases. It is theorised that ignoring this contribution should not affect the overall result much, unless the pairwise interaction between Cu and Sn is order of magnitude greater than the interaction with Al. This is because for the numerical experiment both Sn and Cu are dilute - at less than 0.02 mol fraction combined. This would ultimately greatly reduce the contribution of Sn-Cu trans interface swaps to the overall redistribution compared to swaps with the much more abundant Al. It should be noted that if it were the case that Cu and Sn were to become enriched in opposite phases (i.e the liquid became Cu enriched, whilst the solid became Sn enriched) this could result in a non-negligible amount of Cu-Sn neighboring each other across the interface and that it would be unrealistic to set their pairwise swapping interaction to zero. Fortunately in this case however both Cu and Sn are depleted in the growing solid

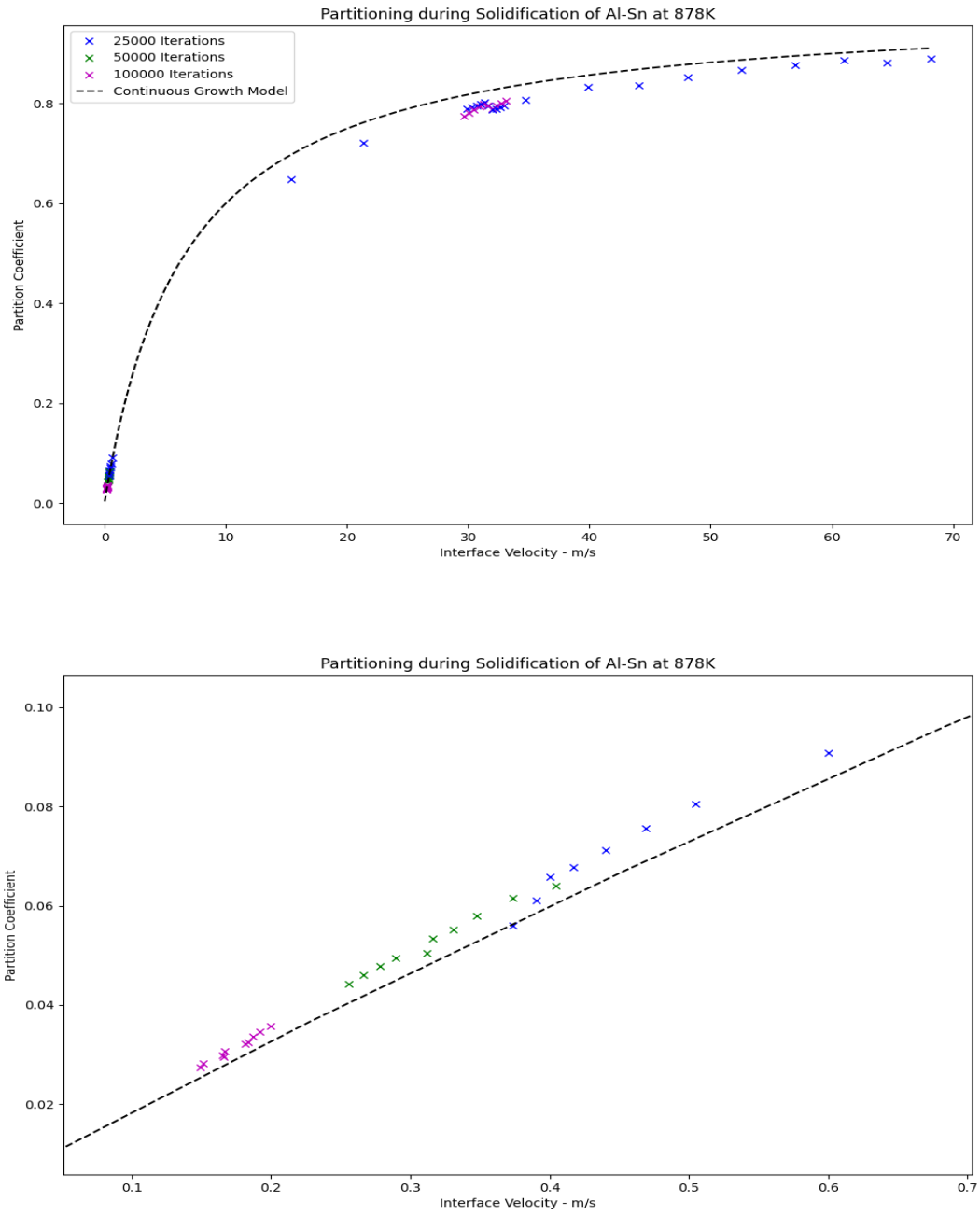


Fig. 22. *Plot of partition coefficent $k(v)$ against interface velocity for the Al Sn Binary at 878K. The dashed line is not fitted to the points in any way, instead both the Phase Field model and CGM are utilizing the parameters in table 7 and demonstrating agreement with each other both at a high (upper graph) and low (lower graph) interface velocity.*

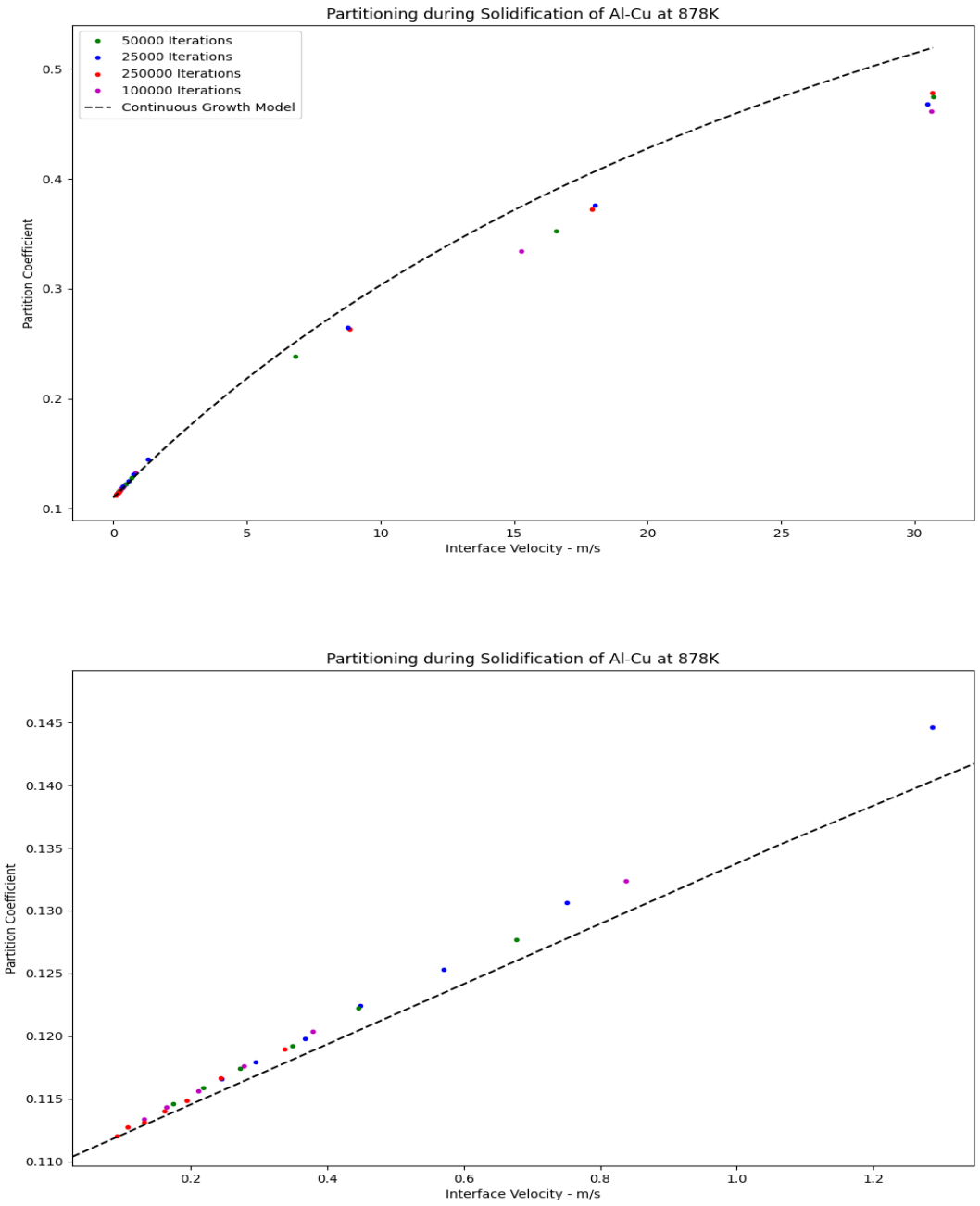


Fig. 23. *Plot of partition coefficent $k(v)$ against interface velocity for the Al Cu Binary, also at 878K. The Phase Field simulation results do not quite match the CGM as well for this system compared to Al-Sn, though the match is still good. Once again, an underestimation of partitioning at low velocities and an overestimation at high velocities is observed.*

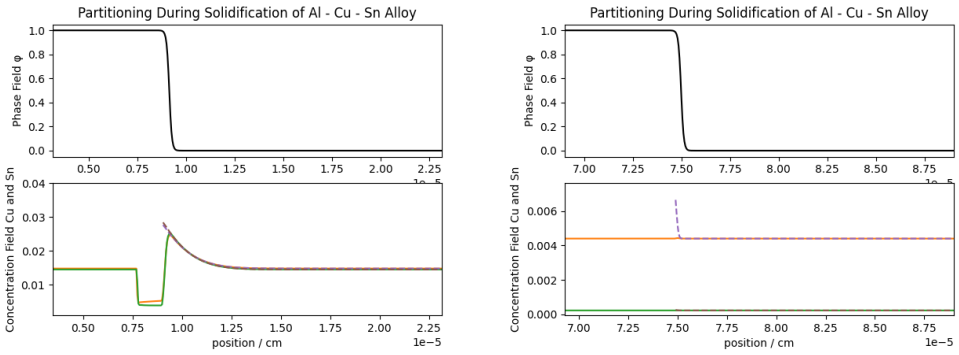


Fig. 24. *A snap shot once again comparing a high partitioning scenario (left) with a low partitioning scenario (right) however for the Al-Sn-Cu Ternary System. For this particular initial condition the concentration fields of Sn (green) and Cu (orange) appear to almost overlap across most the domain - however it can be observed in the small solidified region that has formed, that much more Cu has been incorporated than Sn. Hence their partition coefficients for each element are markedly different.*

phase.

Finding something to compare the results of the phase-field simulation with in the Ternary case is ultimately a bit more challenging than the binary case, that is because as far as the authors are aware the CGM has not been used to characterise the partitioning in rapid solidification experiments involving more than two elements. Appealing once again to the diluteness of the solution, it is postulated that the partitioning behaviour of the Cu and Sn elements would be approximately the same as the partitioning behaviour expected in a binary, but utilising the partition coefficients derived from the ternary phase diagram for the Al - Sn - Cu system. With these caveats in mind the match seen between the CGM and phase field models is once again quite close as shown in figure 25. In contrast to the binary cases we instead observe that the partitioning of the Al-Cu subsystem is consistently underestimated. This underestimation however may be a necessary result of overestimating

the partitioning in the Al - Sn subsystem in the low interface velocity regime, between 0 and 1 ms.

6.3 Discussion of Partitioning Results

The numerical experiments in this paper have demonstrated that CGM like behaviour can be produced across a wide range of interface velocities for a diffuse interface phase field model, when explicitly considering averaged concentration of solute either side of the interface. Compared to the approach by Reuther and Steinbach in a recent application of the Finite Interface Dissipation Model to the Al-Cu system [85], our model manages to fit the experimental k - v relation from Aziz and Smith [18] much better. In the finite interface dissipation model, different interface permeabilities (analogous to the γ_{ij} factors in this work) had to be used in order to better capture the partitioning at high and low interface velocities as show in figure 26. It should be noted however, that some of this may be down to differences in how the partition coefficient was defined in each piece of work.

Qualitatively the PFM also behaved similarly to the Al-Cu rapid solidification experiment with two distinct modes of solidification, one where growth was controlled and inhibited by a solute pile up, and another where there was little to no pile up and the interface grew at a much faster rate. A clear distinction between these modes can be seen in figure 21, with the stratification of interface velocities being most clear for the Al-Sn system show by the distinct gap between the cluster of simulations resulting in low velocity interfaces (solutally controlled), and simulations resulting in much higher velocities (non-solutally controlled). Although a clustering of velocities was observed, the clustering of velocities seen in our numerical experiments did not match the clustering seen in the actual rapid solidifica-

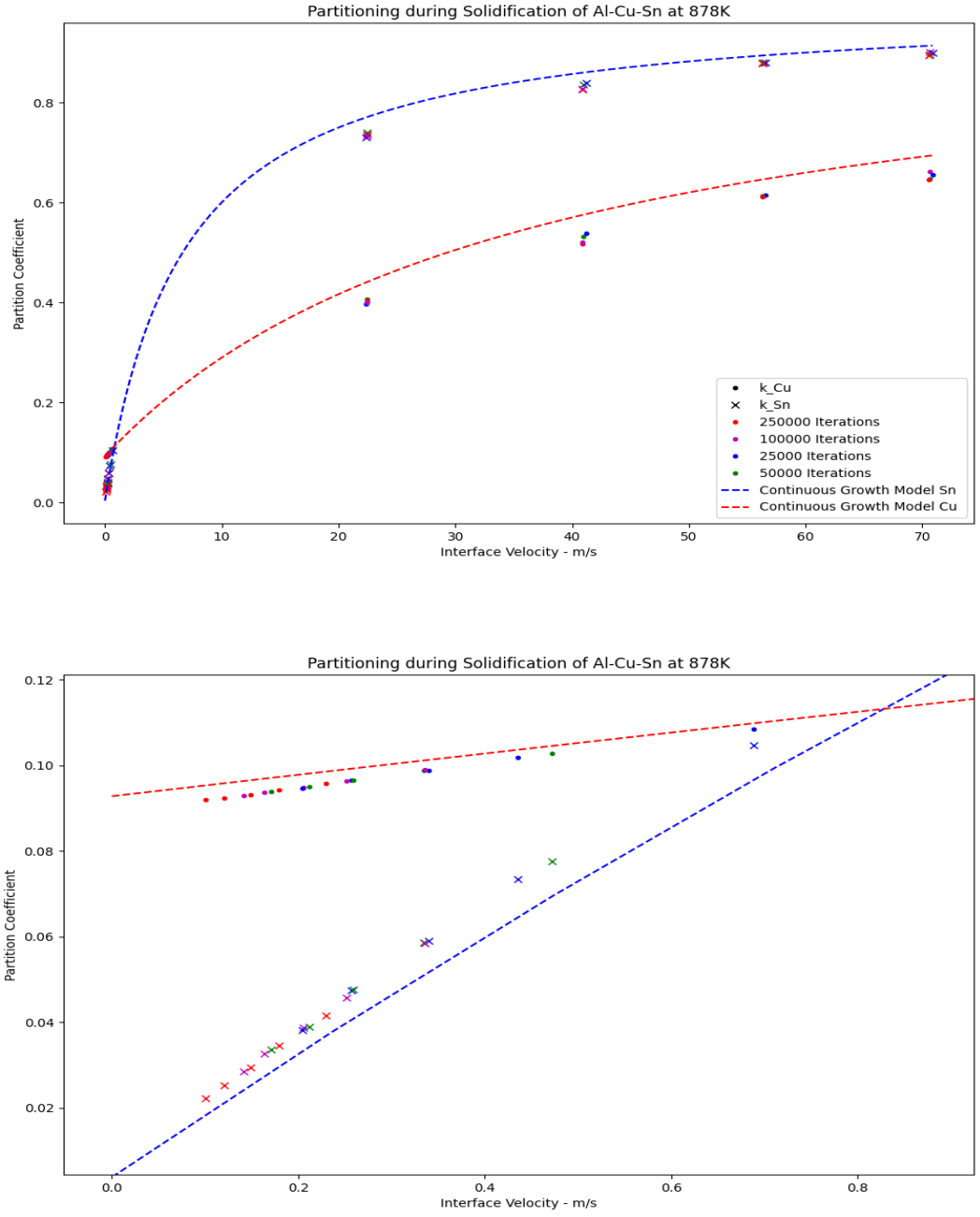


Fig. 25. *Plot of the partition velocity versus solute partitioning in an Al-Cu-Sn Ternary Alloy. This graph was produced by taking compositions along the tie line between solidus composition 0.0044 mol frac Cu, 0.000229 mol frac Sn and liquidus composition Cu-0.0044 Sn-0.0474. These compositions correspond to the the tie line for which a system evolution trajectory is plotted in figure 18. Once again the simulation was performed at 878K utilising the parameters in table 7*

tion experiment by Aziz and Smith [18]. In our simulations most solute controlled growth happened around 0.1 - 1 m/s whereas non-solutally controlled growth modes would have interface velocities beyond 10 m/s, unlike the experimentally observed clusters which appeared at around 1.5 and 5 m/s respectively. This would indicate the interfaces response to driving forces (specifically V_C in the cooperative growth phase field terms) would need some further tuning in order to better reflect reality. In this comparison however the interfaces actual response to a driving force is unimportant as it was only necessary to generate interfaces moving at different velocities in order to see if the k-v relationship matched the CGM. For these purposes the interface velocity might as well have been arbitrarily imposed.

It was reasonable to predict that the PFM would reproduce the behaviour of the CGM given that the evolution of the diffuse interface was designed to mirror the fluxes proposed in the original derivation of the CGM [16]. As the interface moves faster, the redistributive flux has less time to partition solute between the solid and liquid phases at points within the diffuse interface, thus a suppression of the overall partitioning being observed as the interface velocity increases was to be expected. This gave confidence that fluxes of the form derived in equation 73 could be used to predict partitioning in systems with 3 or even more elements, and could offer an approach to creating 2 or 3 dimensional phase-field models with accurate multi element partitioning.

The redistribution fluxes in the phase field model derived in section 4.1.2 were ultimately found to significantly over predict the amount of partitioning observed, thus in order to produce a more accurate partitioning the redistributive fluxes were multiplied by a factor of 0.5 effectively suppressing them. There may well be a conceptual reason that has been missed in the derivation that ought to justify including this factor of a half - given that a

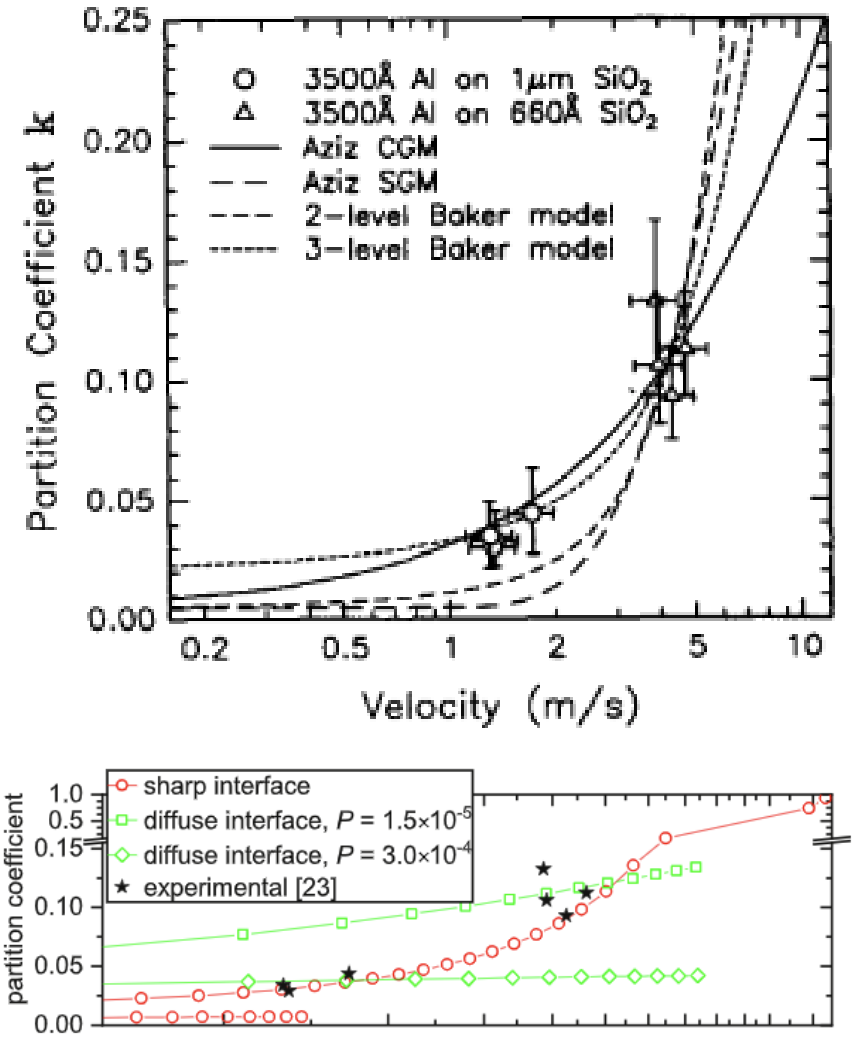


Fig. 26. *Comparison of the solute partitioning observed in Smith and Azizs Experiments with rapidly solidifying Al-Cu [18](top) with the finite interface dissipation models attempt to match those results (bottom) [85]. It can be seen that the finite interface dissipation model required different P (interface permeability) values in order to get an accurate k - v relationship for high and low interface velocities.*

half is quite a nice round factor that yields a very good fit to CGM model. Alternatively the measure of partition coefficient itself may have been inappropriate, and that instead the explicit amount of material that was redistributed ought to have been tracked and compared to the continuous growth model. Such a measure ought to consider the amount of solute redistributed over a given distance, as opposed to over a given time interval. This would be an interesting avenue for further work, to see if more appropriate or robust definitions of the partition coefficient still result in good fits between the CGM and the phase field model.

Ultimately the primary limitation to using this model to predict partitioning in systems with many elements is simply the fact that there is a dearth of binary partitioning experiments to draw redistribution velocities from for pairs of elements in the alloy. Given that many alloys of interest under rapid solidification conditions contain many elements, such as Inconel 718 with its 9 constituent elements, there are likely to be pairs of elements in the alloy which do not form a solidifying phase at the temperature of interest and thus it would be a challenge to characterise their redistribution rate at that temperature. This problem can be mitigated somewhat by assuming that the only swapping procedure that it is meaningful to model accurately would be swaps involving only the major element in a system - as could potentially be done with 316L stainless steel, though in the case of Inconel 718 this may be a poor assumption to make as its single most common constituent Nickel only constitutes 50% of the weight. Furthermore the assumption that the redistribution of solute in systems containing three or more elements can be adequately modelled by effectively independent binary redistribution reactions may ultimately prove to be inadequate. It may instead be necessary to consider the higher order interactions between triples or even quadruples of elements.

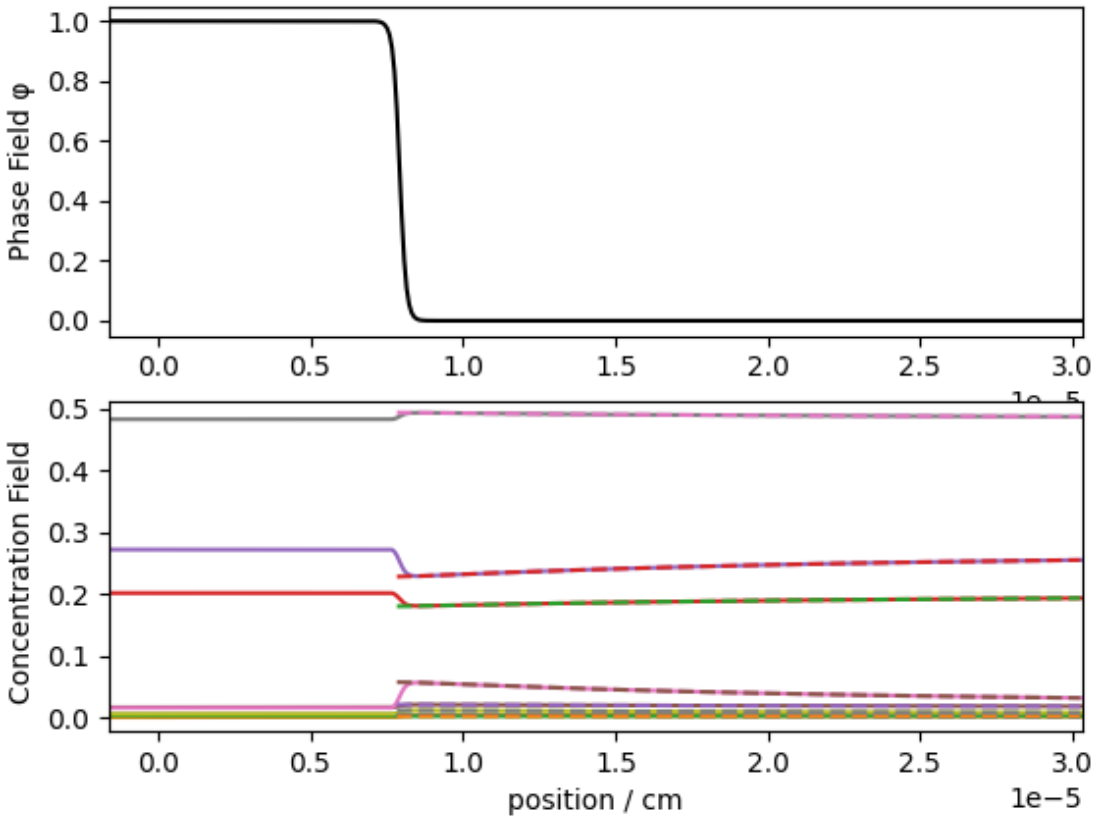


Fig. 27. *Partitioning observed in full Inconel system demonstrating the generality of the model.*

6.4 Inconel System Demonstration

Despite some of difficulties outlined above with extending the phase field model to make predictions for higher order systems, it was still deemed worthwhile to at least demonstrate the phase field model could in principle be applied to the Inconel system. Parameters for this demonstration were taken from Karayagiz et als simulation of a Ni-Nb system [11], meant as a representative analogue for Nickel super alloys. The results for a preliminary simulation of the Inconel718 system can be seen in figure 27 where it was demonstrated that it would be possible to extend the phase field model to this system.

The simulation was performed for 250000 iterations at 1520K for a system composed of 50% Nickel, 17% Chromium, 0.25% Cobalt, 2.8% Molybdenum, 4.75 % Niobium, 0.65% Titanium, 0.2% Aluminium, 0.04% Carbon with the remainder being Iron (Percentages are given in weight % rather than molar percentage). However without verifiably accurate thermodynamics, and reasonable assumptions for redistribution rates - it was deemed that it was not currently possible to make an informed prediction of the partitioning for the Inconel system.

7 Conclusions

The conclusions of this thesis are presented here. In the overview section the motivations for this work are reviewed to explain what was investigated and why, then the main achievements and core thrust of the project are summarised. Some findings deviated slightly from the core thrust of this project however they were still deemed interesting and important enough to highlight and are covered in the Other Findings section. Finally, The Potential Future Work section outlines the most immediately promising lines of enquiry that are still left to explore.

7.1 Overview

7.1.1 Motivation

It is generally useful to be able to predict which microstructures form during manufacturing processes, as these microstructures can be correlated with presence of defects detrimental to the performance of a material [21]. In many modern manufacturing processes such as Laser Powder Bed Fusion the thermal conditions and resultant solidification rates are much more extreme than conventional casting processes [19] [20], as a result many of the assumptions and models developed for predicting microstructure morphologies needed to be re-evaluated.

To this end, the motivation for this work was to develop a phase-field model capable of studying morphologies and microstructures that form over a wide range of solidification rates. Such a model would be useful for modelling the LPBF process as it would contribute to the general multi-scale modelling approaches [11] [24] [41] which weakly couple meso-scale models of temperature fields and fluid flows with micro-scale models of microstructure formation such as dendrite formation and morphology. Additionally the kinetic parameters in

the model developed in this thesis could also be informed by Molecular Dynamics simulations as previously demonstrated in [74].

7.1.2 Model Development

A necessary feature for an accurate model of microstructure formation, and as a result a core component of the work in this thesis, is to reproduce physically correct solute partitioning and segregation at the interface between a solid and liquid phase. It is extremely important to get this solute partitioning right as the size and shape of the solute concentration profile around the interface directly determines which morphologies will develop during solidification [34]. Thus the focus of this thesis was on developing a model that could accurately capture the relationship between an interfaces velocity and the amount of solute partitioning that occurs.

Solidification models such as the Continuous Growth Model (CGM) [16] and Local Non-Equilibrium Model (LNM) [17] are generally considered premier models of solute partitioning, however unlike phase-field models they are not straight forwardly applicable to 2D or 3D simulation of microstructure. It is currently an active area of research to develop phase field models that are capable of reproducing the behaviour of the CGM and LNM [86] [14] [15], and it was decided early on to develop a novel phase field model to contribute to these efforts.

The resultant model was based on work done by N Warnken on a phase field model for non-local equilibrium phase transformations [78] [79], and conceptually mirrored the approach of Steinbach, Zhang and Plapp in their finite interface dissipation model [15] [85] however with the "dissipation" process being informed directly by the atomistic processes and fluxes at the interface. These atomistic processes were the cooperative growth mechanism, and

the redistributive flux each described in sections 3.3.1 and 3.3.2, which are generalisations of the atomistic processes that are assumed in the CGM. The manner in which these processes could be represented and incorporated into a phase-field model were then detailed in sections 4.1.1 and 4.1.2. The explicit consideration of the atomistic process was itself reminiscent of and inspired by the work Larsson and Borgstam [73] [75] simulating how cooperative and diffusive growth fluxes would evolve a system.

Overall this approach to developing a rapid solidification model yielded three important advantages:

- Can easily apply the kinetic parameters found in CGM models to a phase field model.
- The Generalised redistribution fluxes that the model is based on allow predictions to be made for partitioning behaviour of Ternary or potentially even higher order systems.
- By virtue of being a phase field model it would be conceptually straight forward to implement in 2D or 3D allowing predictions of microstructure morphologies to incorporate solute partitioning dynamics from the CGM.

7.1.3 Notable Results

It was demonstrated in section 6.1 that the model could straight forwardly utilise kinetic parameters from a CGM to reproduce the CGM solute partitioning behaviour across a wide range of interface velocities (from 0.01 - 40 m/s). This was performed for the Al-Sn and the Al-Cu systems, as those systems had robust experimental observations (courtesy once again of Aziz and Smith) and other models (such as the finite interface dissipation model [85]) had also been used to attempt to characterise the observed partitioning behaviour. Ultimately

the model presented in this thesis provided a simple and successful incorporation of CGM kinetics.

The redistribution fluxes originally proposed in the CGM were for a binary alloy, however their generalisation in chapter 3.3.1 permitted the new PFM to make predictions for partitioning in a ternary system - given the kinetic parameters describing its binary-subsystems. Predictions were made for the Al-Cu-Sn ternary system utilising the kinetic parameters from the Al-Sn and Al-Cu simulations, subject to a few assumptions outlined in chapter 5.3. It would be interesting to see whether or not this prediction can be validated by actual experiments, unfortunately to date there do not appear to be any ternary rapid solidification experiments utilizing the same thin film pulsed laser melting technique used to gather the rapid solidification solute partitioning data for the Al-Cu and Al-Sn binaries [59].

In section 6.4 it was shown that the model could in principle be used to model the full chemical system for Inconel718, a popular Nickel Super Alloy of interest for LPBF, demonstrating the scalability of the model. However, due to lack of data on partitioning rates for elements in the system at such extreme temperatures (1520K), it was not possible to make informed predictions of partitioning for that particular system.

7.2 Other Findings

7.2.1 Redistributive Flux as a description of Diffusion

The redistributive flux derived in section 3.3.1 had several properties that made it potentially useful for modelling the diffusion of solute throughout a material as opposed to exclusively across an interface. The most important property being the number fixed nature of the

flux, ie. the sum over all the redistributive fluxes for all species crossing some boundary is 0. It shares this property with the conventional descriptions of number fixed frame (NFF) diffusion (based on considering lattice fixed frame fluxes in a different velocity frame) utilized by CALPHAD models of diffusivity and is useful for numerical simulation [69]. In section 3.4 the properties of diffusion described by a conventional NFF flux were compared to diffusion modelled with a redistributive flux, however the only scenario under which it was found that the two processes were equivalent was when the Mobilities for diffusion across all elements in the system were the same. There may have been other equivalent scenarios, however this was the only one found in this work. Although this does not completely invalidate the idea of utilizing a redistributive flux to describe diffusion through the bulk of a material, it does make it much more difficult to relate the kinetic parameters in the redistributive flux to kinetic parameters (such as Diffusivity and Mobility) used by NFF models, which have already enjoyed widespread success in modelling diffusion.

7.2.2 Curvature Potential in Diffuse Interfaces

When incorporating the redistributive flux into a phase field model in section 4.1.2 it was necessary to modify the thermodynamic description of the mixture of phases at point in the diffuse interface in order to reflect any curvature of the interface between the phases. Though it was not necessary for the 1-D simulations in this work, it would be necessary for 2D and 3D simulations as curvature would effect the local equilibrium compositions that points in the diffuse interface should evolve towards. This quantity, denoted as curvature potential $\Delta\mu^C$, would need to be uniform across the direction normal to the diffuse interface (ie along the vector $\nabla\phi$), and it would be convenient to be able to determine it locally. By considering

standard travelling wave solutions to a phase field equation for a uniformly curved particle- and the driving force necessary to stabalise such a particle, such a quantity was found, with the full derivation given in the appendix:

$$\Delta\mu^C = -\frac{\epsilon}{\sqrt{2H}}\frac{RT}{\phi(1-\phi)}\frac{\delta F_{int}}{\delta\phi} \tag{110}$$

7.2.3 Non-Phase Field Diffuse Interface

The general approach model development in this thesis has been to try to model the effect of discrete atomistic processes, such the redistributive flux and the cooperative growth mechanism, as explicitly and directly as possible. The Phase Field Model however is simply a useful phenomenological tool onto which these processes were projected. An attempt was made to instead derive a diffuse interface model from first principles, based on atomistic processes and is presented in section 4.3. Although the model produced a stable diffuse interface, characterising its behaviour and incorporating redistributive flux and cooperative growth mechanism was deemed beyond the scope of this project, and would have delayed the gathering of useful results.

7.3 Potential Future Work

7.3.1 Solute Partitioning Predictions

One of the advantages and goals of the model in this project was to be able to predict the solute partitioning behaviour for multi-component systems. In future work it would be interesting to verify whether or not the model is capable of doing so for more complex systems.

To this end it would invaluable to gather experimentally results for solute partitioning for the Al-Cu-Sn system to see whether or not the assumptions regarding predictions for dilute alloys still held for multi-component systems. Admittedly however, it may turn out to be difficult to adapt the experiments on binary partitioning to consider a ternary alloy. Currently the simulations for Al-Cu-Sn could only be compared to a rudimentary CGM that assumed independent binary redistribution processes.

In order to apply system to non-dilute alloys with many components the challenges addressed in chapter 5.3 (the chapter where the concern about whether or not binary can be used to predict ternary system is most important) would also need to be addressed. In aid of this the Generalised redistribution fluxes proposed in section 3.3.1 offer a frame work for characterising the rates of solute redistribution in multi-component systems. This could be utilised similarly to how thermodynamic modelling approaches such as CALPHAD predict and interpolate the equilibrium compositions for coexisting phases. By building up a database of the redistribution velocities between many pairs of elements for many phases it would be possible to construct redistributive flux models for multi-component systems - if it is the case that multi component system can be accurately modelled as a many independent pairwise redistribution processes. Even if not it may in principle be possible to extend the swapping procedure to consider 3 element interactions instead of just pair wise interactions.

7.3.2 Prediction of Microstructure Morphology

In order to begin using this model in 2 or 3D simulations for predicting which microstructures form, there are couple of questions that would need to be addressed. The sensitivity of results to different definitions of the partition coefficient as discussed in chapter 6.3 would have to

be addressed, and an appropriate definition of the partition coefficient ought to be verified. Additionally even though the γ_{ij} factors appear to produce the correct partitioning for a given velocity, it would need to be verified that the V_C (max crystallisation velocity) used in this model produces the correct interface velocity for a given interface condition. The interface condition is it self still ambiguous for this diffuse interface, it should relate the composition profile across the interface to the compositions of the solid and liquid phase either side of a sharp interface. Solving the ambiguity in what the appropriate partition coefficient should be however, would immediately solve the problem of determining what the interface condition it self is.

Once these issues are addressed there would be the scaling issues that may need to be tackled either by improving compute resources (GPU parallelism) or by an adaptive meshing approach such as (P4est Amrex). For this model in particular it may be especially necessary for multi-component systems given how the number of swap interactions that need to be considered for the redistribution flux scales as n(n-1)/2 where n is number of elements in the system.

8 APPENDIX

8.1 Low Driving force limit of Pair Wise Swapping Scheme

Starting from a flux derived from a simple reaction rate model of diffusion and as a simplification assuming that $\Delta\eta_i < 0$ for all i:

$$\begin{aligned} j_i/\delta = X_i(z)\exp\left(\frac{\eta_i(z)-\eta_i(z+\delta z)}{RT}\right)\cdot\sum_j \gamma_{ij}X_j(z+\delta z) \\ -X_i(z+\delta z)\cdot\sum_j \gamma_{ij}X_j(z)\exp\left(\frac{\eta_j(z)-\eta_j(z+\delta z)}{RT}\right) \end{aligned} \tag{111}$$

we make substitutions of the following form in order to derive a flux within a bulk phase in the continuum limit:

$$\begin{aligned} X_i(z+\delta z) = X_i + \delta\nabla X_i \\ \eta_i(z+\delta z) = \eta_i + \delta\nabla\eta \end{aligned} \tag{112}$$

these substitutions yield:

$$\begin{aligned} j_i/\delta = X_i\exp\left(\frac{-\delta\nabla\eta_i}{RT}\right)\cdot\sum_j \gamma_{ij}(X_j+\delta\nabla X_j) \\ -\left(X_i+\delta\nabla X_i\right)\cdot\sum_j \gamma_{ij}X_j\exp\left(\frac{-\delta\nabla\eta_j}{RT}\right) \end{aligned} \tag{113}$$

For a low thermodynamic driving force, i.e when $-\delta\nabla\eta_j$ is small the following approximation can be made:

$$\exp\left(\frac{-\delta\nabla\eta_i}{RT}\right) \approx 1 - \frac{\delta\nabla\eta_i}{RT} \tag{114}$$

substituting this back into the expression for j_i yields:

$$j_i/\delta = X_i \left[1 - \frac{\delta \nabla \eta_i}{RT}\right] \cdot \sum_j \gamma_{ij}(X_j + \delta \nabla X_j) \\ -(X_i + \delta \nabla X_i) \cdot \sum_j \gamma_{ij} X_j \left[1 - \frac{\delta \nabla \eta_j}{RT}\right] \tag{115}$$

utilising the identities:

$$\sum_j \nabla X_j = 0 \\ \nabla \eta_i = \nabla \mu_i - RT \frac{\nabla X_i}{X_i} \tag{116}$$

These are substituted into j_i to give:

$$j_i/\delta = X_i \left[1 - \frac{\delta \nabla \mu_i}{RT} + \delta \nabla X_i / X_i\right] \cdot \sum_j \gamma_{ij}(X_j + \delta \nabla X_j) \\ -(X_i + \delta \nabla X_i) \cdot \sum_j \gamma_{ij} X_j \left[1 - \frac{\delta \nabla \mu_j}{RT} + \delta \nabla X_i / X_i\right] \tag{117}$$

it will be assumed that $X_i \approx X_i + \delta \nabla X_i$ given that δ is quite small. Thus the following form for a flux j_i is arrived that, which can be related to the conventional number fixed frame transformation under certain circumstances.

$$j_i/\delta = X_i \left[1 - \frac{\delta \nabla \mu_i}{RT}\right] \cdot \sum_j \gamma_{ij} X_j - X_i \cdot \sum_j \gamma_{ij} X_j \left[1 - \frac{\delta \nabla \mu_j}{RT}\right] \tag{118}$$

now just do a bit of rearrangement to yield:

$$j_i/\delta = X_i \left[-\frac{\delta \nabla \mu_i}{RT}\right] \cdot \sum_j \gamma_{ij} X_j - X_i \cdot \sum_j \gamma_{ij} X_j \left[-\frac{\delta \nabla \mu_j}{RT}\right] \tag{119}$$

8.2 Derivation of Curvature Potential

An expression for the curvature potential for phase field model 60 and energy function 59. The concept of curvature potential was introduced by N Warnkenn in [79] as a locally evaluatable

potential that simultaneously accounts for diffuse interface stabilisation and macroscopic particle curvature. The curvature potential is ultimately something that is phase field model and Energy Functional specific, so would need to be rederived if a different phase field model was being used as a substrate from which to build a model of the style presented in this work.

$$F_{int} = \int_{\Omega} d\Omega \left[\frac{\varepsilon^2}{2} |\nabla \phi|^2 + H\phi^2(1-\phi)^2 \right] \tag{120}$$

for a particle with radius R, we can take the variational derivative of the above expression in the interfacial region and it will evaluate to:

$$\frac{\delta F_{int}}{\delta \phi} = -\varepsilon^2 \frac{1}{r} \frac{\partial}{\partial r} \phi(r) \approx -\varepsilon^2 \frac{1}{R} \frac{\partial}{\partial r} \phi(r) \tag{121}$$

as this will be the residual term assuming a fully relaxed diffuse interface profile.

$$\frac{\delta F_{int}}{\delta \phi} = -\frac{\varepsilon}{R} \sqrt{2H} \phi(1-\phi) \tag{122}$$

gathering the constant terms onto one side we know that for an interface of given curvature R, you have the following:

$$\frac{\delta F_{int}}{\delta \phi} \cdot \frac{1}{\phi(1-\phi)} = -\frac{\varepsilon}{R} \sqrt{2H} \tag{123}$$

This will be useful in a moment. Now we consider an equation of motion like equation 60.

$$\frac{\partial \phi}{\partial t} = -V_C \left[\frac{\delta F_{int}}{\delta \phi} + \frac{\sqrt{2H}}{\epsilon} \phi(1-\phi) P \right] \tag{124}$$

Let us consider what driving force would need to added to P in order for this for a curved particle of radius R to be balance in equilibrium. This driving force is the curvature potential, $\Delta\mu^C$.

$$P = 1 - \exp\left(-\frac{\Delta\mu^C}{RT}\right) \approx \frac{\Delta\mu^C}{RT} \tag{125}$$

if this $\Delta\mu^C$ is in equilibrium with the curvature of the particle then using equations 123 and 124 we know that:

$$\frac{\epsilon^2}{R} = \frac{\Delta\mu^C}{RT} \tag{126}$$

comparing this back to equation 123 then yields an expression for curvature potential that can be evaluated locally across a diffuse interface:

$$\Delta\mu^C = -\frac{\epsilon}{\sqrt{2H}}\frac{RT}{\phi(1-\phi)}\frac{\delta F_{int}}{\delta\phi} \tag{127}$$

8.3 anti derivative of $\phi(1-\phi)$ for standard travelling wave solution

for the travelling wave solutions of the form:

$$\phi(x,t) = \frac{1}{2}\left(1 - \tanh\left(\frac{\sqrt{W}}{\epsilon\sqrt{2}}(x - v\cdot t)\right)\right) \tag{128}$$

these can be differentiated with respect to x in order to yield:

$$\frac{\partial\phi}{\partial x} = 2\frac{\sqrt{H}}{\epsilon\sqrt{2}}\phi(1-\phi) \tag{129}$$

which is a result we can use to straight forwardly calculated what the integral of $\phi(1-\phi)$ is:

$$\begin{aligned}\int_{-\infty}^{\infty} 2\frac{\sqrt{H}}{\epsilon\sqrt{2}}\phi(1-\phi)dx &= \int_{-\infty}^{\infty}\frac{\partial\phi}{\partial x}dx \\ &= \int_0^1 d\phi = 1\end{aligned} \tag{130}$$

therefore:

$$\int_{-\infty}^{\infty}\phi(1-\phi)dx = \frac{\epsilon}{\sqrt{2H}} \tag{131}$$

References

[1] D D Gu, W Meiners, K Wissenbach, and R Poprawe. Laser additive manufacturing of metallic components: materials, processes and mechanisms. *International Materials Reviews*, 57(3):133–164, 2012.

[2] David Bourell, Jean Pierre Kruth, Ming Leu, Gideon Levy, David Rosen, Allison M. Beese, and Adam Clare. Materials for additive manufacturing. *CIRP Annals - Manufacturing Technology*, 66:659–681, 2017.

[3] S. Pratheesh Kumar, S. Elangovan, R. Mohanraj, and J. R. Ramakrishna. A review on properties of inconel 625 and inconel 718 fabricated using direct energy deposition. volume 46, pages 7892–7906. Elsevier Ltd, 2021.

[4] M. Karmuhilan and Somasundaram Kumanan. A review on additive manufacturing processes of inconel 625. *Journal of Materials Engineering and Performance*, 31(4):2583–2592, Apr 2022.

[5] M. J.K. Lodhi, K. M. Deen, M. C. Greenlee-Wacker, and Waseem Haider. Additively manufactured 316l stainless steel with improved corrosion resistance and biological response for biomedical applications. *Additive Manufacturing*, 27:8–19, 5 2019.

[6] Abdollah Saboori, Alberta Aversa, Giulio Marchese, Sara Biamino, Mariangela Lombardi, and Paolo Fino. Application of directed energy deposition-based additive manufacturing in repair. *Applied Sciences (Switzerland)*, 9, 8 2019.

[7] E. Liverani, S. Toschi, L. Ceschini, and A. Fortunato. Effect of selective laser melting (slm) process parameters on microstructure and mechanical properties of 316l austenitic stainless steel. *Journal of Materials Processing Technology*, 249:255 – 263, 2017.

[8] Joel Heang Kuan Tan, Swee Leong Sing, and Wai Yee Yeong. Microstructure modelling for metallic additive manufacturing: a review. *Virtual and Physical Prototyping*, 15(1):87–105, 2020.

[9] J. P. Oliveira, T. G. Santos, and R. M. Miranda. Revisiting fundamental welding concepts to improve additive manufacturing: From theory to practice. *Progress in Materials Science*, 107, 1 2020.

[10] A Farzadi, M Do-Quang, S Serajzadeh, A H Kokabi, and G Amberg. Phase-field simulation of weld solidification microstructure in an al–cu alloy. *Modelling and Simulation in Materials Science and Engineering*, 16(6):065005, aug 2008.

[11] Kubra Karayagiz, Luke Johnson, Raiyan Seede, Vahid Attari, Bing Zhang, Xueqin Huang, Supriyo Ghosh, Thien Duong, Ibrahim Karaman, Alaa Elwany, and Raymundo Arróyave. Finite interface dissipation phase field modeling of ni–nb under additive manufacturing conditions. *Acta Materialia*, 185:320–339, feb 2020.

[12] Seong Gyoon Kim, Won Tae Kim, and Toshio Suzuki. Phase-field model for binary alloys. *Phys. Rev. E*, 60:7186–7197, Dec 1999.

[13] M. Ode, T. Suzuki, S.G. Kim, and W.T. Kim. Phase–field model for solidification of fe–c alloys. *Science and Technology of Advanced Materials*, 1(1):43–49, jan 2000.

[14] D Jou P Ganlenko. Diffuse-interface model for rapid phase transformations in nonequilibrium systems. *Physical Review*, E 71:NA, 01 2005.

[15] Ingo Steinbach, Lijun Zhang, and Mathis Plapp. Phase-field model with finite interface dissipation. *Acta Materialia*, 60:2689–2701, 4 2012.

[16] Michael J Aziz and Theodore Kaplan. Continuous growth model for interface motion during alloy solidification. *Acta Metallurgica*, 36(8):2335 – 2347, 1988.

[17] S. L. Sobolev. Local non-equilibrium diffusion model for solute trapping during rapid solidification. *Acta Materialia*, 60:2711–2718, 4 2012.

[18] Patrick M. Smith and M.J. Aziz. Solute trapping in aluminum alloys. *Acta Metallurgica et Materialia*, 42(10):3515–3525, 1994.

[19] W. E. King, A. T. Anderson, R. M. Ferencz, N. E. Hodge, C. Kamath, S. A. Khairallah, and A. M. Rubenchik. Laser powder bed fusion additive manufacturing of metals; physics, computational, and materials challenges. *Applied Physics Reviews*, 2(4):041304, 2015.

[20] William J. Sames, Frederick Alyious List, III, Sreekanth Pannala, Ryan R. Dehoff, and Sudarsanam Suresh Babu. The metallurgy and processing science of metal additive manufacturing. *International Materials Reviews*, 61(5), 3 2016.

[21] Hossein Taheri, Mohammad Rashid Bin Mohammad Shoaib, Lucas W. Koester, Timothy A. Bigelow, Peter C. Collins, and Leonard J. Bond. Powder-based additive manufacturing - a review of types of defects, generation mechanisms, detection, property

evaluation and metrology. *International Journal of Additive and Subtractive Materials Manufacturing*, 1(2):172–209, 2017.

[22] Bintao Wu, Zengxi Pan, Donghong Ding, Dominic Cuiuri, Huijun Li, Jing Xu, and John Norrish. A review of the wire arc additive manufacturing of metals: properties, defects and quality improvement. *Journal of Manufacturing Processes*, 35:127–139, 2018.

[23] Stéphane Gorsse, Christopher Hutchinson, Mohamed Gouné, and Rajarshi Banerjee. Additive manufacturing of metals: a brief review of the characteristic microstructures and properties of steels, ti-6al-4v and high-entropy alloys. *Science and Technology of Advanced Materials*, 18(1):584–610, 2017. PMID: 28970868.

[24] Saad A. Khairallah, Andrew T. Anderson, Alexander Rubenchik, and Wayne E. King. Laser powder-bed fusion additive manufacturing: Physics of complex melt flow and formation mechanisms of pores, spatter, and denudation zones. *Acta Materialia*, 108:36 – 45, 2016.

[25] Pavel Krakhmalev, Gunnel Fredriksson, Krister Svensson, Igor Yadroitsev, Ina Yadroitsava, Mattias Thuvander, and Ru Peng. Microstructure, solidification texture, and thermal stability of 316 l stainless steel manufactured by laser powder bed fusion. *Metals*, 8(8), 2018.

[26] Zhongji Sun, Xipeng Tan, Shu Beng Tor, and Wai Yee Yeong. Selective laser melting of stainless steel 316l with low porosity and high build rates. *Materials and Design*, 104:197 – 204, 2016.

[27] Mostafa Yakout, M. A. Elbestawi, and Stephen C. Veldhuis. On the characterization of stainless steel 316l parts produced by selective laser melting. *The International Journal of Advanced Manufacturing Technology*, 95(5):1953–1974, Mar 2018.

[28] K. Saeidi, X. Gao, Y. Zhong, and Z.J. Shen. Hardened austenite steel with columnar sub-grain structure formed by laser melting. *Materials Science and Engineering: A*, 625:221 – 229, 2015.

[29] P. Krakhmalev, I. Yadroitsava, G. Fredriksson, and I. Yadroitsev. In situ heat treatment in selective laser melted martensitic aisi 420 stainless steels. *Materials and Design*, 87:380 – 385, 2015.

[30] I. Yadroitsev, P. Krakhmalev, I. Yadroitsava, S. Johansson, and I. Smurov. Energy input effect on morphology and microstructure of selective laser melting single track from metallic powder. *Journal of Materials Processing Technology*, 213(4):606 – 613, 2013.

[31] H.B. Dong and P.D. Lee. Simulation of the columnar-to-equiaxed transition in directionally solidified al–cu alloys. *Acta Materialia*, 53(3):659 – 668, 2005.

[32] J. W. Elmer, S. M. Allen, and T. W. Eagar. Microstructural development during solidification of stainless steel alloys. *Metallurgical Transactions A*, 20(10):2117–2131, Oct 1989.

[33] M. Rappaz. Modelling of microstructure formation in solidification processes. *International Materials Reviews*, 34(1):93–124, 1989.

[34] W. W. Mullins and R. F. Sekerka. Stability of a planar interface during solidification of a dilute binary alloy. *Journal of Applied Physics*, 35(2):444–451, 1964.

[35] R Trivedit and W Kurz. Morphological stability of a planar interface under rapid solidification conditions, 1986.

[36] Rohit Trivedi and W Kurz. Dendritic growth. *International Materials Reviews*, 39:49–74, 01 1994.

[37] Shaun McFadden and David J. Browne. A generalised version of an ivantsov-based dendrite growth model incorporating a facility for solute measurement ahead of the tip. *Computational Materials Science*, 55:245–254, 4 2012.

[38] Min Yang, Lu Wang, and Wentao Yan. Phase-field modeling of grain evolutions in additive manufacturing from nucleation, growth, to coarsening. *npj Computational Materials*, 7, 12 2021.

[39] Mohammad Amin Jabbareh and Hamid Assadi. Modelling of microstructure evolution during laser processing of intermetallic containing ni-al alloys. *Metals*, 11, 7 2021.

[40] Balasubramaniam Radhakrishnan, Sarma B. Gorti, John A. Turner, Ranadip Acharya, John A. Sharon, Alexander Staroselsky, and Tahany El-Wardany. Phase field simulations of microstructure evolution in in718 using a surrogate ni–fe–nb alloy during laser powder bed fusion. *Metals*, 9, 1 2019.

[41] Patcharapit Promoppatum, Shi-Chune Yao, P. Chris Pistorius, and Anthony D. Rollett. A comprehensive comparison of the analytical and numerical prediction of the thermal

history and solidification microstructure of inconel 718 products made by laser powder-bed fusion. *Engineering*, 3(5):685–694, 2017.

[42] Sepideh Kavousi, Brian R. Novak, Jeffrey Hoyt, and Dorel Moldovan. Interface kinetics of rapid solidification of binary alloys by atomistic simulations: Application to ti-ni alloys. *Computational Materials Science*, 184:109854, 2020.

[43] J.A. Kittl, P.G. Sanders, M.J. Aziz, D.P. Brunco, and M.O. Thompson. Complete experimental test of kinetic models for rapid alloy solidification. *Acta Materialia*, 48(20):4797–4811, 2000.

[44] J. Los and E. Flöter. Construction of kinetic phase diagrams. *Phys. Chem. Chem. Phys.*, 1:4251–4257, 1999.

[45] Michael J. Aziz. Crystal growth and solute trapping. *MRS Online Proceedings Library (OPL)*, 23:369, 1983.

[46] W.C. Carter, A.R. Roosen, J.W. Cahn, and J.E. Taylor. Shape evolution by surface diffusion and surface attachment limited kinetics on completely faceted surfaces. *Acta Metallurgica et Materialia*, 43(12):4309 – 4323, 1995.

[47] T. Ihle and H. Müller-Krumbhaar. Fractal and compact growth morphologies in phase transitions with diffusion transport. *Phys. Rev. E*, 49:2972–2991, Apr 1994.

[48] Alain Karma and Wouter-Jan Rappel. Phase-field method for computationally efficient modeling of solidification with arbitrary interface kinetics. *Phys. Rev. E*, 53:R3017–R3020, Apr 1996.

[49] A. G. Khachaturyan. Long-range order parameter in field model of solidification. *Philosophical Magazine A*, 74(1):3–14, 1996.

[50] Ryo Kobayashi. A numerical approach to three-dimensional dendritic solidification. *Experiment. Math.*, 3(1):59–81, 1994.

[51] B. I. Halperin, P. C. Hohenberg, and Shang-keng Ma. Renormalization-group methods for critical dynamics: I. recursion relations and effects of energy conservation. *Phys. Rev. B*, 10:139–153, Jul 1974.

[52] Supriyo Ghosh. Predictive modeling of solidification during laser additive manufacturing of nickel superalloys: recent developments, future directions. 2018.

[53] J. J. Hoyt, Mark Asta, and Alain Karma. Atomistic and continuum modeling of dendritic solidification. 2003.

[54] Ingo Steinbach. Phase-field models in materials science. *Modelling and Simulation in Materials Science and Engineering*, 17(7):073001, jul 2009.

[55] Mathis Plapp. Unified derivation of phase-field models for alloy solidification from a grand-potential functional. *Physical review. E, Statistical, nonlinear, and soft matter physics*, 84 3 Pt 1:031601, 2011.

[56] I. Steinbach and M. Apel. Multi phase field model for solid state transformation with elastic strain. *Physica D: Nonlinear Phenomena*, 217(2):153 – 160, 2006.

[57] Tomohiro Takaki. Phase-field modeling and simulations of dendrite growth. *ISIJ International*, 54(2):437–444, 2014.

[58] A. A. Wheeler, W. J. Boettinger, and G. B. McFadden. Phase-field model for isothermal phase transitions in binary alloys. *Phys. Rev. A*, 45:7424–7439, May 1992.

[59] Michael J. Aziz. Interface attachment kinetics in alloy solidification. *Metallurgical and Materials Transactions A*, 27(3):671–686, Mar 1996.

[60] Igor Rasin. *Numerical simulation of microstructure of the GeSi alloy.* PhD thesis, 02 2007.

[61] Jun Fan, Michael Greenwood, Mikko Haataja, and Nikolas Provatas. Phase-field simulations of velocity selection in rapidly solidified binary alloys. *Physical review. E, Statistical, nonlinear, and soft matter physics*, 74:031602, 10 2006.

[62] Sukeharu Nomoto, Masahito Segawa, and Hiroshi Wakameda. Non-equilibrium phase field model using thermodynamics data estimated by machine learning for additive manufacturing solidification. 08 2018.

[63] P. K. Galenko, E. V. Abramova, D. Jou, D. A. Danilov, V. G. Lebedev, and D. M. Herlach. Solute trapping in rapid solidification of a binary dilute system: A phase-field study. *Phys. Rev. E*, 84:041143, Oct 2011.

[64] Martin Ostoja-Starzewski. A derivation of the maxwell–cattaneo equation from the free energy and dissipation potentials. *International Journal of Engineering Science*, 47(7):807 – 810, 2009.

[65] Peter Hänggi, Peter Talkner, and Michal Borkovec. Reaction-rate theory: fifty years after kramers. *Rev. Mod. Phys.*, 62:251–341, Apr 1990.

[66] Lars Onsager. Reciprocal relations in irreversible processes. i. *Phys. Rev.*, 37:405–426, Feb 1931.

[67] Henry Eyring. The activated complex in chemical reactions. *The Journal of Chemical Physics*, 3(2):107–115, 1935.

[68] W. E. Roseveare, R. E. Powell, and Henry Eyring. The structure and dynamics of liquids. *Journal of Applied Physics*, 12:669–679, 1941.

[69] M Hillert. The discrete lattice model for diffusion revisited. *Scripta Materialia*, 44(7):1095 – 1097, 2001.

[70] Mats Hillert. Fundamentals of diffusion in phase transformations. *Phase Transformations in Steels*, 1:94–125, 2012.

[71] Mark D. Kluge and John R. Ray. Velocity versus temperature relation for solidification and melting of silicon: A molecular-dynamics study. *Phys. Rev. B*, 39:1738–1746, Jan 1989.

[72] David Turnbull. On the relation between crystallization rate and liquid structure. *The Journal of Physical Chemistry*, 66(4):609–613, 1962.

[73] Henrik Larsson, Henrik Strandlund, and Mats Hillert. Unified treatment of kirkendall shift and migration of phase interfaces. *Acta Materialia*, 54(4):945 – 951, 2006.

[74] Li-li Zhou, Jia-ming Pan, Lin Lang, Ze-an Tian, Yun-fei Mo, and Ke-jun Dong. Atomic structure evolutions and mechanisms of the crystallization pathway of liquid al during rapid cooling. *RSC Adv.*, 11:39829–39837, 2021.

[75] Henrik Larsson and Annika Borgenstam. Trans-interface diffusivity in the fe–ni system. *Scripta Materialia*, 56(1):61–64, 2007.

[76] Jan-Olof Andersson and John Ågren. Models for numerical treatment of multicomponent diffusion in simple phases. *Journal of Applied Physics*, 72(4):1350–1355, 1992.

[77] U. R. Kattner and C. E. Campbell. Modelling of thermodynamics and diffusion in multicomponent systems. *Materials Science and Technology*, 25:443–459, 4 2009.

[78] Nils Warnkenn. private communication, Febuary 2019.

[79] Michael Johnsson Nils Warnkenn, Bashir Mitchell. manuscript in preperation, 2023.

[80] J-O Andersson, Thomas Helander, Lars Höglund, Pingfang Shi, and Bo Sundman. Thermo-calc & dictra, computational tools for materials science. *Calphad*, 26(2):273–312, 2002.

[81] Ales Kroupa. Modelling of phase diagrams and thermodynamic properties using calphad method – development of thermodynamic databases. *Computational Materials Science*, 66:3–13, 2013. Multiscale simulation of heterogeneous materials and coupling of thermodynamic models.

[82] Mats Hillert. The compound energy formalism, 2001.

[83] T. A.M. Langlands and B. I. Henry. The accuracy and stability of an implicit solution method for the fractional diffusion equation. *Journal of Computational Physics*, 205:719–736, 5 2005.

[84] W.A Tiller, K.A Jackson, J.W Rutter, and B Chalmers. The redistribution of solute atoms during the solidification of metals. *Acta Metallurgica*, 1(4):428–437, 1953.

[85] Klemens Reuther, Stephan Hubig, Ingo Steinbach, and Markus Rettenmayr. Solute trapping in non-equilibrium solidification: A comparative model study. *Materialia*, 6, 6 2019.

[86] Tatu Pinomaa and Nikolas Provatas. Quantitative phase field modeling of solute trapping and continuous growth kinetics in quasi-rapid solidification. *Acta Materialia*, 168:167–177, 4 2019.